NASA TM X-64

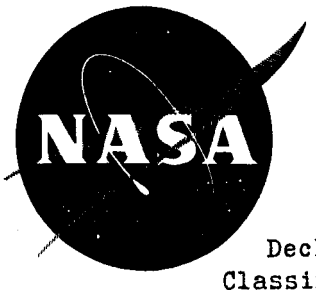

TECHNICAL MEMORANDUM

X - 64

MEASUREMENTS OF FLOW PROPERTIES IN THE VICINITY OF THREE WING-FUSELAGE COMBINATIONS AT MACH NUMBERS OF 1.61 AND 2.01

By Harry W. Carlson

Langley Research Center
Langley Field, Va.

NATIONAL AERONAUTICS AND SPACE ADMINISTRATION
WASHINGTON
October 1959

NATIONAL AERONAUTICS AND SPACE ADMINISTRATION

TECHNICAL MEMORANDUM X-64

MEASUREMENTS OF FLOW PROPERTIES IN THE VICINITY OF THREE WING-FUSELAGE COMBINATIONS AT MACH NUMBERS OF 1.61 AND 2.01*

By Harry W. Carlson

SUMMARY

This investigation has been conducted in order to study in detail the actual flow below the wing of wing-body combinations by the use of wind-tunnel flow surveys. For a number of sample cases, the linearized theory has been used to calculate the flow properties and is compared with experiment in an effort to demonstrate the range of applicability of the theory, to point out its limitations, and to suggest means of improvement.

The tests were made in the Langley 4- by 4-foot supersonic pressure tunnel at Mach numbers of 1.61 and 2.01 for three wing-body combinations employing a swept wing, a trapezoidal wing, and a delta wing. Reynolds numbers for the tests corresponding to the Mach numbers were 2.8×10^6 and 2.3×10^6 per foot. Local Mach number, pressure coefficient, downwash, and sidewash were measured at angles of attack of 0°, 4°, and 8°.

INTRODUCTION

In recent years, several investigations have dealt with the problem of the prediction of store forces due to interference effects from the parent airplane (refs. 1 to 4). Although the agreement that has been obtained between experiment and simple theories has often been surprisingly good, just as often it has been inadequate.

A first-order theoretical prediction of store forces requires, first, the calculation of the flow field surrounding the airplane and, second, an evaluation of the effect of this flow on the store. In references 1 to 4 calculated forces are compared directly with the experimental force

*Title, Unclassified.

measurements. A comparison, at the intermediate stage, between calculated and measured flow properties has not been attempted. Such a comparison is desirable to determine the ability of linearized theory to predict wing-body flow fields and to aid in the discovery of the source of the discrepancies between predicted and measured store forces.

The purpose of this investigation is to study in detail the actual flow about wing-body combinations by using wind-tunnel flow surveys. For a number of sample cases, linearized theory has been used to calculate the flow properties and is compared with experiment in an effort to demonstrate the range of applicability of the theory, point out its limitations, and suggest means of improvement.

These tests were made in the Langley 4- by 4-foot supersonic pressure tunnel at Mach numbers of 1.61 and 2.01 for three wing-body combinations employing a swept wing, a trapezoidal wing, and a delta wing. Reynolds numbers for the tests corresponding to the Mach numbers were 2.8×10^6 and 2.3×10^6 per foot. Local Mach number, pressure coefficient, downwash, and sidewash were measured at angles of attack of 0°, 4°, and 8°.

SYMBOLS

q_∞	free-stream dynamic pressure
p_∞	free-stream static pressure
$p_{t,\infty}$	free-stream stagnation pressure
M_∞	free-stream Mach number
β	cotangent of Mach angle, $\sqrt{M_\infty^2 - 1}$
p	local static pressure
C_p	pressure coefficient, $\frac{p - p_\infty}{q_\infty}$
M	local Mach number
ϵ	downwash angularity, positive down, deg
σ	sidewash angularity, positive out, deg

i	total flow angularity, $\approx \sqrt{\epsilon^2 + \sigma^2}$, deg
ϕ	angle between radial component of flow and horizontal plane, $\approx \tan^{-1} \frac{\epsilon}{\sigma}$, deg
x,y,z	Cartesian coordinates referenced to wing-fuselage combinations as shown in figure 1
x,r	cylindrical coordinates (origin at fuselage nose, axis coincident with fuselage center line)
α	wing-fuselage angle of attack, deg
ξ,η,ζ	Cartesian coordinates of sources giving rise to theoretical flow
m	cotangent of sweep angle of line source
λ	slope of wing surface, dz/dx at surface
b	wing semispan
c	wing chord

MODELS AND APPARATUS

Sketches of the models used in these tests are shown in figure 1. The wings were constructed of steel and the fuselages of steel and aluminum alloy. Transition strips composed of No. 120 carborundum grains were used at the fuselage nose and at the 10-percent wing-chord stations. The models themselves contained no instrumentation.

Also shown in figure 1 is a drawing of the survey apparatus. The probe actuator provided a remotely controlled longitudinal travel of 23 inches. The lateral distance was varied by means of the permanent tunnel-sting traversing mechanism. Thus, during one run, the probe could be placed at any point (within defined limits) in a plane parallel to the chord plane of the wing. Provision was made for a manual adjustment of the vertical height and the angle of attack.

Details of the conical tip probe are shown at the lower left of figure 1. Each of the five orifices was connected to a separate Baldwin gage. A card-punch data-recording system was used.

TESTING TECHNIQUES

For this investigation a method of data recording and reduction demanding a minimum of manual operations was employed. The five probe pressures were measured by individual Baldwin gages having a range of 15 lb/sq in. and an accuracy of 0.1 percent full scale. The outputs of these gages were fed directly to a Brown self-balancing potentiometer and then to an IBM card punch. The data reduction was performed by IBM electronic data processing machines.

The task of finding flow angularity and Mach number from the five pressures is complicated by the fact that one must be known in order to determine the other. A simultaneous solution may be found when the calibration data are prepared in chart form. However, this method is quite laborious.

A method has been developed whereby the answers can be found rapidly by use of the tables for supersonic flow around cones (refs. 5 to 7) and by use of machine computing. In this method the angularity is first approximated so that the Mach number may be calculated, and finally the angularity is accurately determined. An experimental check established the validity of using the M.I.T. cone tables (refs. 5 to 7) alone in relating cone pressures to Mach number and flow angularity. This was done at both test Mach numbers by testing the cone through an angle-of-attack range in the known flow of the tunnel test section with no model present. The equations obtained directly from the cone tables provided Mach number and flow-angularity data that agreed well with the known values. Thus, the cone could be used as a flow-measuring instrument without extensive calibrations.

The following equations for the ratio of the surface pressure on an unyawed cone to the free-stream static pressure ahead of the cone $\bar{p}_s/p$ and for the ratio of the surface pressure on a yawed cone to that on an unyawed cone $p_s/\bar{p}_s$ have been taken from the cone tables:

$$\frac{\bar{p}_s}{p} = K_0$$

$$\frac{p_s}{\bar{p}_s} = 1 + K_1 i \cos \psi + K_2 i^2 + K_3 i^2 \cos 2\psi$$

where

$$K_0 = \left(\frac{\bar{a}_s^2}{\bar{a}_w^2}\right)^{\frac{\gamma}{\gamma-1}}\left(\frac{2\gamma}{\gamma+1}M^2\sin^2\theta_w - \frac{\gamma-1}{\gamma+1}\right)$$

$$K_1 = \frac{n}{\bar{p}_s}$$

$$K_2 = \frac{\bar{p}_{t,\infty}}{\bar{p}_s} + \frac{\gamma}{2}\left(\frac{\bar{U}_s}{\bar{a}_s}\right)^2 + \frac{1}{2}\cot\theta_s\left(\frac{n}{\bar{p}_s}\right)$$

$$K_3 = \frac{\bar{p}_w}{\bar{p}_s} + \frac{\gamma}{2}\left(\frac{\bar{U}_s}{\bar{a}_s}\right)^2 - \frac{1}{2}\cot\theta_s\left(\frac{n}{\bar{p}_s}\right)$$

The terminology used in these equations is defined as follows:

M	Mach number of flow ahead of cone (local Mach number)
p	static pressure of flow ahead of cone (local static pressure)
$\bar{p}_s$	static pressure on surface of unyawed cone
p_s	static pressure on surface of yawed cone
$\bar{p}_w$	static pressure immediately behind shock wave of unyawed cone
$\bar{p}_{t,\infty}$	stagnation pressure behind shock wave of unyawed cone
$\bar{a}_s$	speed of sound at surface of unyawed cone
$\bar{a}_w$	speed of sound immediately behind shock of unyawed cone
$\bar{U}_s$	radial velocity component at surface of unyawed cone
n	Fourier expansion coefficients as defined in reference 5
γ	ratio of specific heats, 1.405
θ_s	semiapex angle of cone

θ_w semiapex angle of shock wave about unyawed cone

ψ angle between radial component of flow and radial line through point on surface of cone where pressure is being evaluated

From these basic equations, the ratio of the average cone surface pressure to the static pressure of the flow ahead of the cone can be written as

$$\frac{p_{s,av}}{p} = \left(1 + K_2 i^2\right) K_0$$

and the ratio of the pressure difference between opposite orifices to the free-stream static pressure can be written as

$$\frac{\Delta p_s}{p} = 2K_0 K_1 i \cos \psi$$

The average surface pressure and the pressure difference can be referred to the stagnation pressure measured behind the normal shock at the probe tip as follows:

$$\frac{p_{s,av}}{\bar{p}_{t,\infty}} = \left(1 + K_2 i^2\right) K_0 \left(\frac{p}{p_{t,\infty}}\right)\left(\frac{p_{t,\infty}}{\bar{p}_{t,\infty}}\right)$$

$$\frac{\Delta p_s}{\bar{p}_{t,\infty}} = 2K_0 K_1 i \cos \psi \left(\frac{p}{p_{t,\infty}}\right)\left(\frac{p_{t,\infty}}{\bar{p}_{t,\infty}}\right)$$

The pressure ratios as a function of Mach number were obtained from the tables of reference 8.

For the cone half-angle used in the survey and over the expected Mach number range, M was plotted as a function of $\frac{p_{s,av}}{\bar{p}_{t,\infty}}$. In addition, $\frac{\epsilon}{\frac{\Delta p_s}{\bar{p}_{t,\infty}}}$ and $\frac{\sigma}{\frac{\Delta p_s}{\bar{p}_{t,\infty}}}$ were plotted as a function of Mach number. (See fig. 2.)

It was found that these curves could be approximated with little error by the power series:

$$M = A + B\frac{\bar{p}_{t,\infty}}{p_{s,av}} + C\left(\frac{\bar{p}_{t,\infty}}{p_{s,av}}\right)^2 + i^2\left[D + E\frac{\bar{p}_{t,\infty}}{p_{s,av}} + F\left(\frac{\bar{p}_{t,\infty}}{p_{s,av}}\right)^2\right]$$

$$\epsilon = i \sin \phi = \left(G + \frac{H}{M} + \frac{J}{M^2}\right)\left(\frac{\Delta p_s}{\bar{p}_{t,\infty}}\right)_{\text{vertical}}$$

$$\sigma = i \cos \phi = \left(G + \frac{H}{M} + \frac{J}{M^2}\right)\left(\frac{\Delta p_s}{\bar{p}_{t,\infty}}\right)_{\text{horizontal}}$$

In evaluating ϵ it is assumed that the orifices lie in a vertical plane and $\psi = 90^\circ - \phi$. In evaluating σ it is assumed that the orifices lie in a horizontal plane and $\psi = \phi$.

In practice, i was first approximated as

$$i \approx \left(G + \frac{H}{M} + \frac{J}{M^2}\right)\sqrt{\left(\frac{\Delta p_s}{\bar{p}_{t,\infty}}\right)^2_{\text{vertical}} + \left(\frac{\Delta p_s}{\bar{p}_{t,\infty}}\right)^2_{\text{horizontal}}}$$

where M was used as the nominal Mach number. This value of i was then used in computing the local Mach number. Finally downwash and sidewash were evaluated.

From a pretest tunnel calibration the accuracies of the probe measurements are estimated to be as follows:

Absolute values of i, deg	Mach number	Angularity, deg	x, in.	y, in.	z, in.
0 to 4	±0.01	±0.25	±0.1	±0.1	±0.1
4 to 8	±.01	±.50	±.1	±.1	±.1
8 to 12	±.02	±.75	±.1	±.1	±.1
12 to 16	±.04	±1.50	±.1	±.1	±.1

THEORY

The linearized-theory line-source method of Robert T. Jones (ref. 9) has been adapted for use in computing machines and has been applied to the wings of these tests. In determining the flow field due to thickness, the airfoil shapes of the wings were approximated by 22 line-source elements as shown in figure 3. When referred to a Cartesian coordinate system, the equations for the pressure coefficient at a point (x,y,z) due to each of the individual line sources of span 2b, cotangent of sweep angle m, and surface slope λ are as shown below:

For subsonic leading edges which are swept back,

$$C_p = \frac{2\lambda}{\pi} \frac{m}{\sqrt{1 - \beta^2 m^2}} \left\{ \cosh^{-1} \frac{x - \beta^2 m y}{\beta \sqrt{(4 - mx)^2 + \left(1 - \beta^2 m^2\right) z^2}} + \right.$$

$$\cosh^{-1} \frac{x + \beta^2 m y}{\beta \sqrt{(y + mx)^2 + \left(1 - \beta^2 m^2\right) z^2}} -$$

$$\cosh^{-1} \frac{\left(x - \frac{b}{m}\right) - \beta^2 m (y - b)}{\beta \sqrt{\left[(y - b) - m\left(x - \frac{b}{m}\right)\right]^2 + \left(1 - \beta^2 m^2\right) z^2}} +$$

$$\left. \cosh^{-1} \frac{\left(x - \frac{b}{m}\right) - \beta^2 m (y + b)}{\sqrt{\left[(y + b) - m\left(x - \frac{b}{m}\right)\right]^2 + \left(1 - \beta^2 m^2\right) z^2}} \right\}$$

For supersonic leading edges which are swept back,

$$C_p = \frac{2\lambda}{\pi} \frac{1}{\sqrt{\beta^2 - \frac{1}{m^2}}} \left\{ \cos^{-1} \frac{x - \beta^2 my}{\beta\sqrt{(y - mx)^2 + \left(1 - \beta^2 m^2\right) z^2}} + \right.$$

$$\cos^{-1} \frac{x + \beta^2 my}{\beta\sqrt{(y + mx)^2 + \left(1 - \beta^2 m^2\right) z^2}} -$$

$$\cos^{-1} \frac{\left(x - \frac{b}{m}\right) - \beta^2 m(y - b)}{\beta\sqrt{\left[(y - b) - m\left(x - \frac{b}{m}\right)\right]^2 + \left(1 - \beta^2 m^2\right) z^2}} +$$

$$\left. \cos^{-1} \frac{\left(x - \frac{b}{m}\right) - \beta^2 m(y + b)}{\beta\sqrt{\left[(y + b) - m\left(x - \frac{b}{m}\right)\right]^2 + \left(1 - \beta^2 m^2\right) z^2}} \right\}$$

For supersonic leading edges which are swept forward,

$$C_p = \frac{2\lambda}{\pi} \frac{1}{\sqrt{\beta^2 - \frac{1}{m^2}}} \left\{ \cos^{-1} \frac{\left(x + \frac{b}{|m|}\right) - \beta^2 |m|(b - y)}{\beta\sqrt{\left[(b - y) - |m|\left(x + \frac{b}{|m|}\right)\right]^2 + \left(1 - \beta^2 m^2\right) z^2}} - \cos \frac{x + \beta^2 |m| y}{\beta\sqrt{(y + |m|x)^2 + \left(1 - \beta^2 m^2\right) z^2}} + \right.$$

$$\left. \cos^{-1} \frac{x + \frac{b}{|m|} - \beta^2 |m|(b + y)}{\beta\sqrt{\left[(b + y) - |m|\left(x + \frac{b}{|m|}\right)\right]^2 + \left(1 - \beta^2 m^2\right) z^2}} - \cos^{-1} \frac{x - \beta^2 |m| y}{\beta\sqrt{(y - |m|x)^2 + \left(1 - \beta^2 m^2\right) z^2}} \right\}$$

[redacted]

[redacted]

In these equations the coordinate system has its origin at the apex of the wing element. Terms are included in the pressure-coefficient equations to account for the wing tip, the opposite wing panel, and the opposite wing tip. The fuselage at the wing-fuselage juncture was assumed to act as a reflection plane. Each individual line source having a supersonic leading edge gives rise to a constant pressure equal to $\frac{2\lambda}{\sqrt{\beta^2 - \frac{1}{m}}}$ in the region between the Mach plane from the leading edge and the Mach cone from the apex, which must be considered separately.

The pressure coefficient due to wing thickness in the field of the complete wing is obtained by a summation of the effects of each of the 22 line sources. Downwash and sidewash were found by a numerical integration to determine the velocity potential and a subsequent differentiation in the desired direction.

The flow about flat-plate wings of the same plan form at an angle of attack of 1° was computed to give the angle-of-attack effects by using only the line sources at the wing leading and trailing edges. These equations, when used for angle-of-attack effects, are valid only ahead of the Mach plane from the trailing edge and inboard of the tip Mach cone. As a matter of interest, the equations were applied in the case of the slightly subsonic leading edge of the swept-wing configuration at $M = 1.61$ and in all cases for flow behind the trailing edge.

The pressure distribution due to thickness of the fuselage was obtained by a numerical integration of the following integral:

$$C_p = 2\int_0^{x-\beta r} \frac{\frac{d}{dx}\left(r\frac{dr}{dx}\right)}{\sqrt{(x-\xi)^2 - \beta^2 r^2}}\, d\xi$$

which can be found in reference 10. The effect of angle of attack on the flow about the fuselage was not considered nor was an attempt made to evaluate mutual interference effects between wing and body.

RESULTS

The flow measurements obtained in this investigation are shown in figures 4 to 17. Local Mach number, static pressure, downwash, and sidewash are plotted as functions of the chordwise location of the tip of the survey probe. On each page, the four flow properties are shown for

a given set of conditions (configuration, angle of attack, Mach number, and spanwise and vertical position). Downwash and sidewash have been plotted with positive values down in order to show the similarity of these curves to those for static pressure and Mach number. Sketches have been included in these figures to show at a glance, the relationship of the survey points to the wing fuselage and to the local wing chord.

In most of the plots a definite jump in the flow properties occurs at the position of the wing leading-edge shock and again at the trailing edge. In fact, the curves are quite similar to those that would appear in two-dimensional flow about the same airfoil sections. The shock from the fuselage nose is outside the range of the plots in most cases.

There appear to be some erroneous data points in the vicinity of the shocks. This may be due to the spacing of the orifices, which may allow a shock front to fall behind some orifices but ahead of others.

An index to the basic data figures is given in table I.

ANALYSIS

Figures 18 to 21 have been prepared in order to illustrate some of the effects of changes in configuration, Mach number, span position, and angle of attack as well as to study the application of linearized theory under a variety of conditions. As in the basic data, the flow properties are plotted as functions of chordwise position. Here the horizontal scale refers to the longitudinal location of the four face orifices instead of the probe tip as was the case for the basic data. Experimental evidence indicated that the effective measuring point of the probe more nearly coincided with the later reference. The local Mach number curves are omitted in these comparisons, since in every case there was a direct relationship between Mach number and static pressure.

Effect of Configuration

Figure 18(a) shows flow properties measured at zero angle of attack below the wing of a swept-wing—fuselage configuration and a trapezoidal-wing—fuselage configuration at a free-stream Mach number of 1.61. The data shown are for a midsemispan position at a distance of approximately 0.2 chord below the wing-chord plane.

The trapezoidal wing with a 4-percent-thick circular-arc section and a sharp, supersonic leading edge apparently had an attached shock. Good agreement is shown between the experimental shock location and the

Mach wave prediction both at the leading edge and at the trailing edge. In fact, good agreement between experiment and theory for all the flow properties is shown over the whole region of the wing-induced disturbances. For the trapezoidal wing there is little deviation from the type of flow associated with a two-dimensional wing, except for the sidewash, which although small is not zero as in the two-dimensional case.

The experimental data for the swept wing indicate a strong detached bow wave appearing some distance ahead of the wing leading edge. The theoretical curves computed for a free-stream Mach number of 1.61 (solid line) show little resemblance to the actual flow in the region of the leading edge. In the region of the trailing-edge disturbances, the agreement is good.

Schlieren photographs made during previous tests of this swept wing confirmed the presence of a shock emanating from the wing-root juncture (ref. 1). The linearity of the shock and its origin near the leading edge at the wing-fuselage juncture suggested the possibility of altering the theory to allow disturbances to propagate along this line instead of along a Mach line. This can be accomplished merely by recomputing the flow for a new and lower Mach number. The theory using this "fictitious" Mach number is shown as a dashed line (fig. 18(a)). The description of the flow (all three quantities) in the vicinity of the leading edge has considerably improved. It is possible that the overestimation of the pressures behind the shock is because of the choice of too large a wedge angle ($\lambda = 0.18$) to approximate the wing section at the leading edge. The remainder of the flow field, however, is not invalidated, being relatively insensitive to this choice.

For the swept wing, quite large values of sidewash are shown, whereas relatively little sidewash was noted for the trapezoidal wing. The pressures and downwash at the midsemispan seem to depend largely on the wing section alone whereas the sidewash is determined in addition by the sweep of the wing elements.

Thus it appears that linearized theory may be used to predict, with some degree of accuracy, the complete flow due to thickness about wing-fuselage configurations. The effect of a thickness-induced bow wave may be approximated by a simple adjustment to the theory if schlieren photographs or other means of locating the shock front are available. Greater deviations of theory and experiment are to be expected when the basic assumptions of the theory are further violated (for example: thicker wings, greater leading-edge radius, and lower-fineness-ratio bodies).

Effect of Mach Number

The data shown in figure 18(b) for $M_\infty = 2.01$ do not agree with the theoretical prediction nearly as well as was the case at $M_\infty = 1.61$ (fig. 18(a)). It is well known that the linearized theory becomes less useful with increasing Mach number, but this much change is difficult to explain. A schlieren photograph of the swept-wing flow field was not available for this Mach number. Therefore, no theory adjusted for the presence of the bow wave is shown.

Effect of Angle of Attack

The effects of angle of attack have been separated from thickness effects by dealing with incremental flow properties. In figure 19 the flow properties at zero angle of attack have been subtracted from those measured at an angle of attack of 4°, the result being plotted as a function of chordwise position. Data are shown for both the swept- and trapezoidal-wing configurations at a free-stream Mach number of 1.61.

The theory treating the angle-of-attack induced flow (as used in this report) is strictly applicable only for special cases. A basic assumption is that the flow everywhere ahead of the leading-edge envelope of Mach cones is that of the undisturbed free stream. This, of course, excludes all subsonic leading-edge conditions. Another assumption made here is that, in the chord plane of the wing behind the wing trailing edge, the flow has no vertical component. Thus, in no case does the theory rigorously apply to the region within the envelope of Mach cone emanating from the wing trailing edge. Nevertheless, as a matter of interest, the theory was computed for all regions. For the swept wing, the fictitious Mach number approximation first shown in figure 18(a) has again been applied. The theory seems to give a reasonable agreement for pressures and downwash about both configurations, except in the modified-theory downwash curve for the swept wing. This poor agreement apparently is one of the penalties paid for the use of the crude attempt to properly define conditions at the bow wave. An adaquate prediction of the sidewash due to angle of attack was not given for either configuration. It should be noted that no theoretical prediction was made of the downwash or sidewash induced by the fuselage at angle of attack. The experiment indicates that the fuselage contributed an upward flow angularity of about 1° at the midsemispan wing leading edge and a sidewash of about $1/2^\circ$.

It appears possible that a first-order approximation of at least the pressure field due to angle of attack can be made over the whole flow region of the wing by using the methods of this paper. For certain conditions and for defined regions of the flow a prediction can be made for all flow properties.

Effect of Spanwise Position

Figures 20 and 21 show a comparison of experimental and theoretical flow properties at an inboard and an outboard station. In general the results are not far different from those obtained at the midsemispan location. The angle-of-attack effects are not predicted as well as the thickness effects, particularly in the region of the wing tip. Here again, one of the assumptions used in the application of the theory may cause errors. In the plane of the wing outboard of the tip the flow was assumed to have no downwash component.

CONCLUSIONS

A study of the results of the flow-survey tests and a comparison with linearized theory provides the following conclusions:

1. The linearized theory may be used to predict, with a reasonable degree of accuracy, the complete flow due to thickness about wing-fuselage configurations. The effect of a thickness-induced wing bow wave may be approximated by an empirical adjustment to the theory if schlieren photographs or other means of locating the shock front in the plane of the wing are available.

2. The agreement between theory and experiment is considerably poorer at a Mach number of 2.0 than at a Mach number of 1.6, a condition not completely understood.

3. A first-order approximation of at least the pressure field due to angle of attack can be made over that portion of the wing flow field covered in this report.

4. For the survey locations of these tests the wing-induced flow predominates over the fuselage flow field. Over large regions of the wing the flow is nearly two dimensional in character except for the sidewash component.

Langley Research Center,
National Aeronautics and Space Administration,
Langley Field, Va., June 17, 1959.

REFERENCES

1. Bobbitt, Percy J., Carlson, Harry W., and Pearson, Albin O.: Calculation of External-Store Loads and Correlation With Experiment. NACA RM L57D30a, 1957.

2. Gapcynski, John P., and Carlson, Harry W.: The Aerodynamic Characteristics of a Body in the Two-Dimensional Flow Field of a Circular-Arc Wing at a Mach Number of 2.01. NACA RM L57E14, 1957.

3. Carlson, Harry W., and Geier, Douglas J.: The Origin and Distribution of Supersonic Store Interference From Measurement of Individual Forces on Several Wing-Fuselage-Store Configurations. V.- Swept-Wing Heavy-Bomber Configuration With Large Store (Nacelle). Mach Number 2.01. NACA RM L55K15, 1956.

4. Morris, Odell A., Carlson, Harry W., and Geier, Douglas J.: Experimental and Theoretical Determination of Forces and Moments on a Store and on a Store-Pylon Combination Mounted on a 45° Swept-Wing—Fuselage Configuration at a Mach Number of 1.61. NACA RM L57K18, 1958.

5. Staff of the Computing Section, Center of Analysis (Under Direction of Zdeněk Kopal): Tables of Supersonic Flow Around Cones. Tech. Rep. No. 1 (NOrd Contract No. 9169), M.I.T., 1947.

6. Staff of the Computing Section, Center of Analysis (Under Direction of Zdeněk Kopal): Tables of Supersonic Flow Around Yawing Cones. Tech. Rep. No. 3 (NOrd Contract No. 9169), M.I.T., 1947.

7. Staff of the Computing Section, Center of Analysis (Under Direction of Zdeněk Kopal): Tables of Supersonic Flow Around Cones of Large Yaw. Tech. Rep. No. 5 (NOrd Contracts No. 8555 and 9169), M.I.T., 1949.

8. Ames Research Staff: Equations, Tables, and Charts for Compressible Flow. NACA Rep. 1135, 1953. (Supersedes NACA TN 1428.)

9. Jones, Robert T.: Thin Oblique Airfoils at Supersonic Speed. NACA Rep. 851, 1946. (Supersedes NACA TN 1107.)

10. Ferri, Antonio: Elements of Aerodynamics of Supersonic Flows. The Macmillan Co., 1949, p. 221.

[redacted]

TABLE I.- INDEX OF BASIC DATA FIGURES

Figure	Configuration	α, deg	M_∞	y, in.	z, in.
4(a)	Swept	0	1.61	3.0	1.15
4(b)				6.6	1.15
4(c)				10.2	1.15
4(d)				3.0	2.1
4(e)				6.6	2.1
4(f)				10.2	2.1
4(g)				6.6	1.50
4(h)				6.6	3.0
4(i)				6.6	4.2
5	Swept	4	1.61	6.6	2.1
6(a)	Swept	8	1.61	3.0	2.1
6(b)				6.6	
6(c)				10.2	
7(a)	Swept	0	2.01	3.0	1.15
7(b)				6.6	
7(c)				10.2	
8(a)	Trapezoidal	0	1.61	3.0	1.15
8(b)				6.6	1.15
8(c)				10.2	1.15
8(d)				3.0	2.1
8(e)				6.6	2.1
8(f)				10.2	2.1
9(a)	Trapezoidal	4	1.61	3.0	2.1
9(b)				6.6	
9(c)				10.2	
10(a)	Trapezoidal	8	1.61	3.0	2.1
10(b)				6.6	
10(c)				10.2	
11(a)	Trapezoidal	0	2.01	3.0	1.15
11(b)				6.6	1.15
11(c)				10.2	1.15
11(d)				3.0	2.1
11(e)				6.6	2.1
11(f)				10.2	2.1
12	Trapezoidal	4	2.01	6.6	2.1
13(a)	Trapezoidal	8	2.01	3.0	2.1
13(b)				6.6	
13(c)				10.2	
14(a)	Delta	0	1.61	3.0	1.15
14(b)				6.6	
14(c)				10.2	
15(a)	Delta	0	2.01	3.0	1.15
15(b)				6.6	
15(c)				10.2	
16(a)	Fuselage	0	1.61	3.0	0
16(b)				6.6	
16(c)				10.2	
17(a)	Fuselage	0	2.01	3.0	0
17(b)				6.6	
17(c)				10.2	

[redacted]

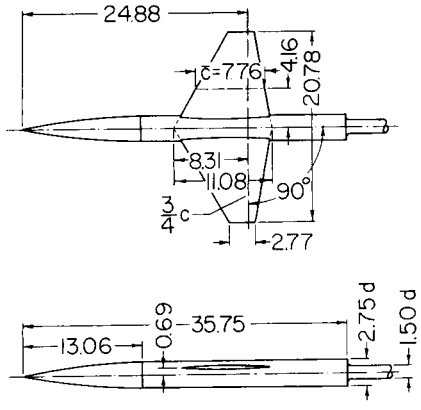

Trapezoidal - wing — fuselage
Aspect ratio 3.0
Taper ratio 0.25
Section 4% circular arc
Area 1.00 sq ft

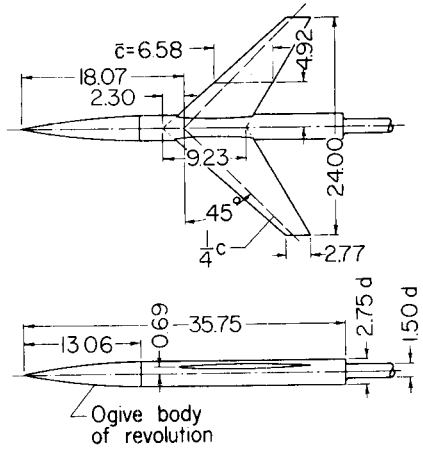

Swept - wing — fuselage
Aspect ratio 4.0
Taper ratio 0.3
Section 65A006
Area 1.00 sq ft

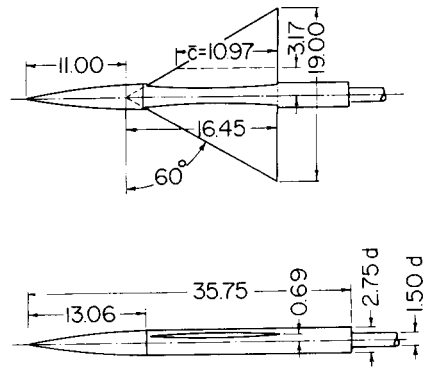

Delta - wing — fuselage
Aspect ratio 2.31
Taper ratio 0
Section 65A004
Area 1.086 sq ft

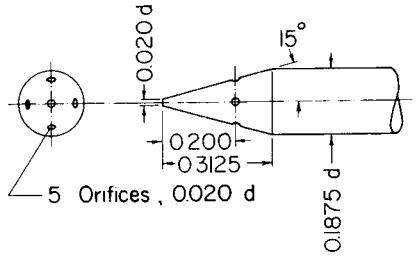

Detail of probe

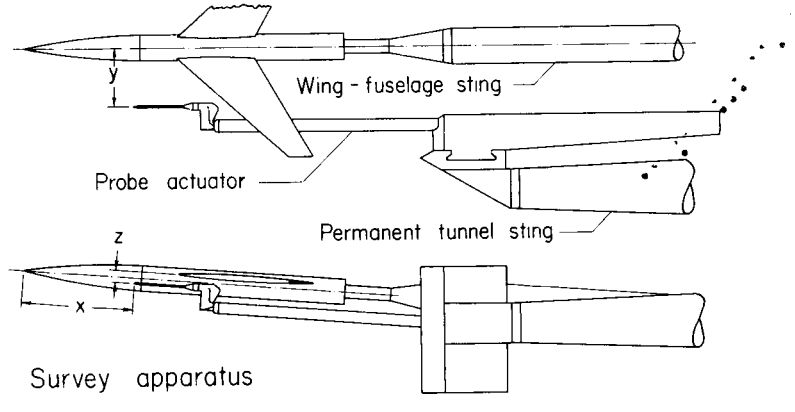

Survey apparatus

Figure 1.- Models and apparatus. All dimensions are in inches.

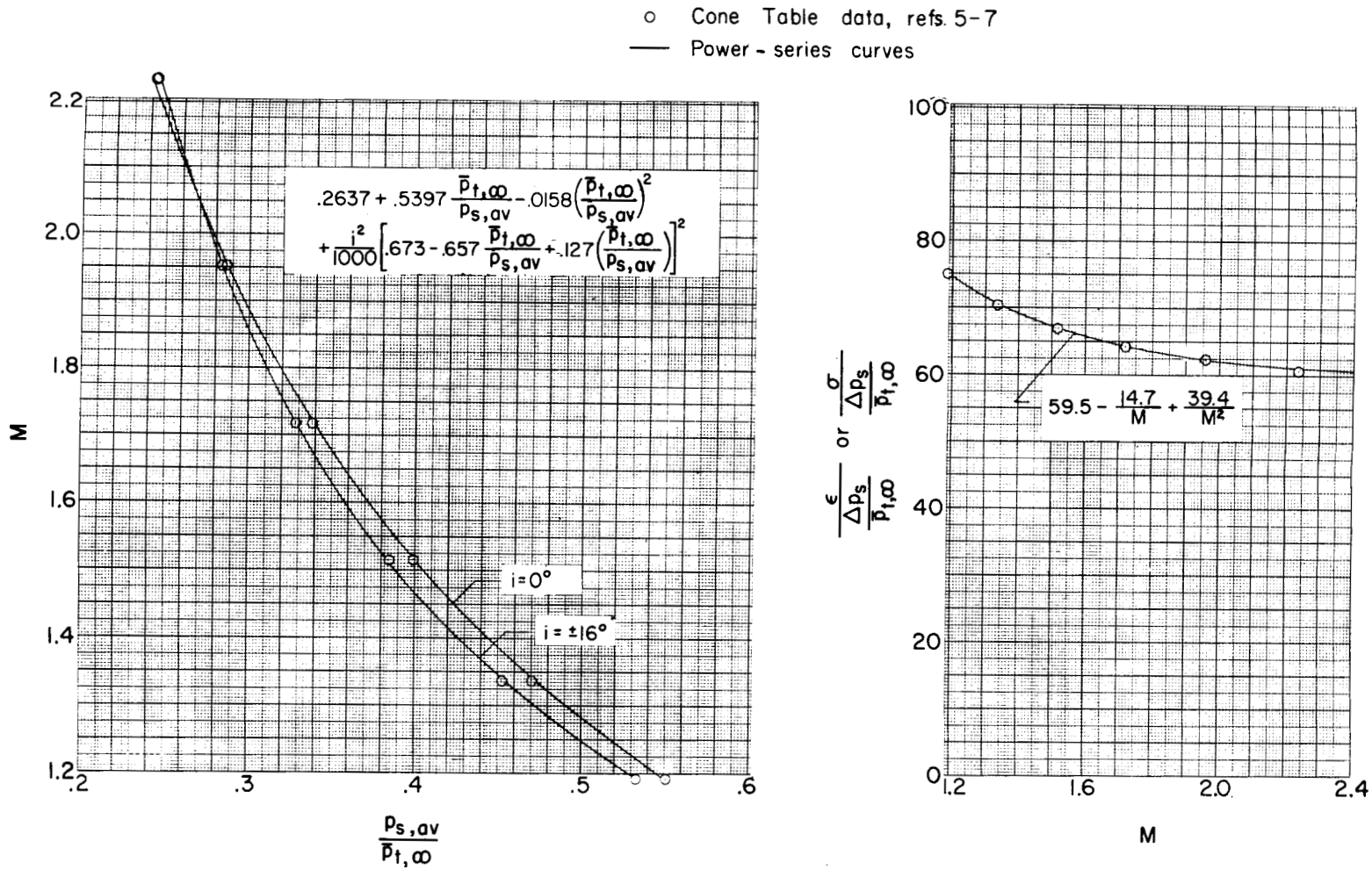

Figure 2.- Relation of Mach number and flow angles to cone pressures.

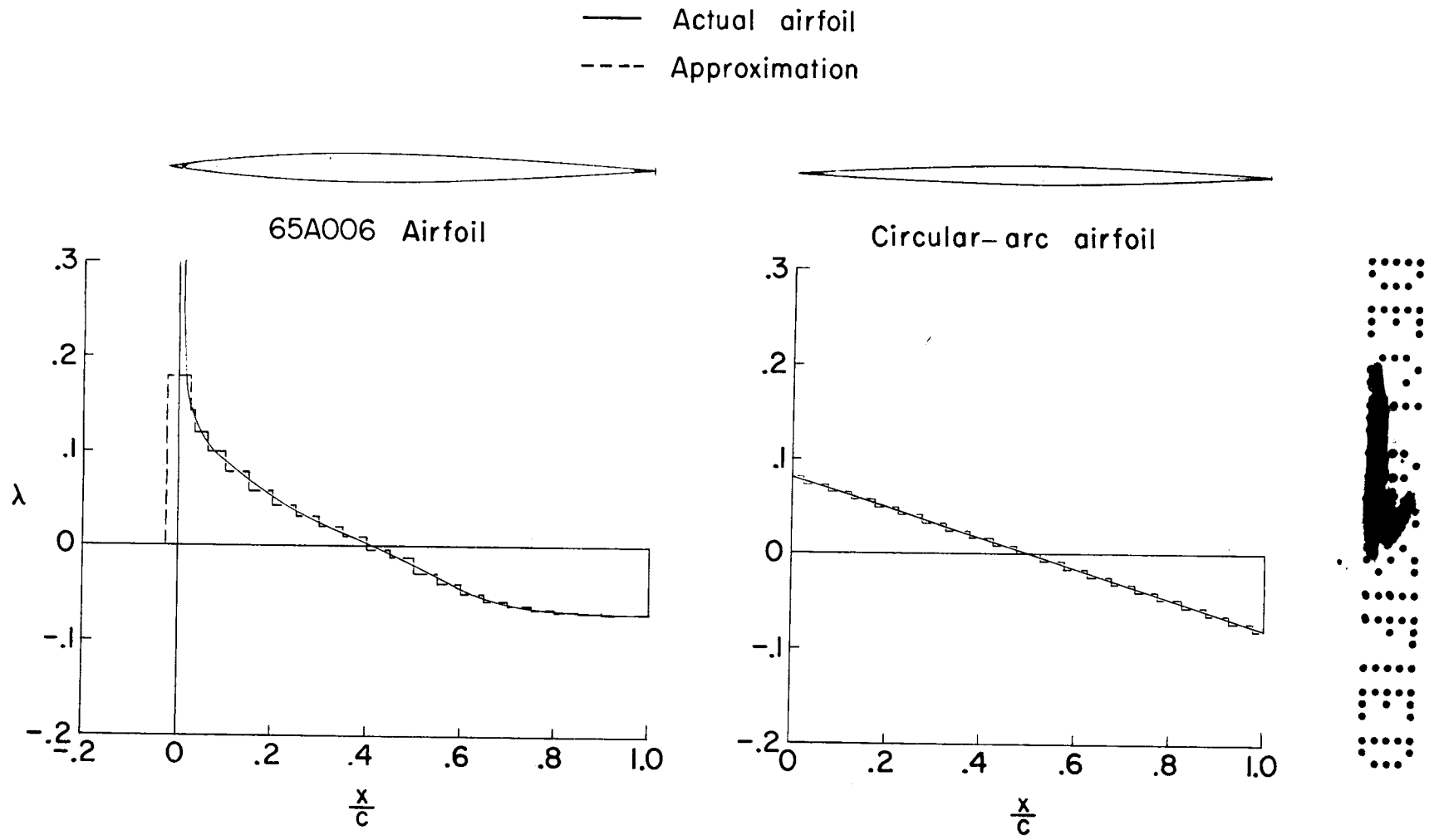

Figure 3.- Actual airfoil sections and line-source approximations.

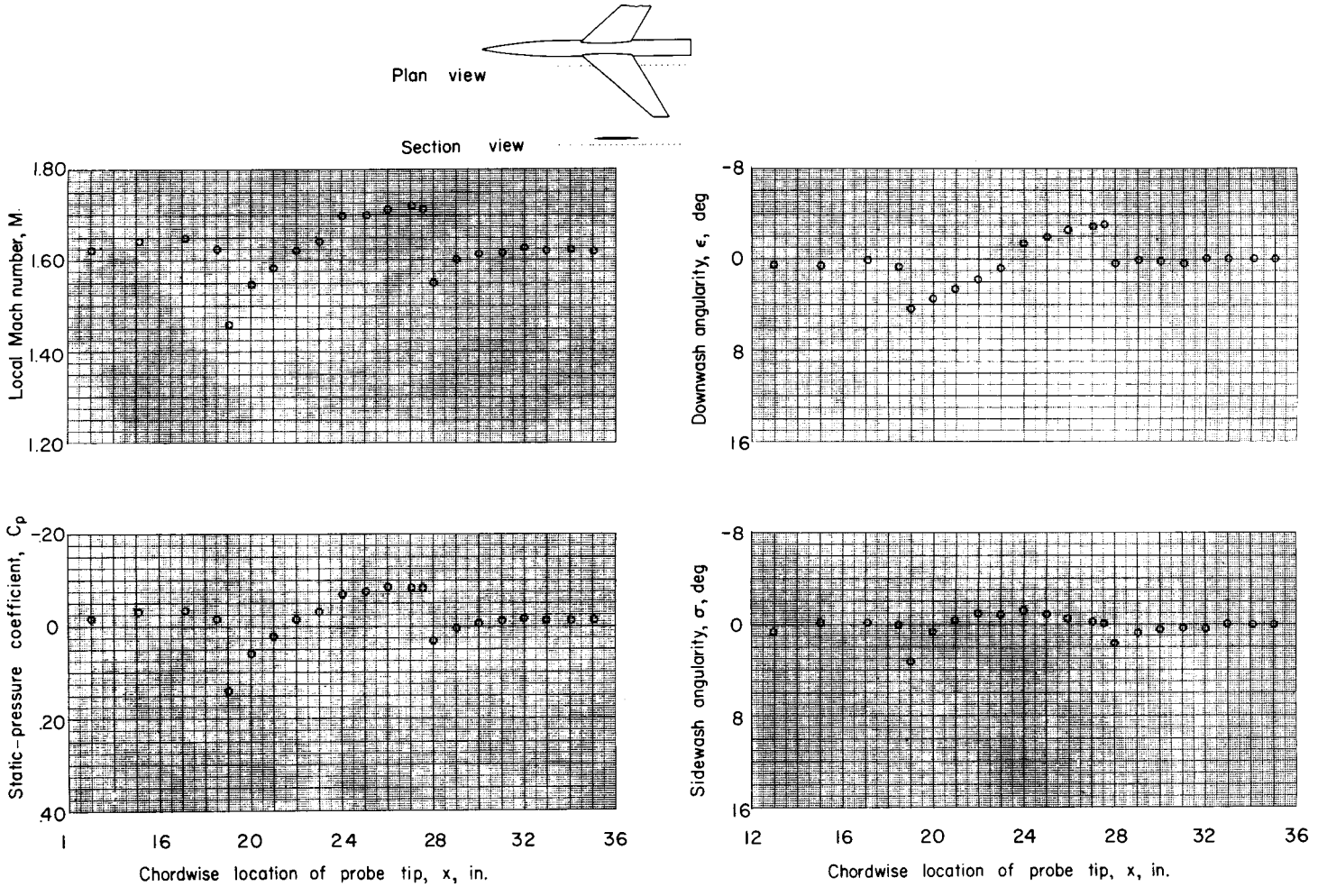

(a) y = 3.0 in.; z = 1.15 in.

Figure 4.- Flow properties measured in the vicinity of a swept-wing—fuselage configuration. $\alpha = 0^{\circ}$; $M_{\infty} = 1.61$.

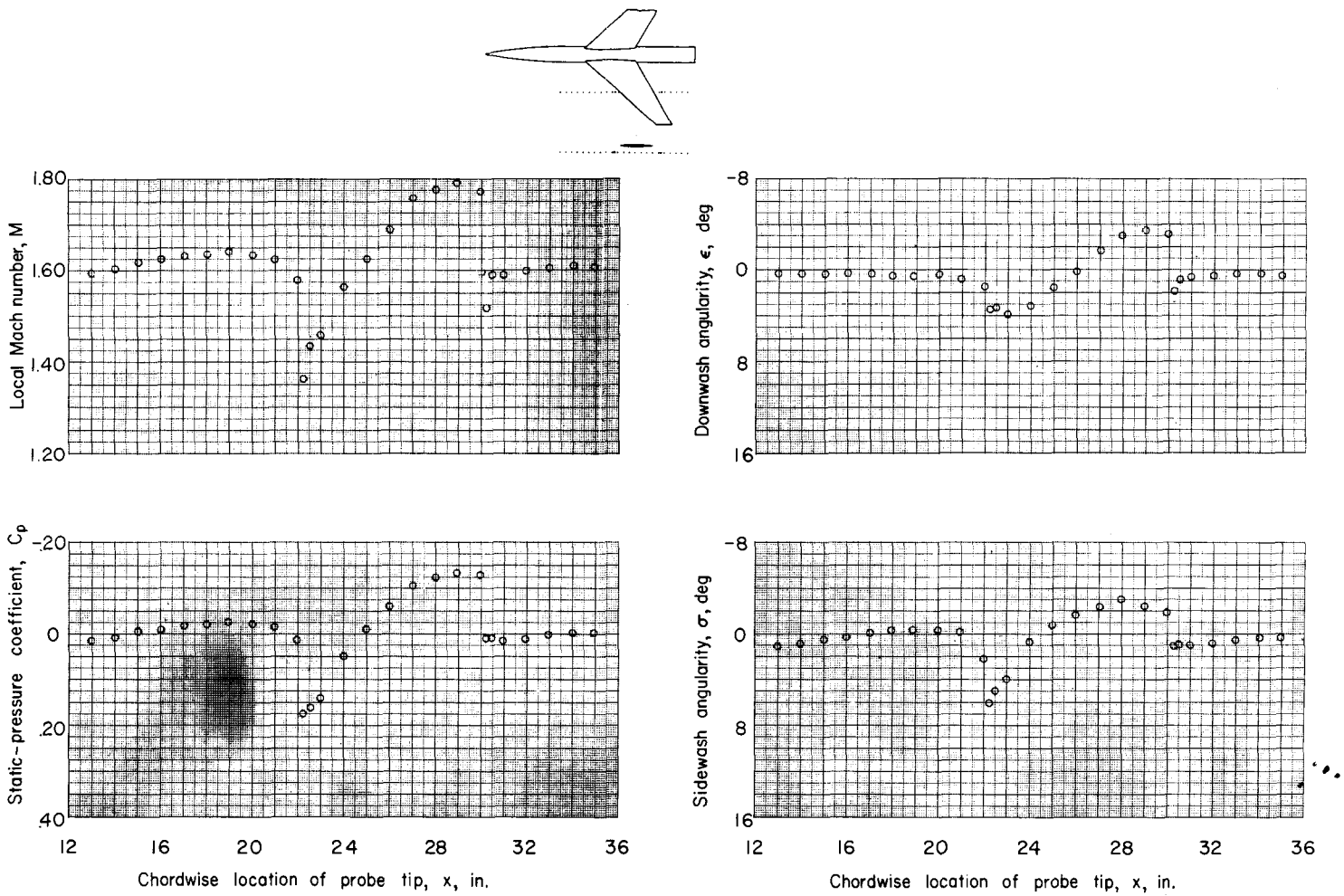

(b) y = 6.6 in.; z = 1.15 in.

Figure 4.- Continued.

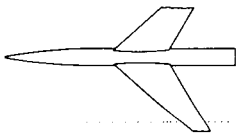

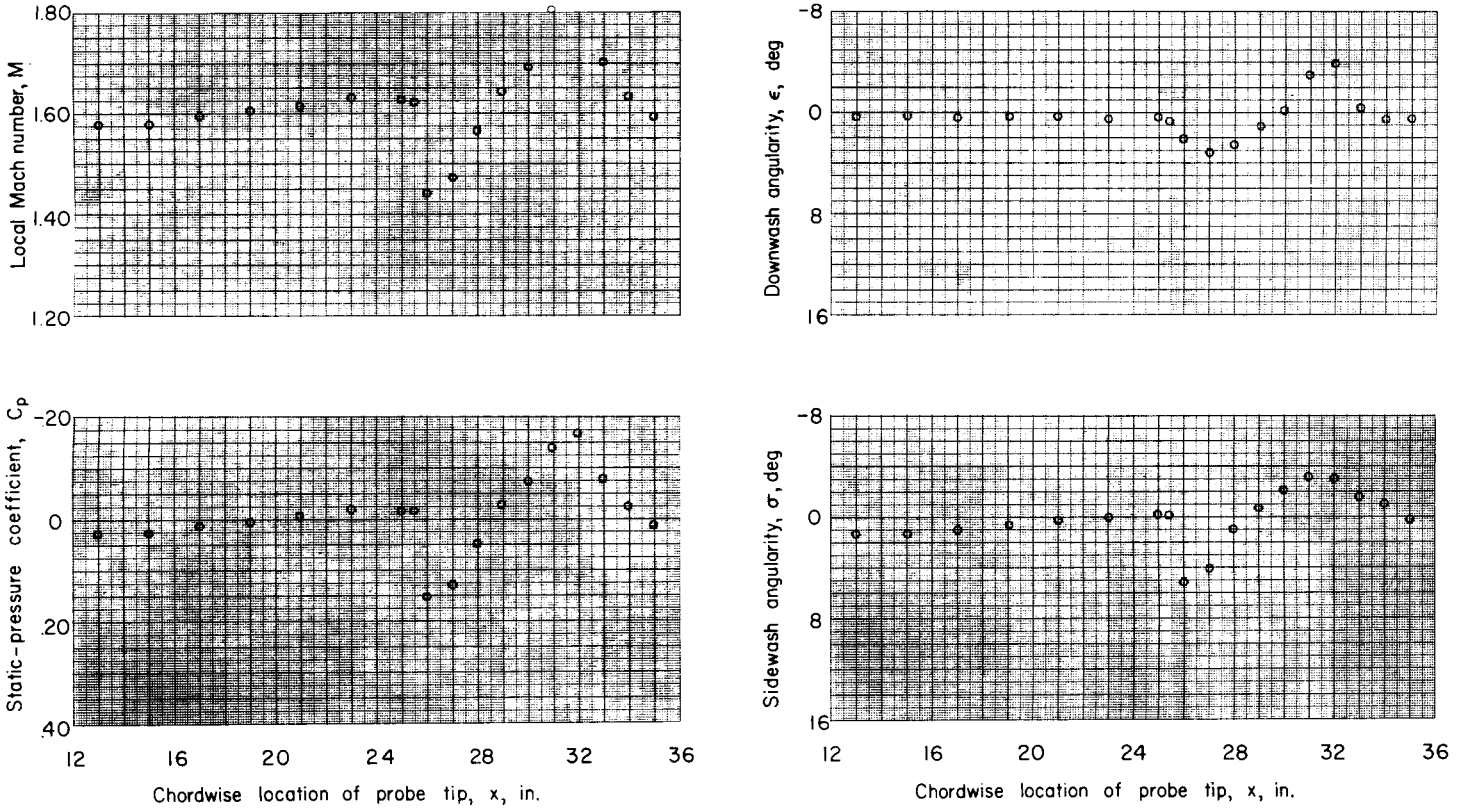

(c) y = 10.2 in.; z = 1.15 in.

Figure 4.- Continued.

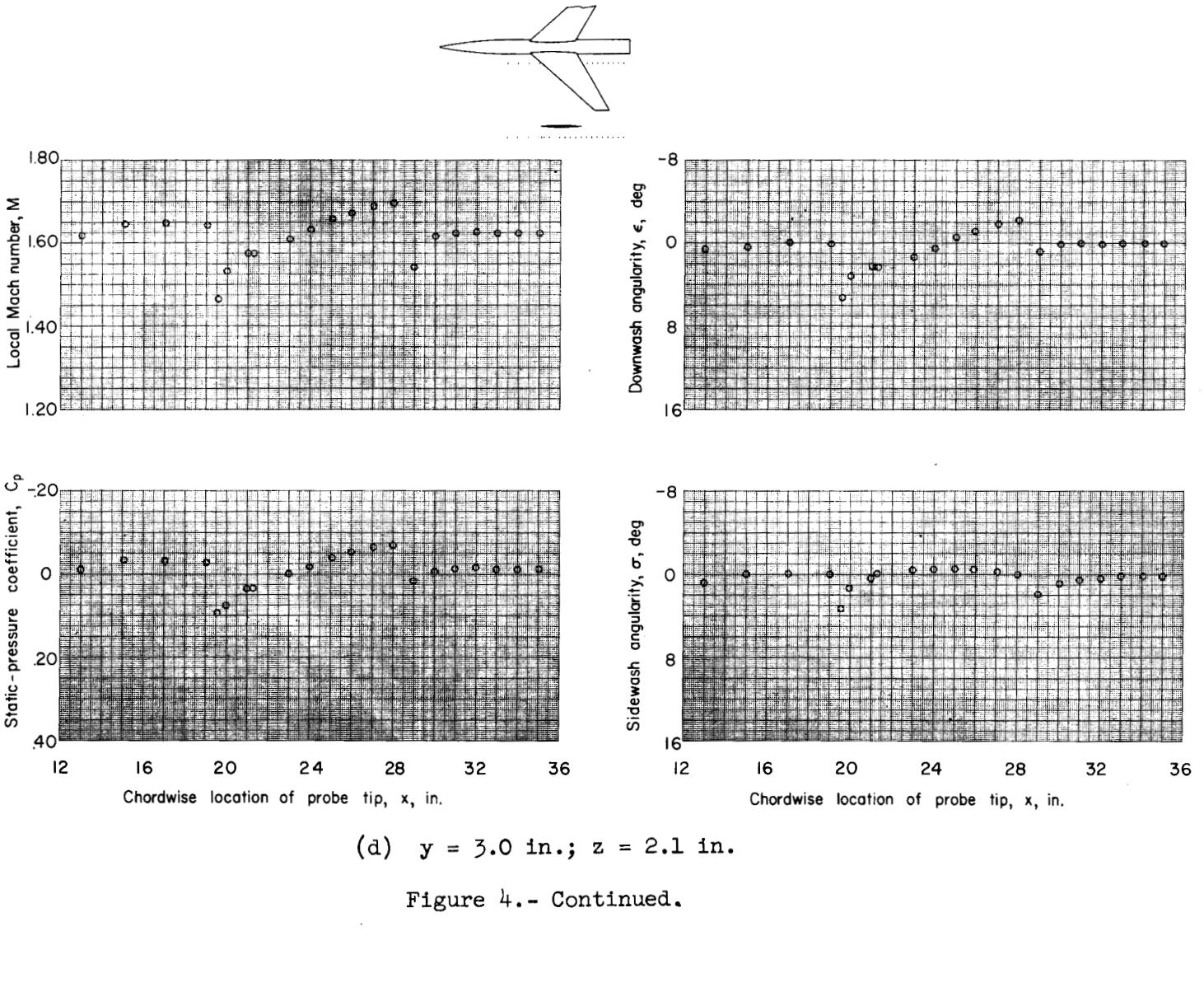

(d) y = 3.0 in.; z = 2.1 in.

Figure 4.- Continued.

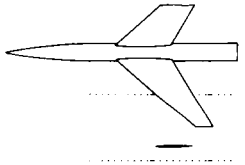

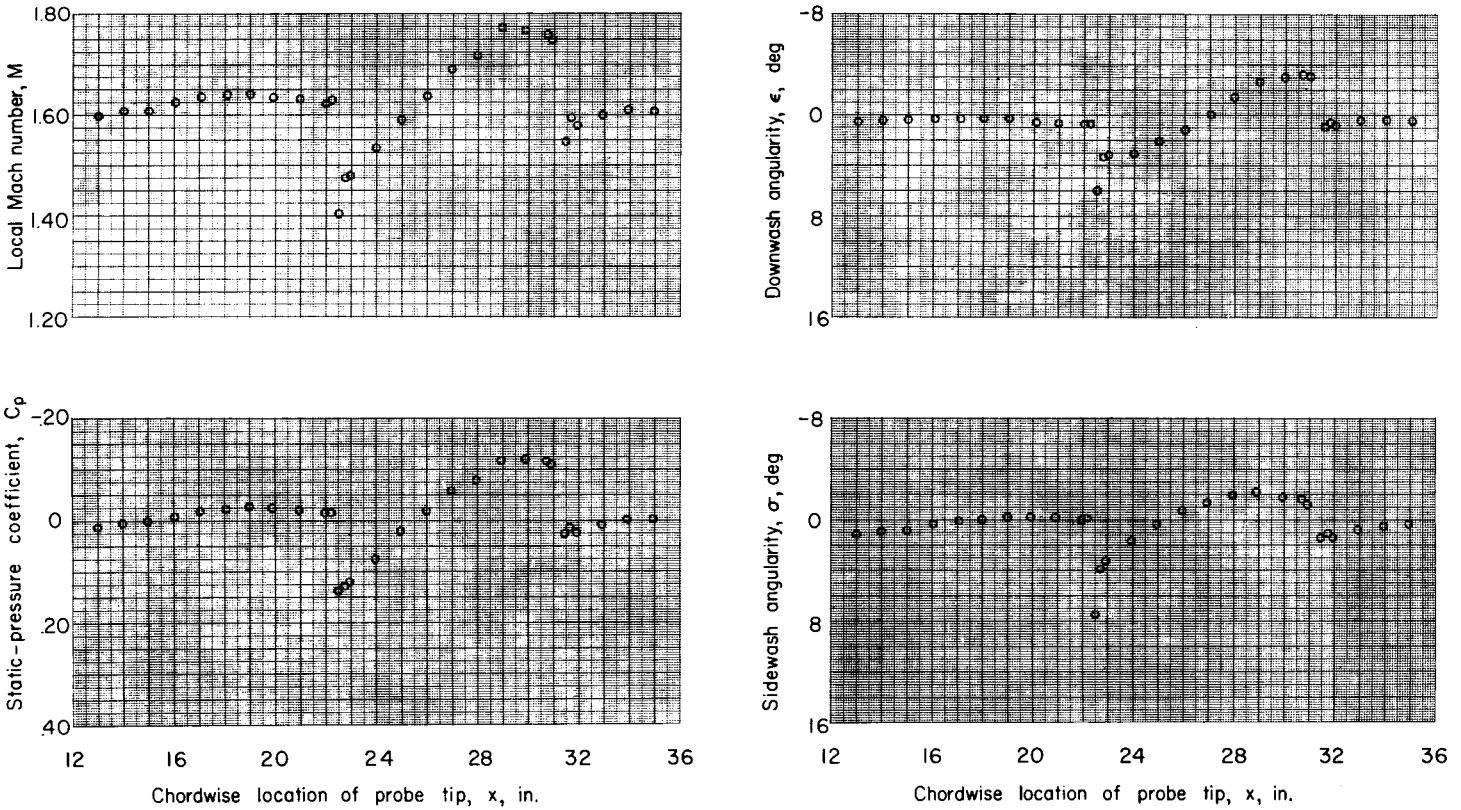

(e) y = 6.6 in.; z = 2.1 in.

Figure 4.- Continued.

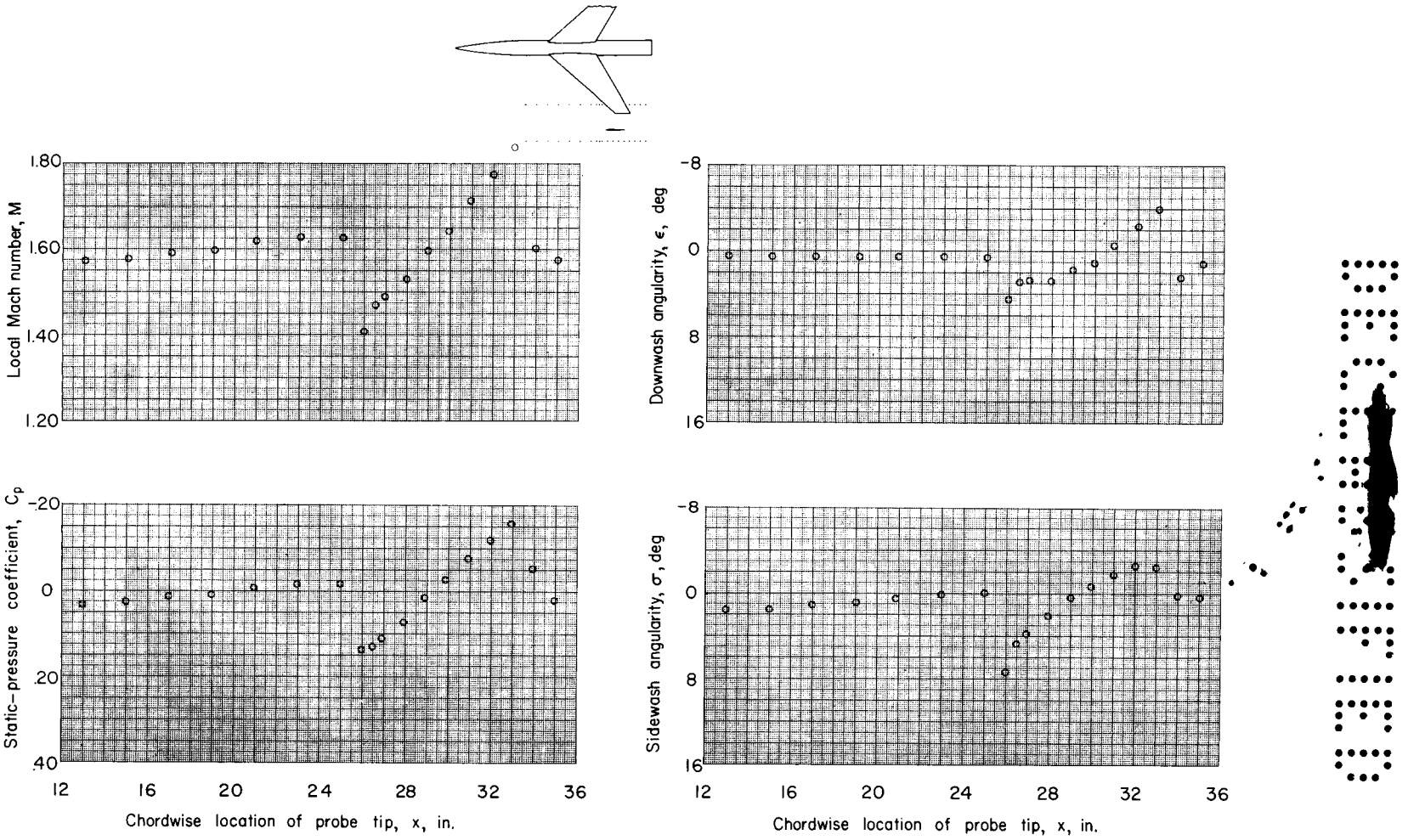

(f) y = 10.2 in.; z = 2.1 in.

Figure 4.- Continued.

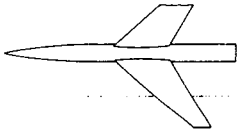

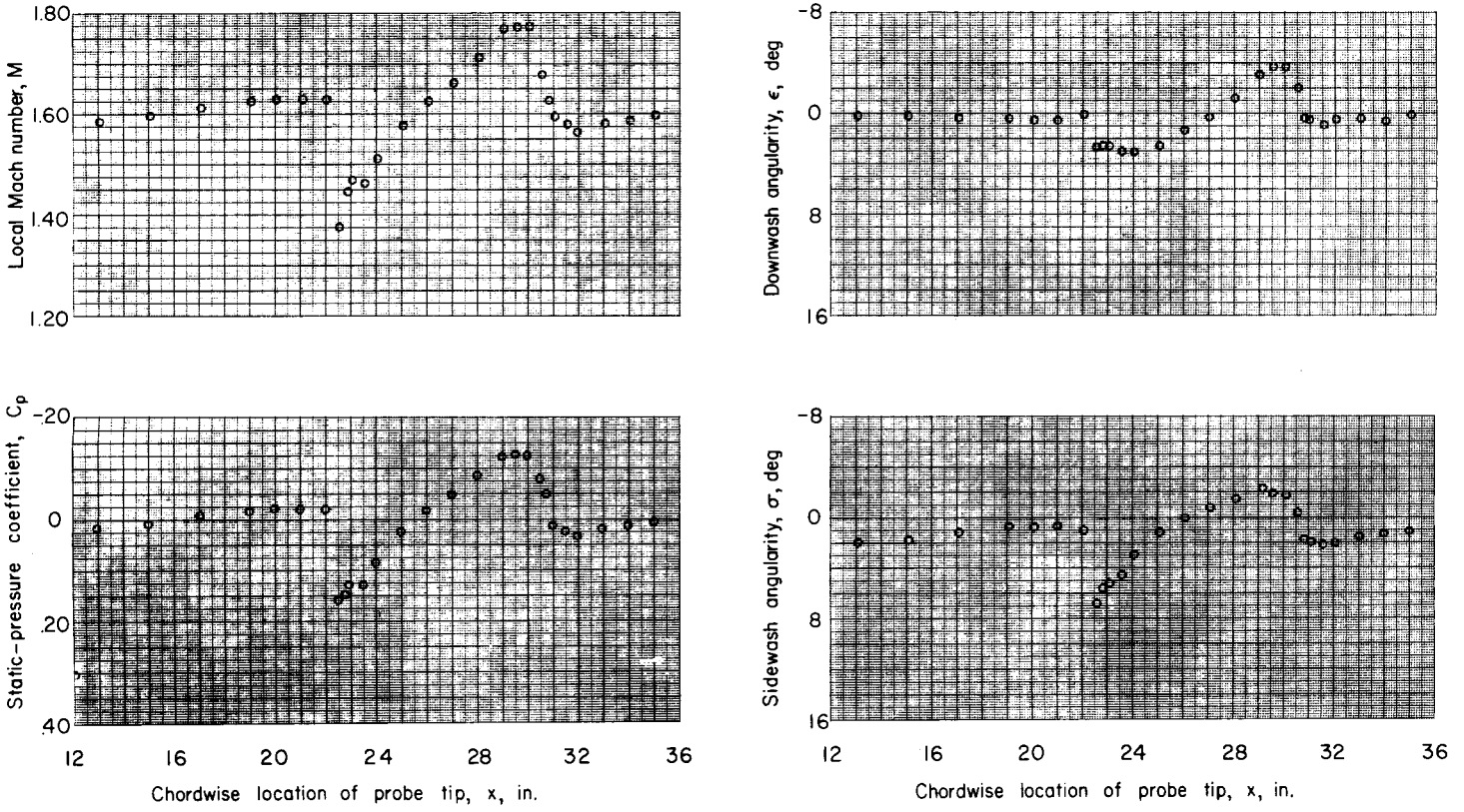

(g) y = 6.6 in.; z = 1.50 in.

Figure 4.- Continued.

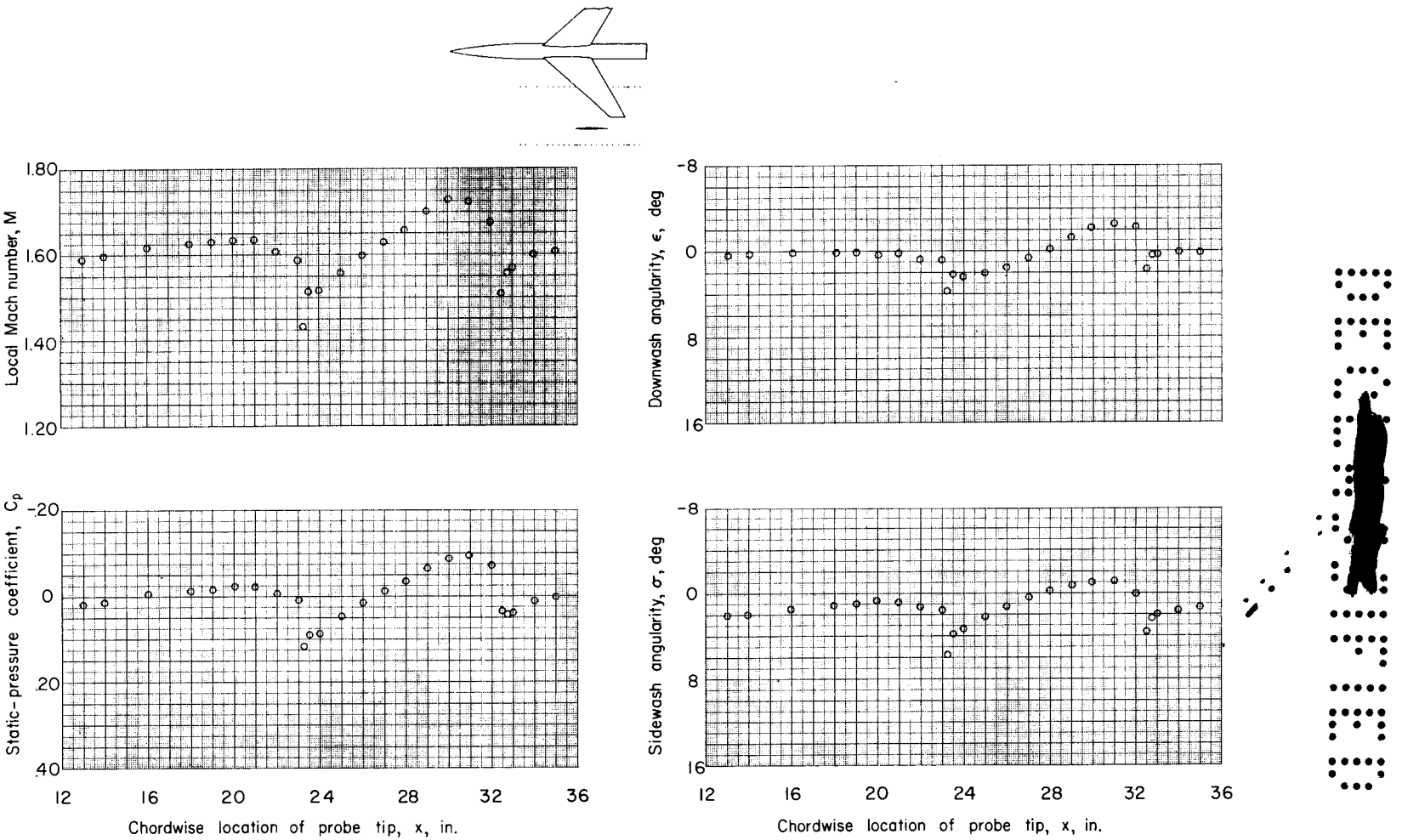

(h) y = 6.6 in.; z = 3.0 in.

Figure 4.- Continued.

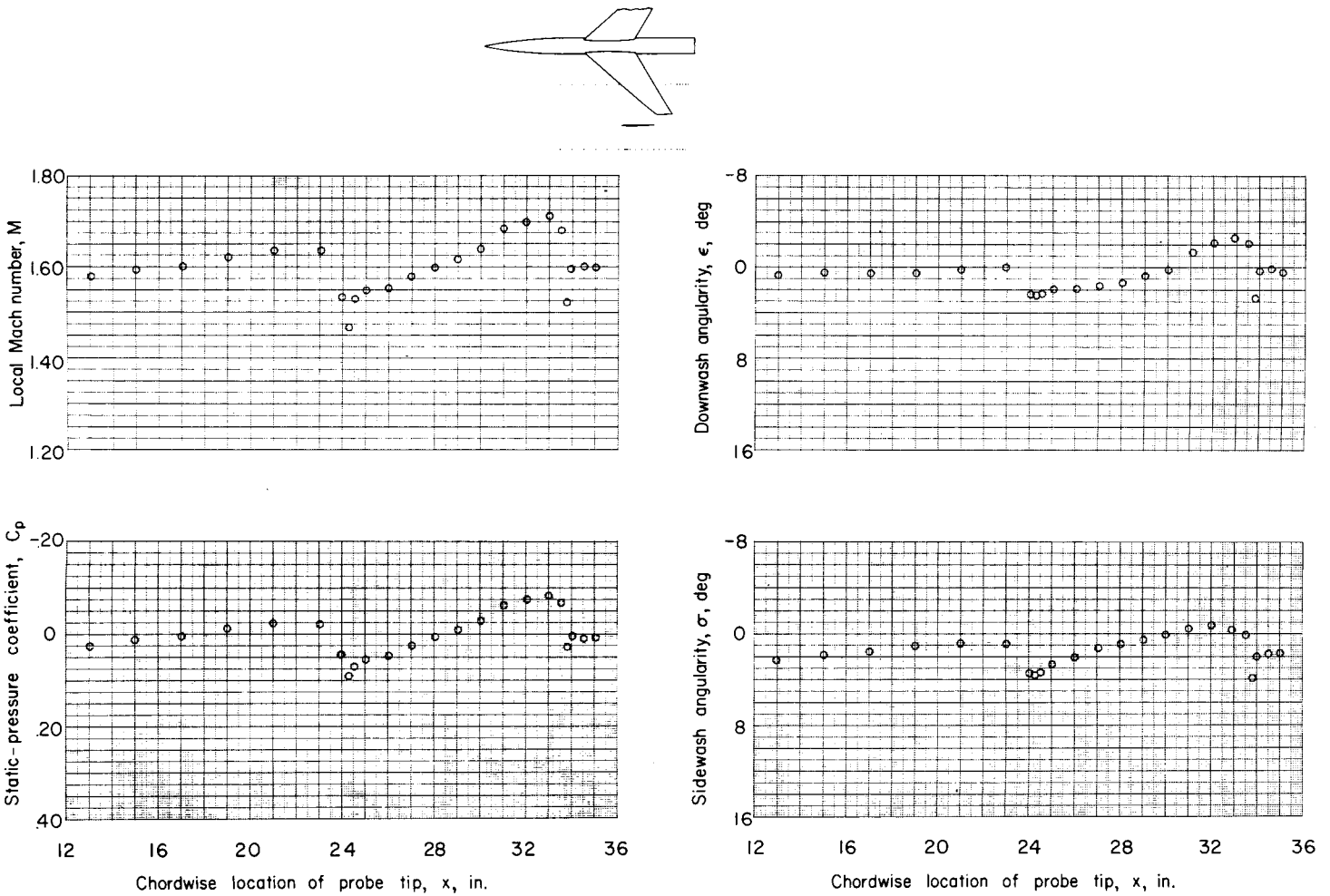

(i) y = 6.6 in.; z = 4.2 in.

Figure 4.- Concluded.

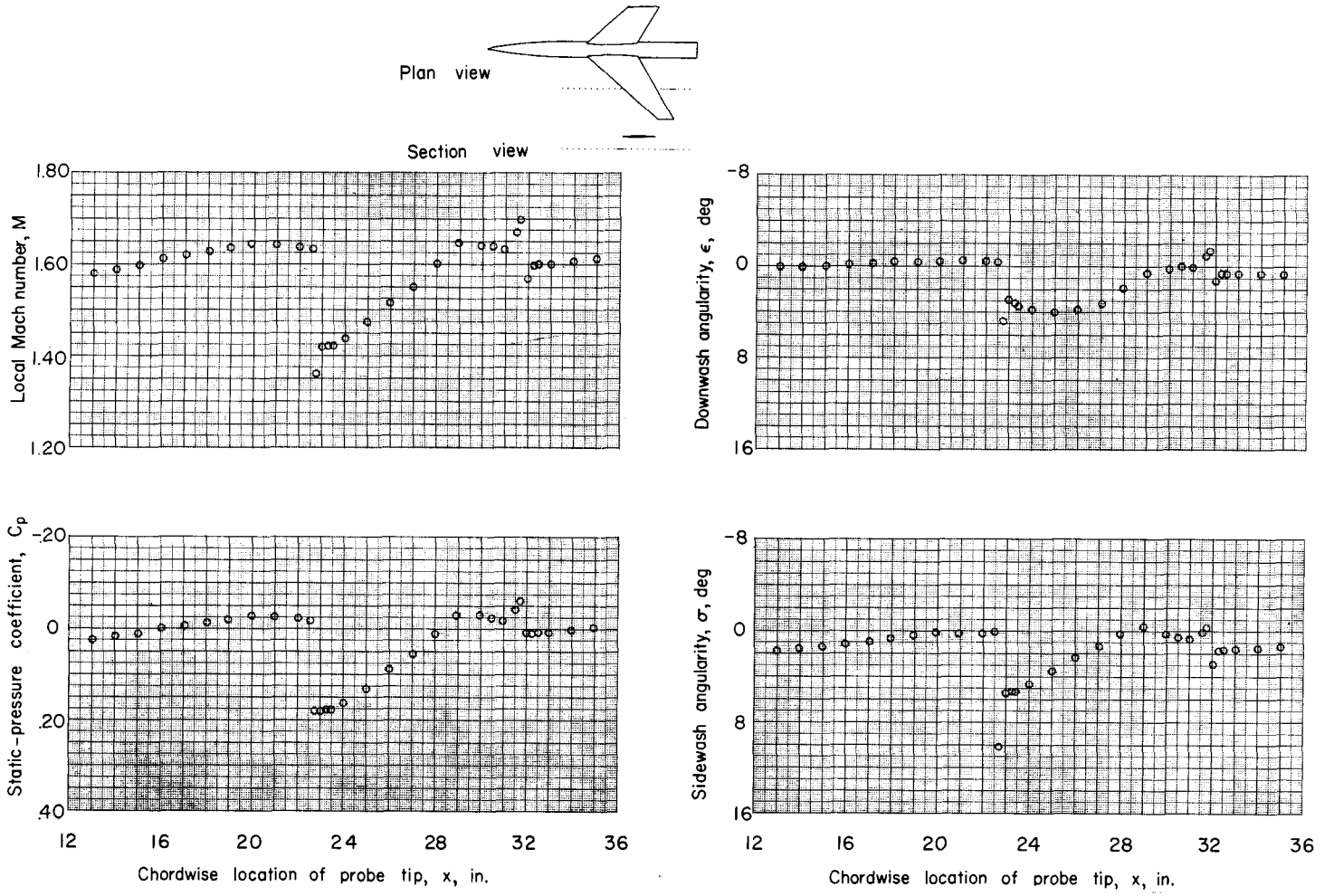

Figure 5.- Flow properties measured in the vicinity of a swept-wing—fuselage configuration. $\alpha = 4^{\circ}$; $M_{\infty} = 1.61$; $y = 6.6$ in.; $z = 2.1$ in.

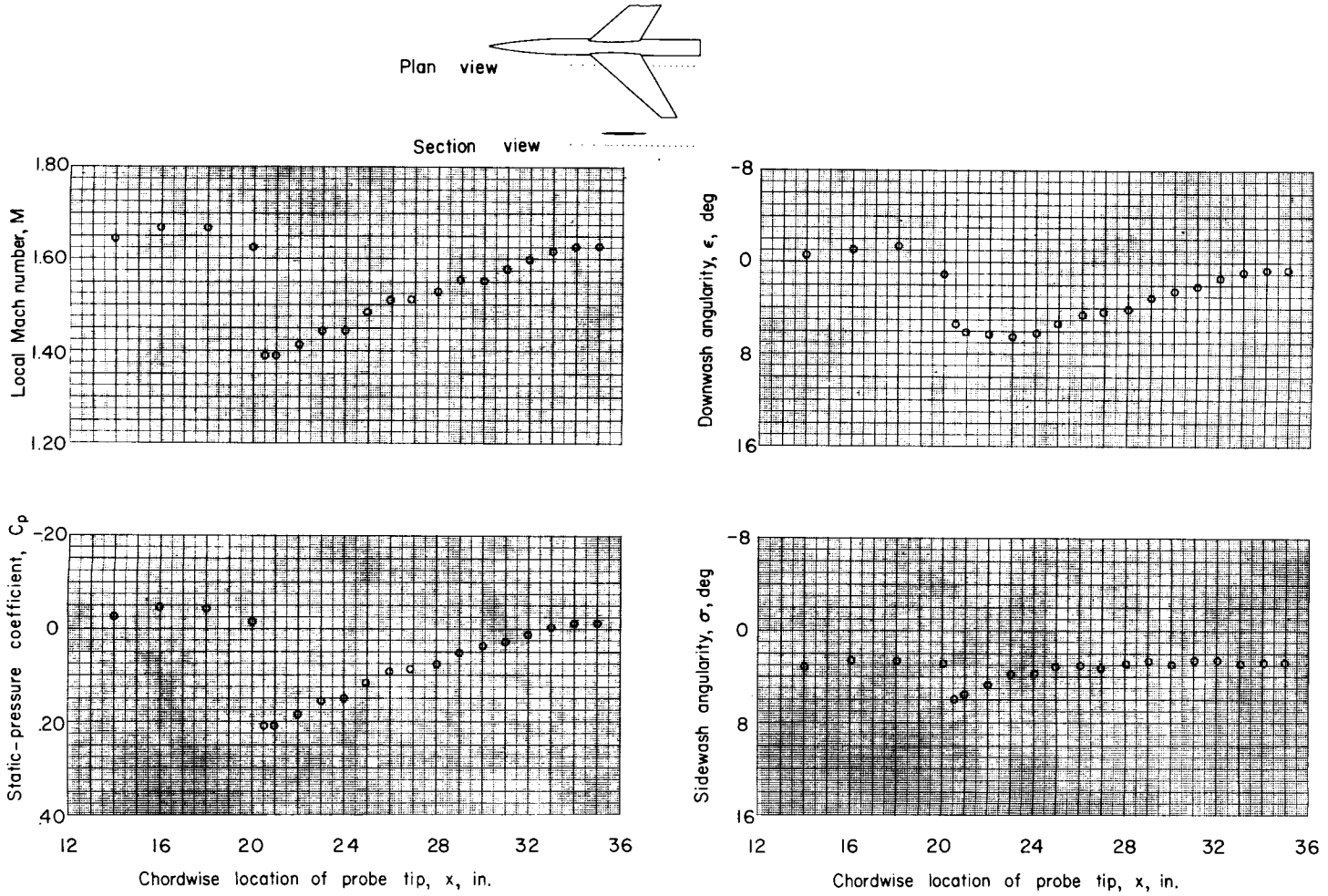

(a) y = 3.0 in.; z = 2.1 in.

Figure 6.- Flow properties measured in the vicinity of a swept-wing—fuselage configuration. $\alpha = 8^{\circ}$; $M_{\infty} = 1.61$.

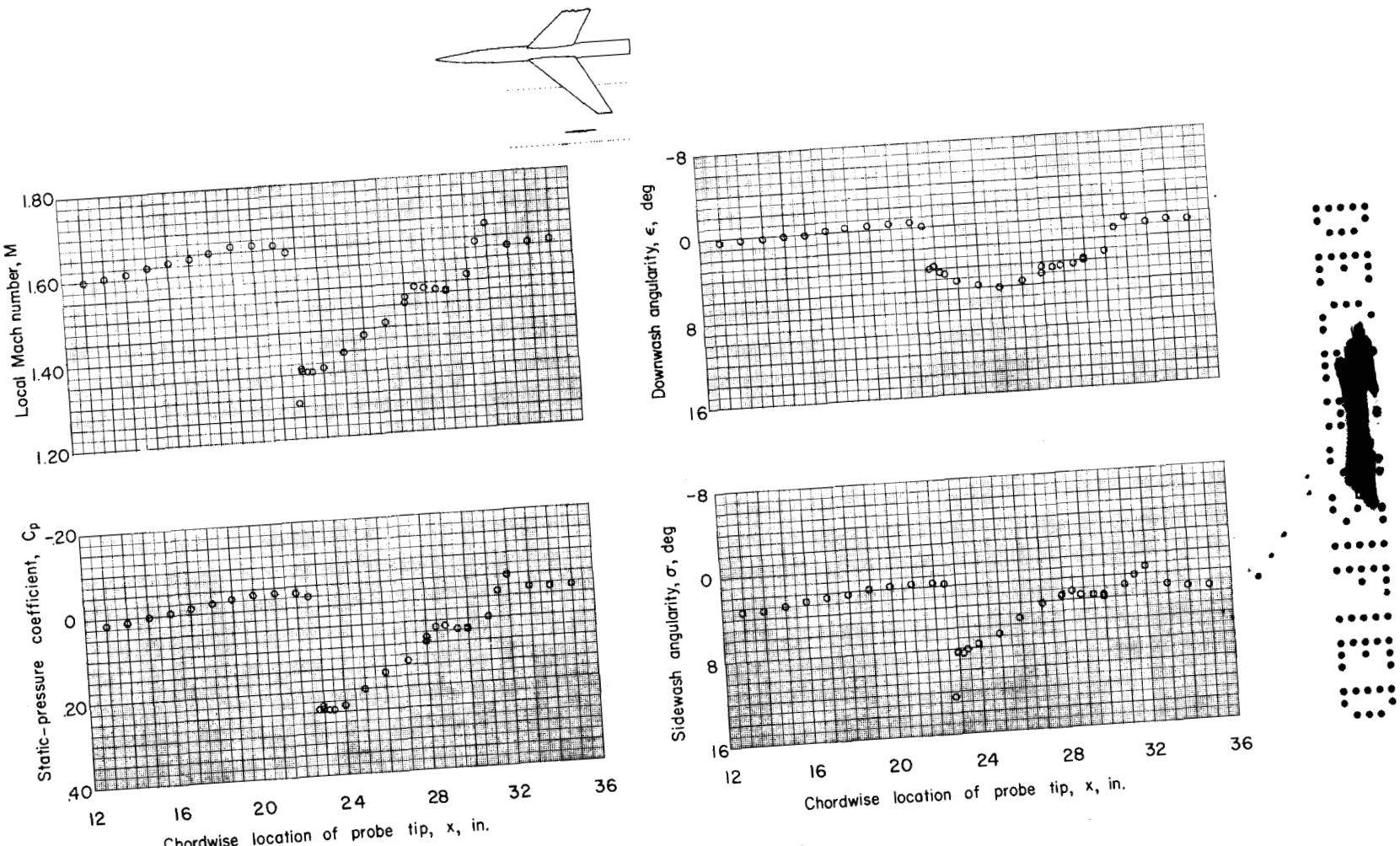

(b) y = 6.6 in.; z = 2.1 in.

Figure 6.- Continued.

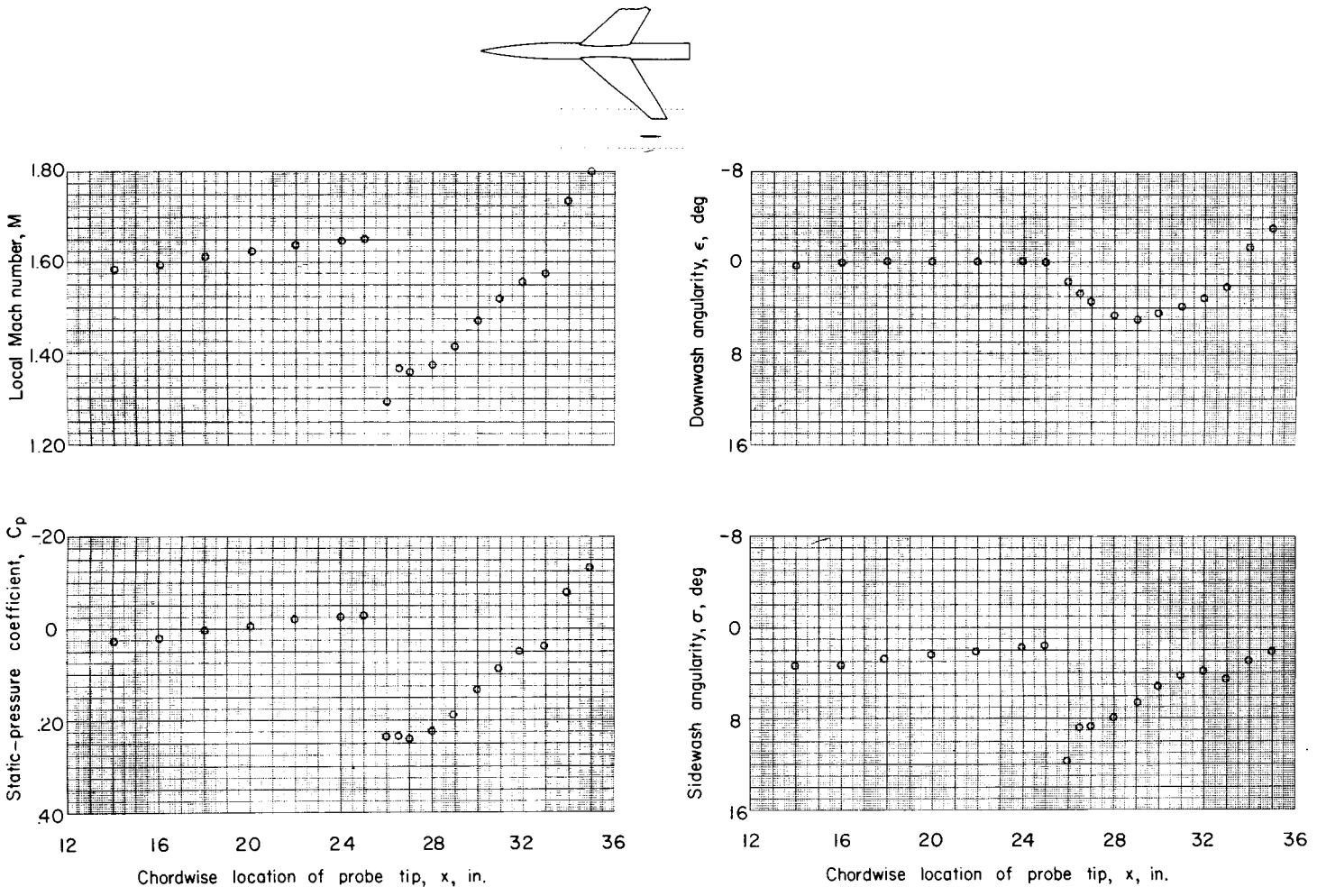

(c) y = 10.2 in.; z = 2.1 in.

Figure 6.- Concluded.

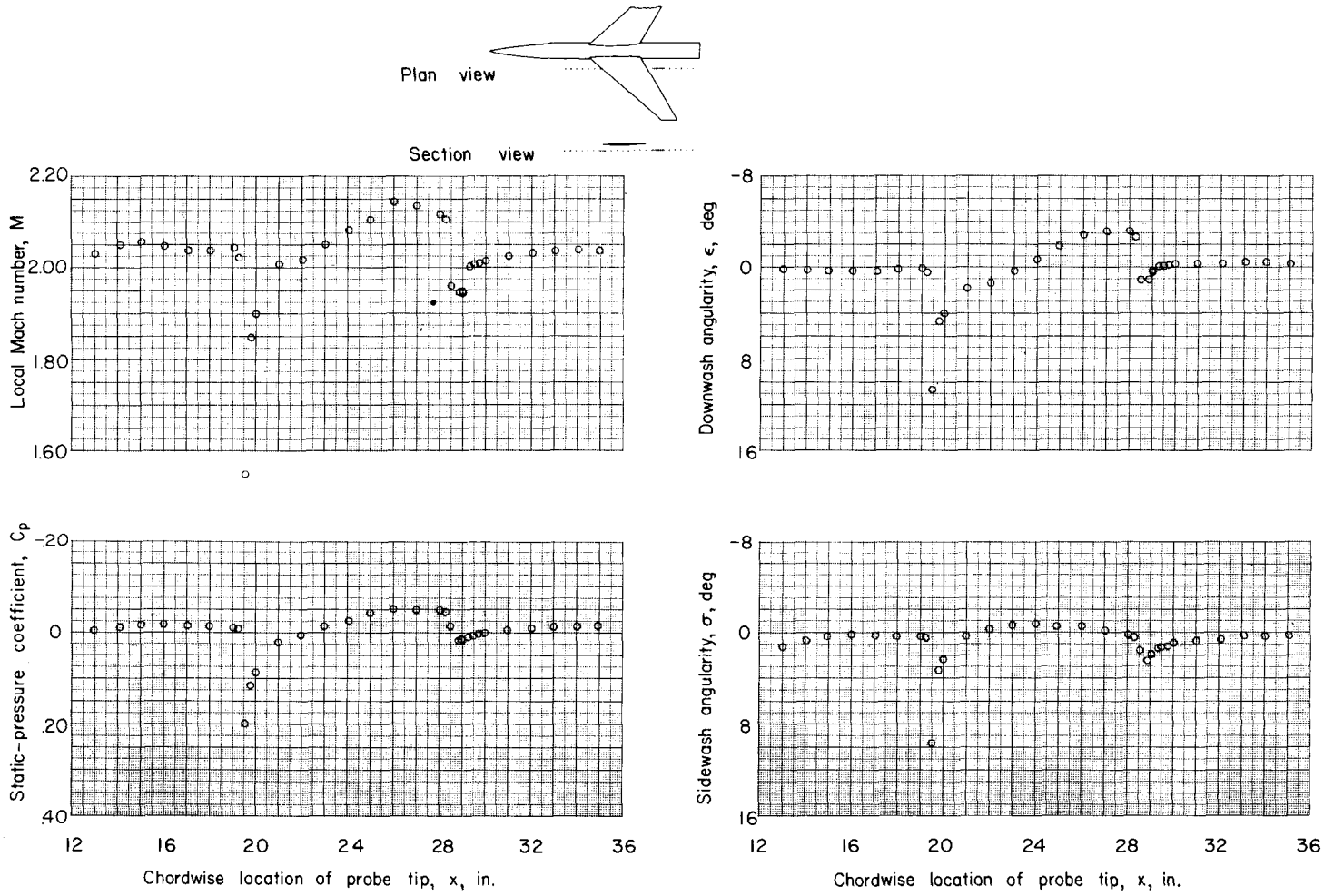

(a) y = 3.0 in.; z = 1.15 in.

Figure 7.- Flow properties measured in the vicinity of a swept-wing—fuselage configuration. $\alpha = 0^{\circ}$; $M_{\infty} = 2.01$.

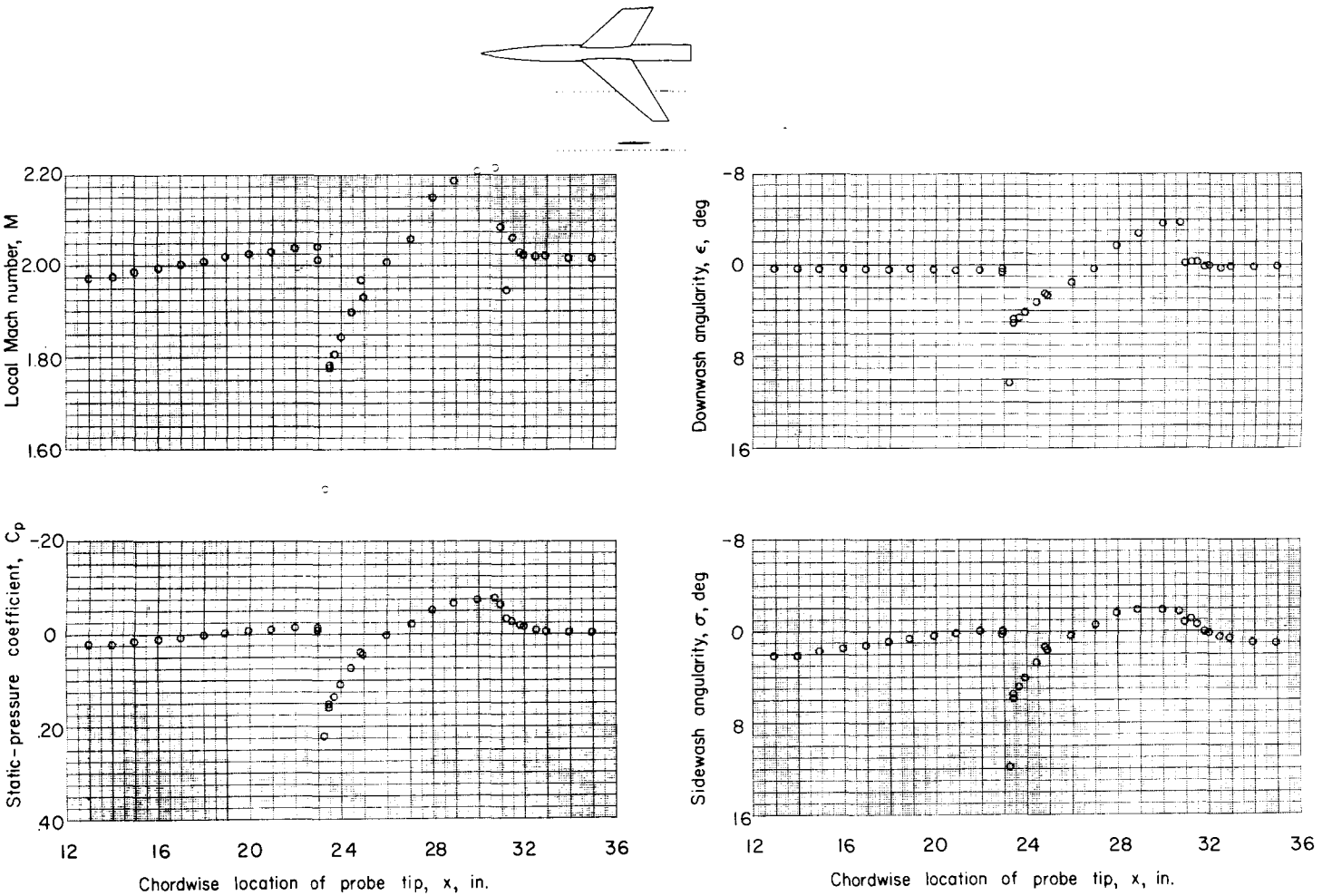

(b) y = 6.6 in.; z = 1.15 in.

Figure 7.- Continued.

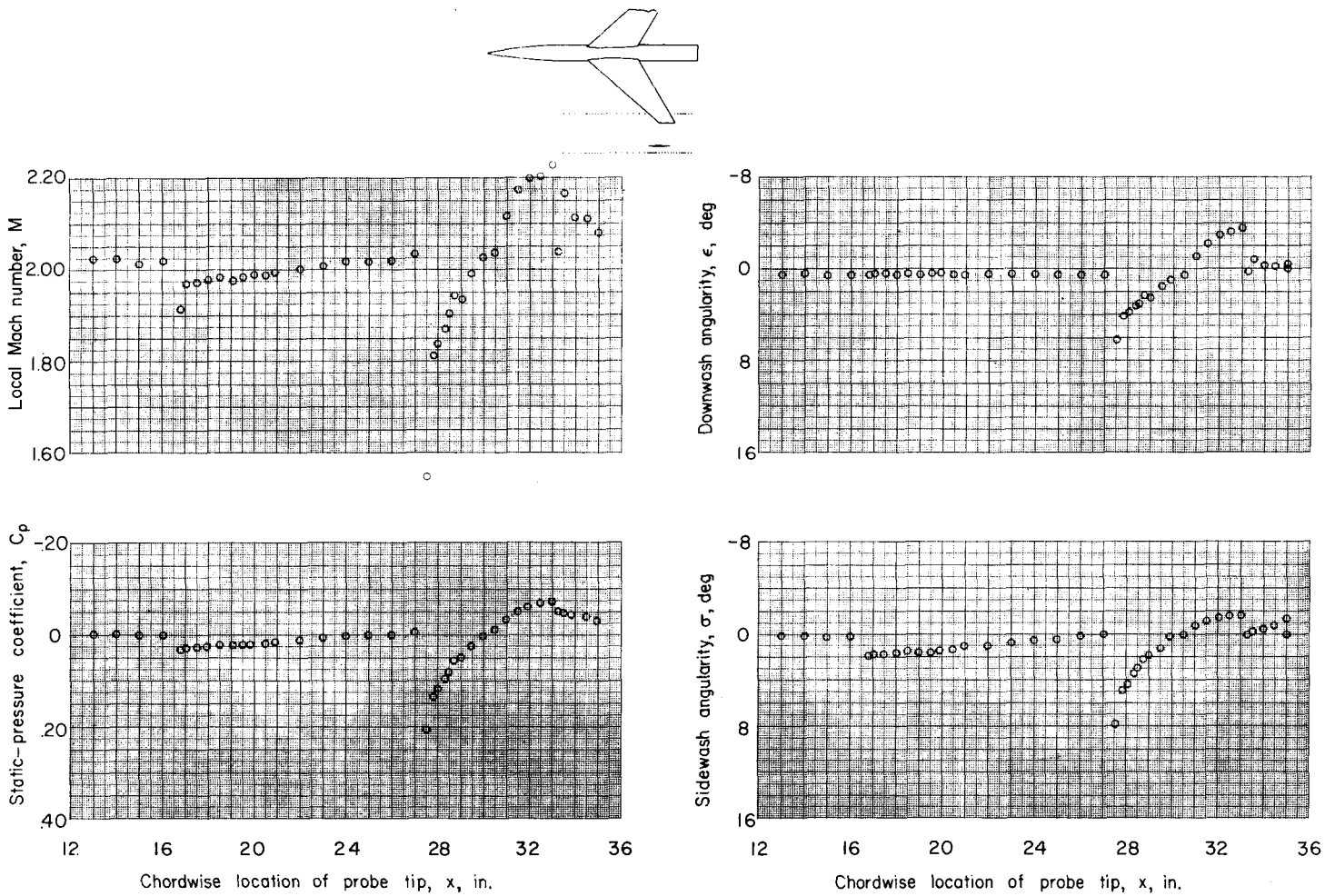

(c) y = 10.2 in.; z = 1.15 in.

Figure 7.- Concluded.

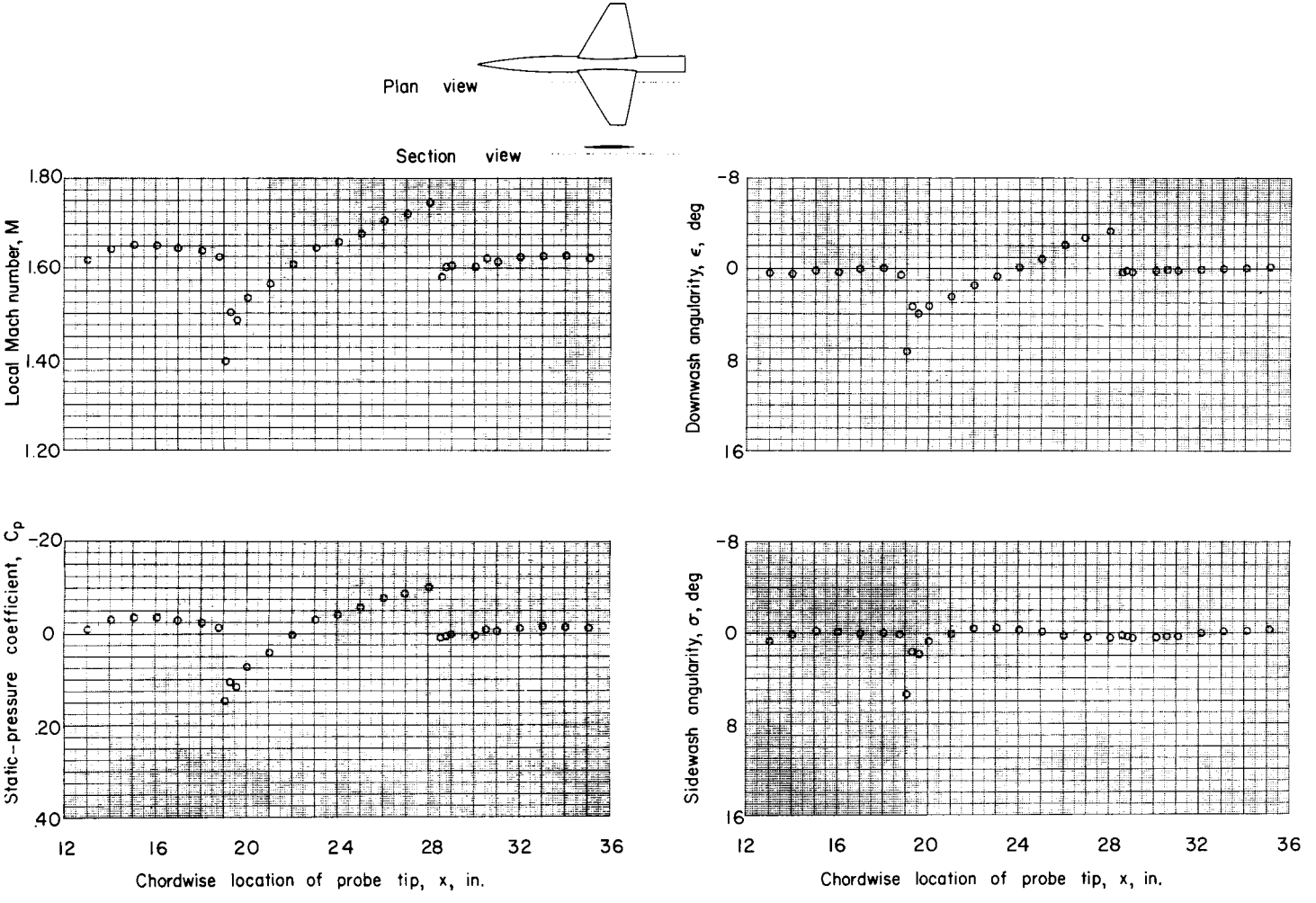

(a) y = 3.0 in.; z = 1.15 in.

Figure 8.- Flow properties measured in the vicinity of a trapezoidal-wing—fuselage configuration. $\alpha = 0^{\circ}$; $M_{\infty} = 1.61$.

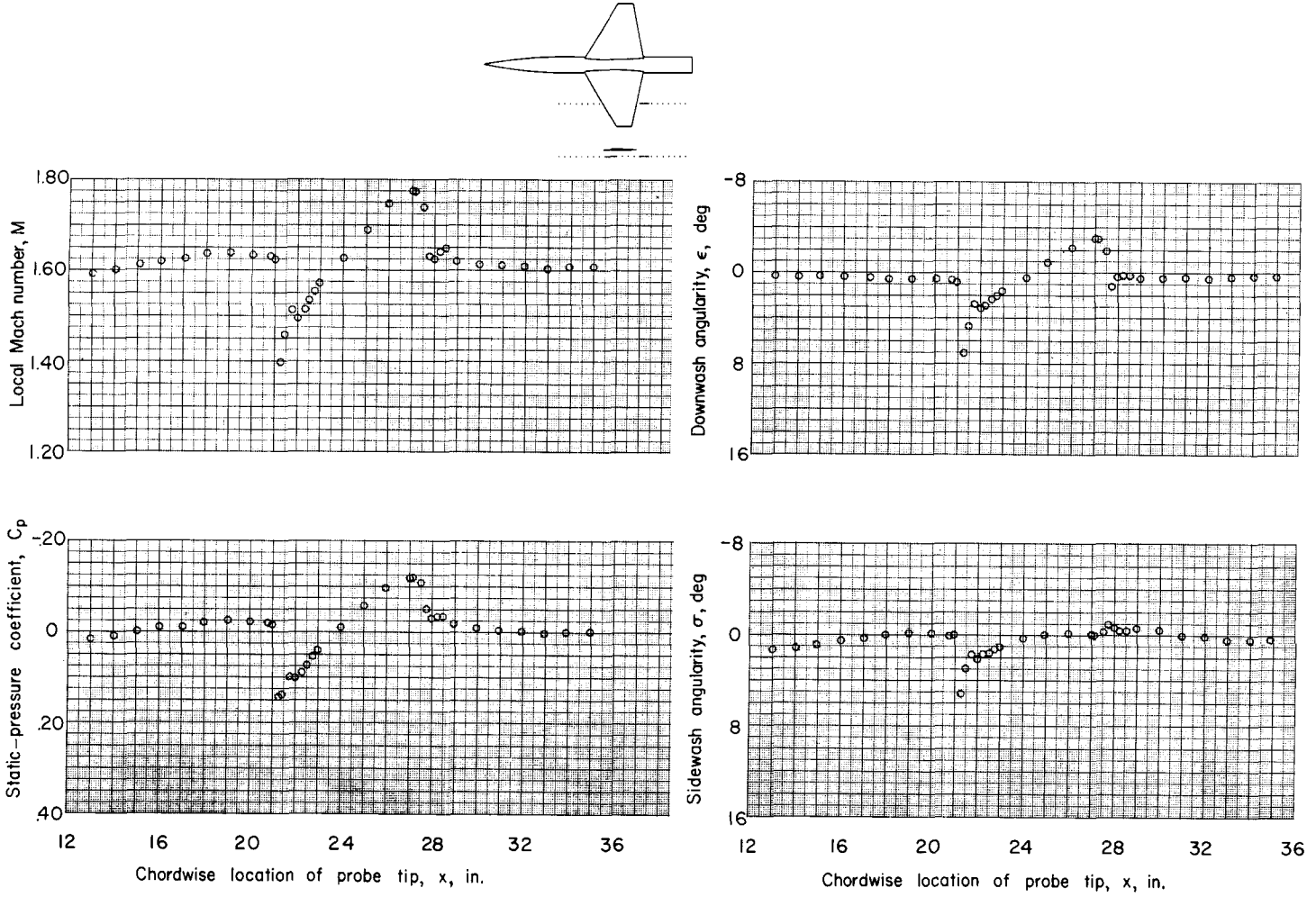

(b) y = 6.6 in.; z = 1.15 in.

Figure 8.- Continued.

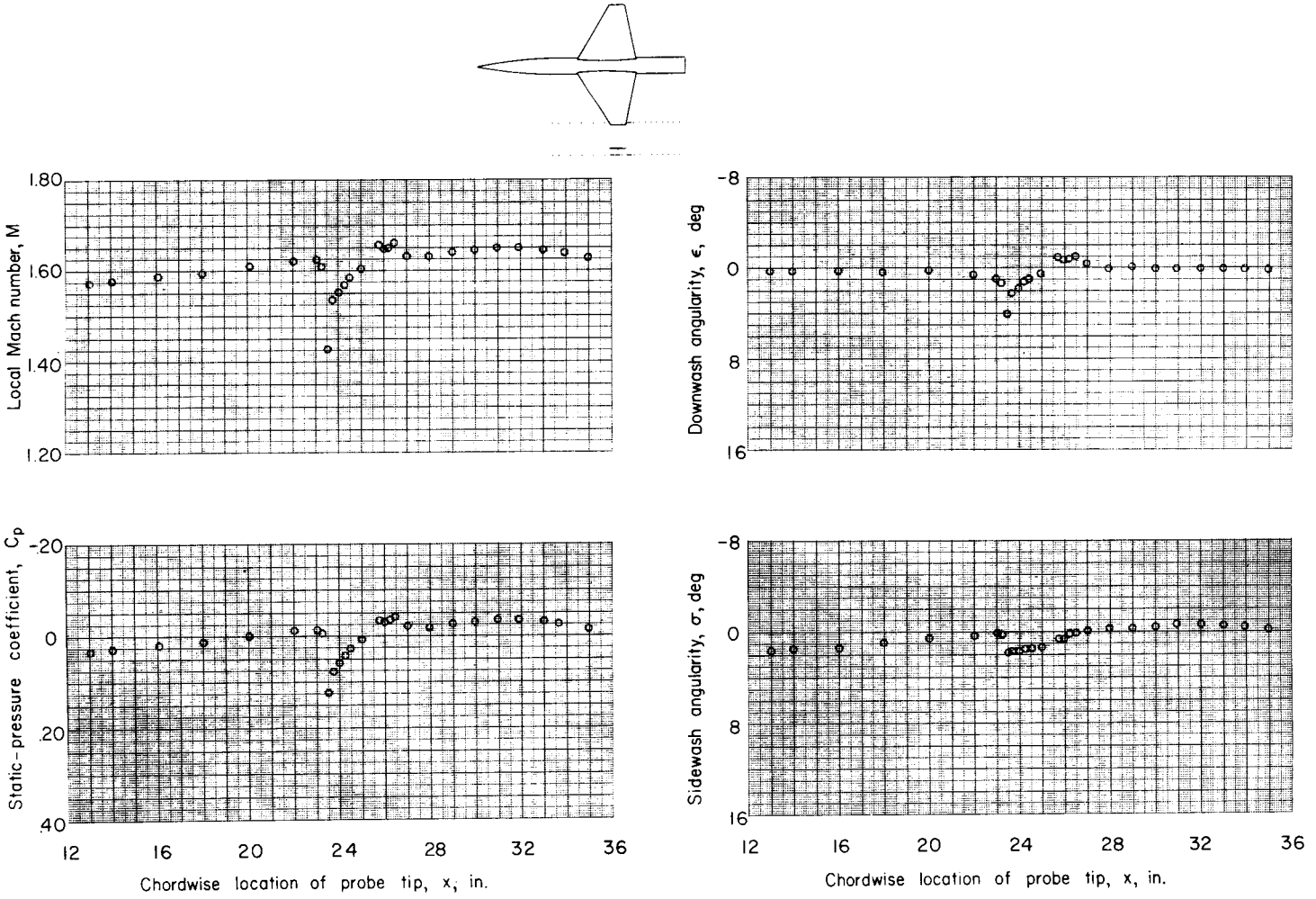

(c) y = 10.2 in.; z = 1.15 in.

Figure 8.- Continued.

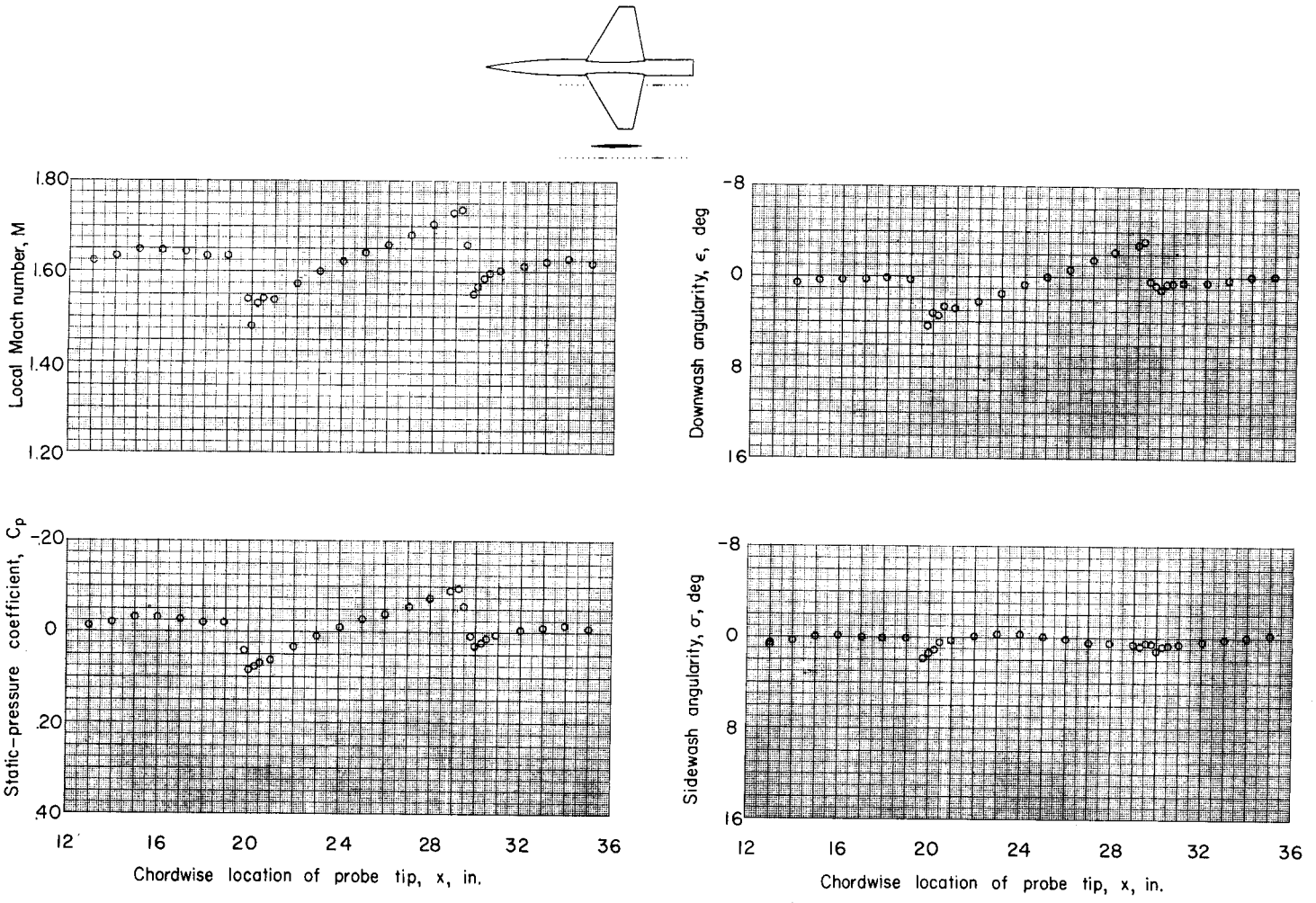

(d) y = 3.0 in.; z = 2.1 in.

Figure 8.- Continued.

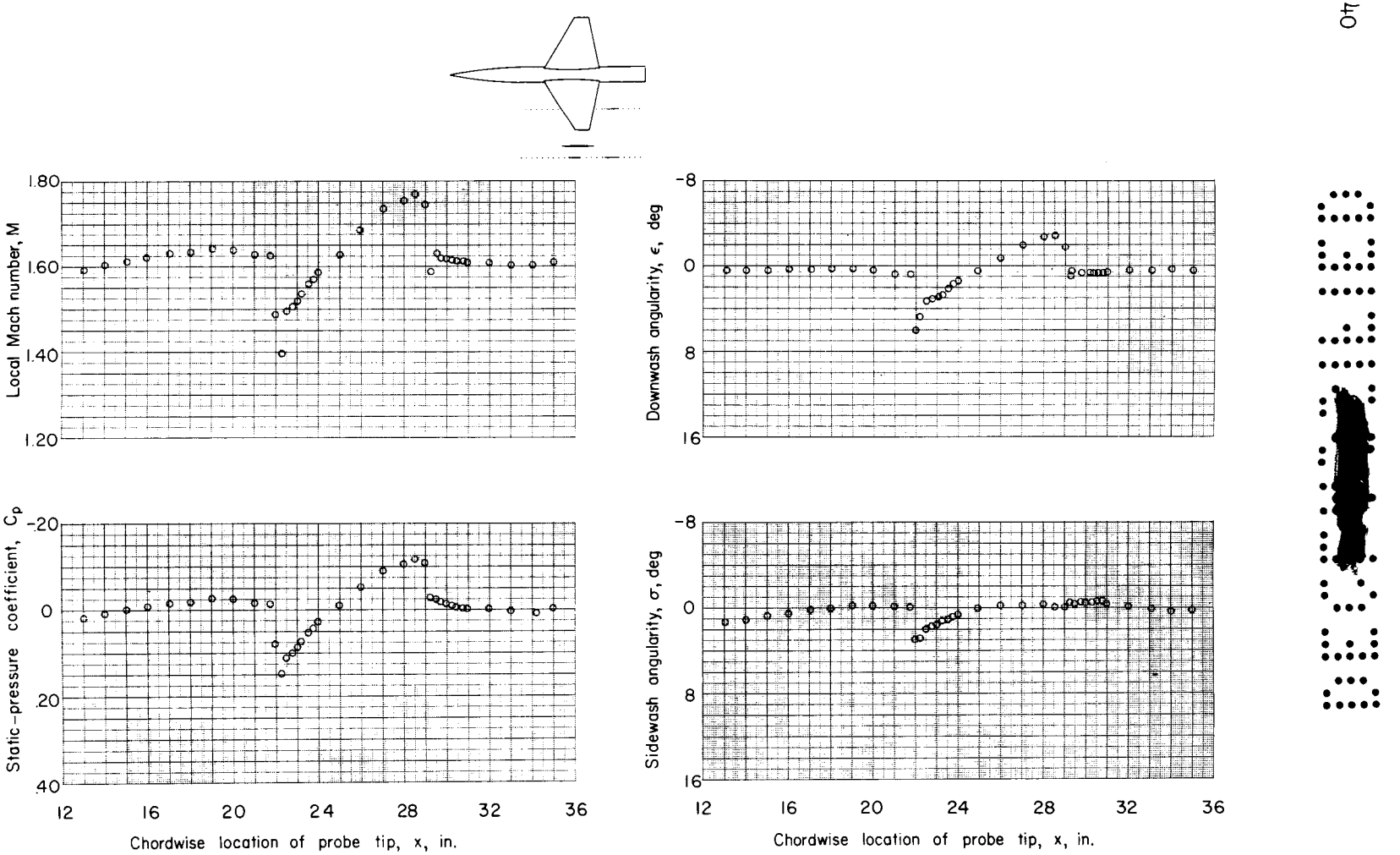

(e) y = 6.6 in.; z = 2.1 in.

Figure 8.- Continued.

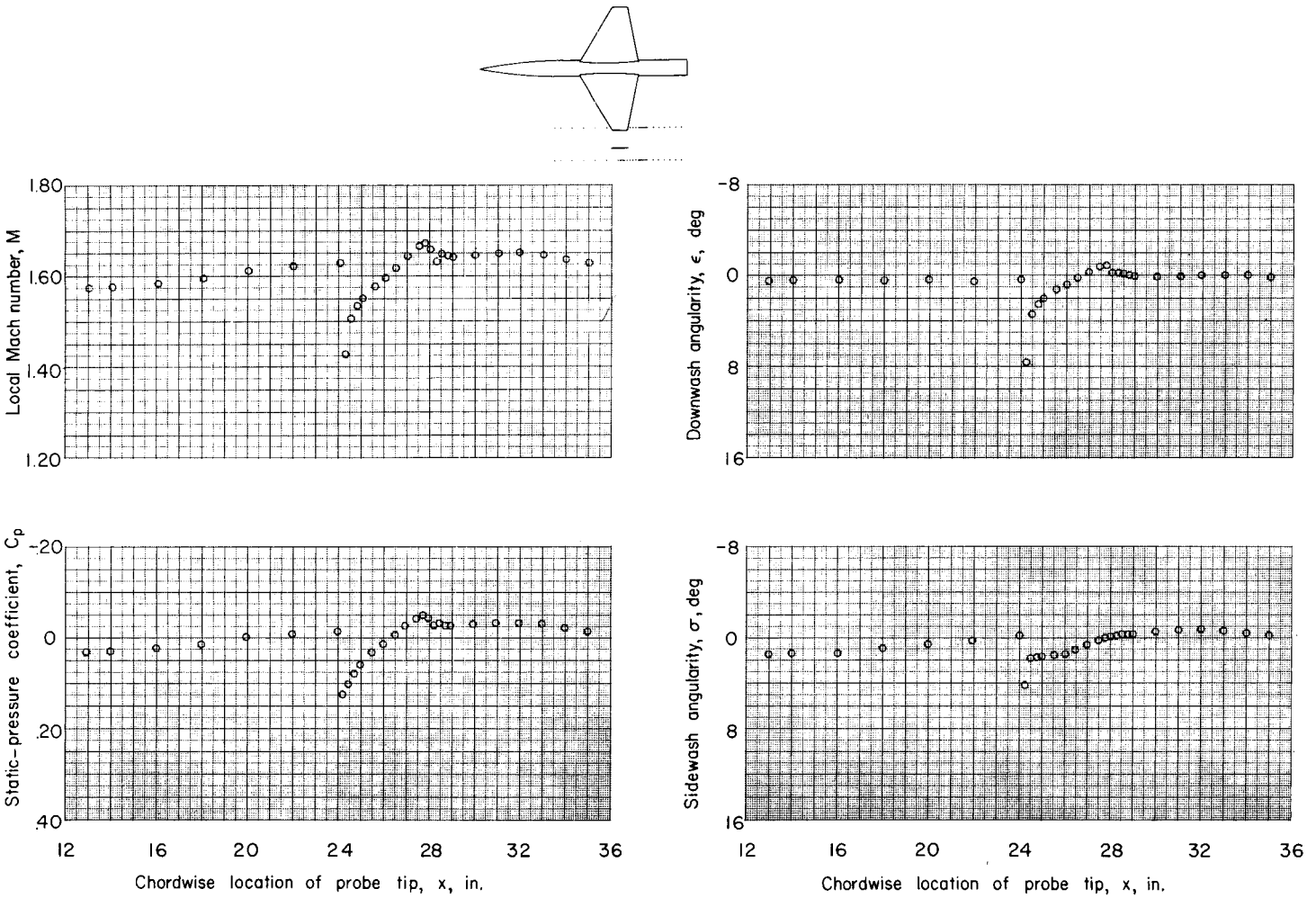

(f) y = 10.2 in.; z = 2.1 in.

Figure 8.- Concluded.

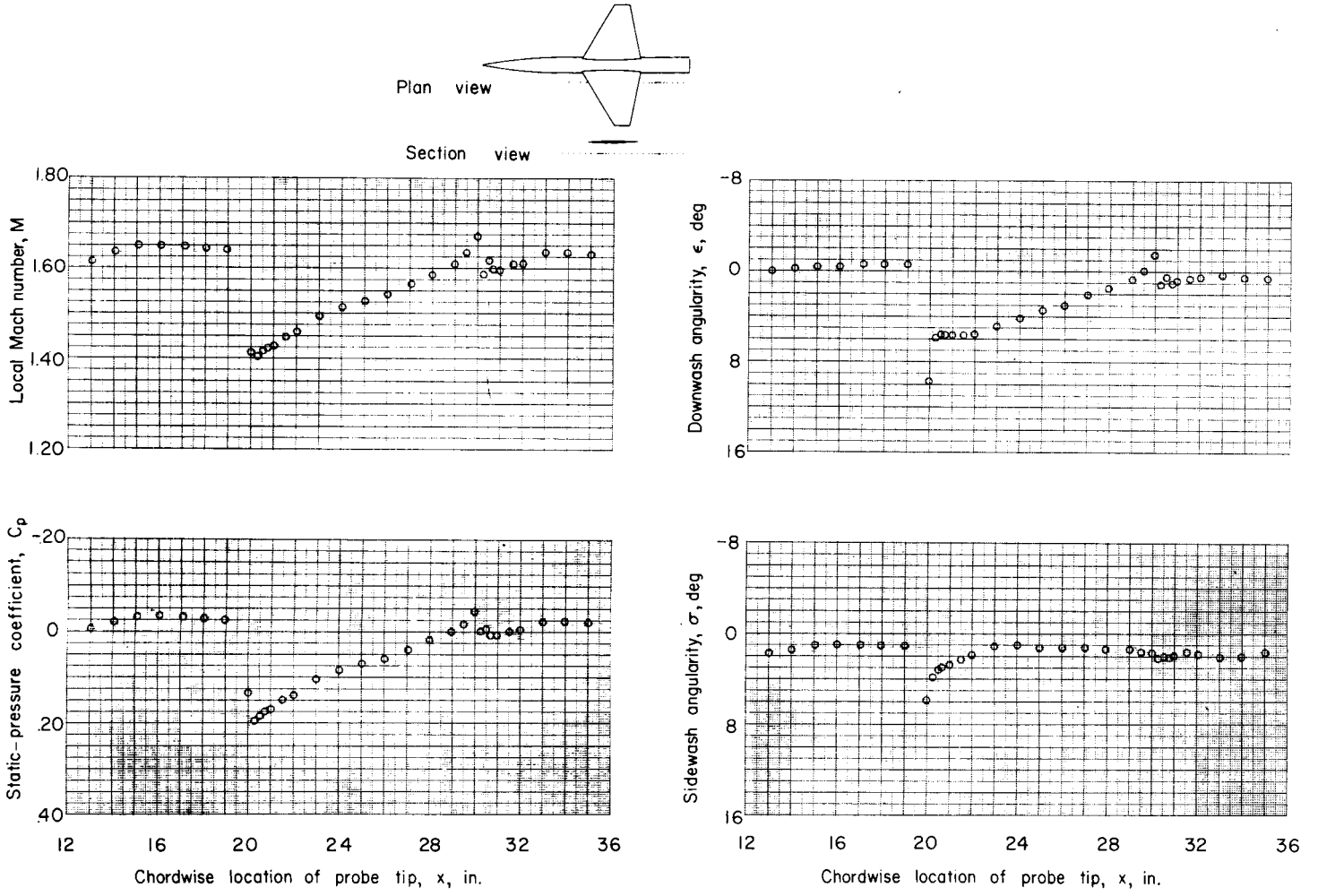

(a) y = 3.0 in.; z = 2.1 in.

Figure 9.- Flow properties measured in the vicinity of a trapezoidal-wing—fuselage configuration. $\alpha = 4^{\circ}$; $M_{\infty} = 1.61$.

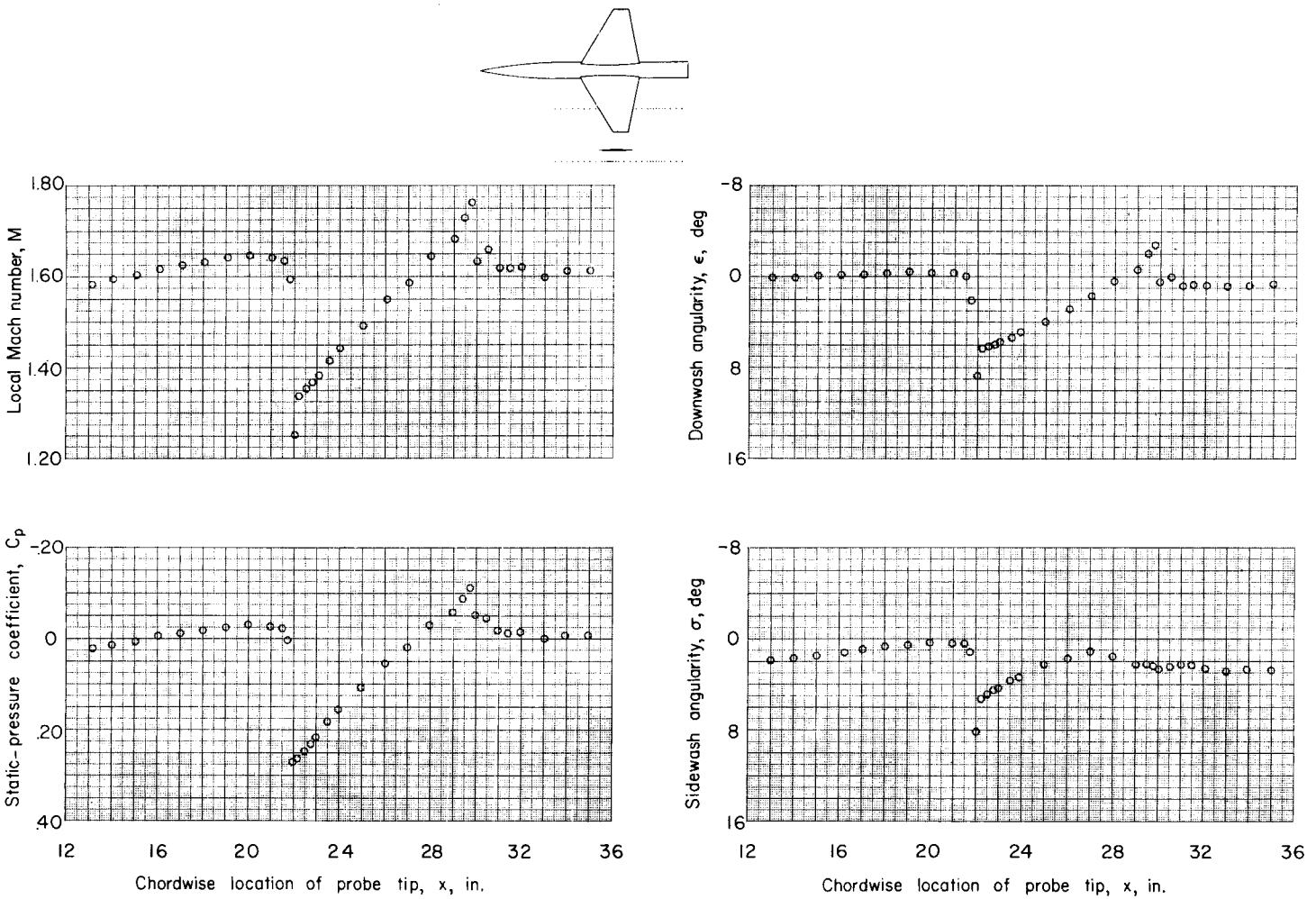

(b) y = 6.6 in.; z = 2.1 in.

Figure 9.- Continued.

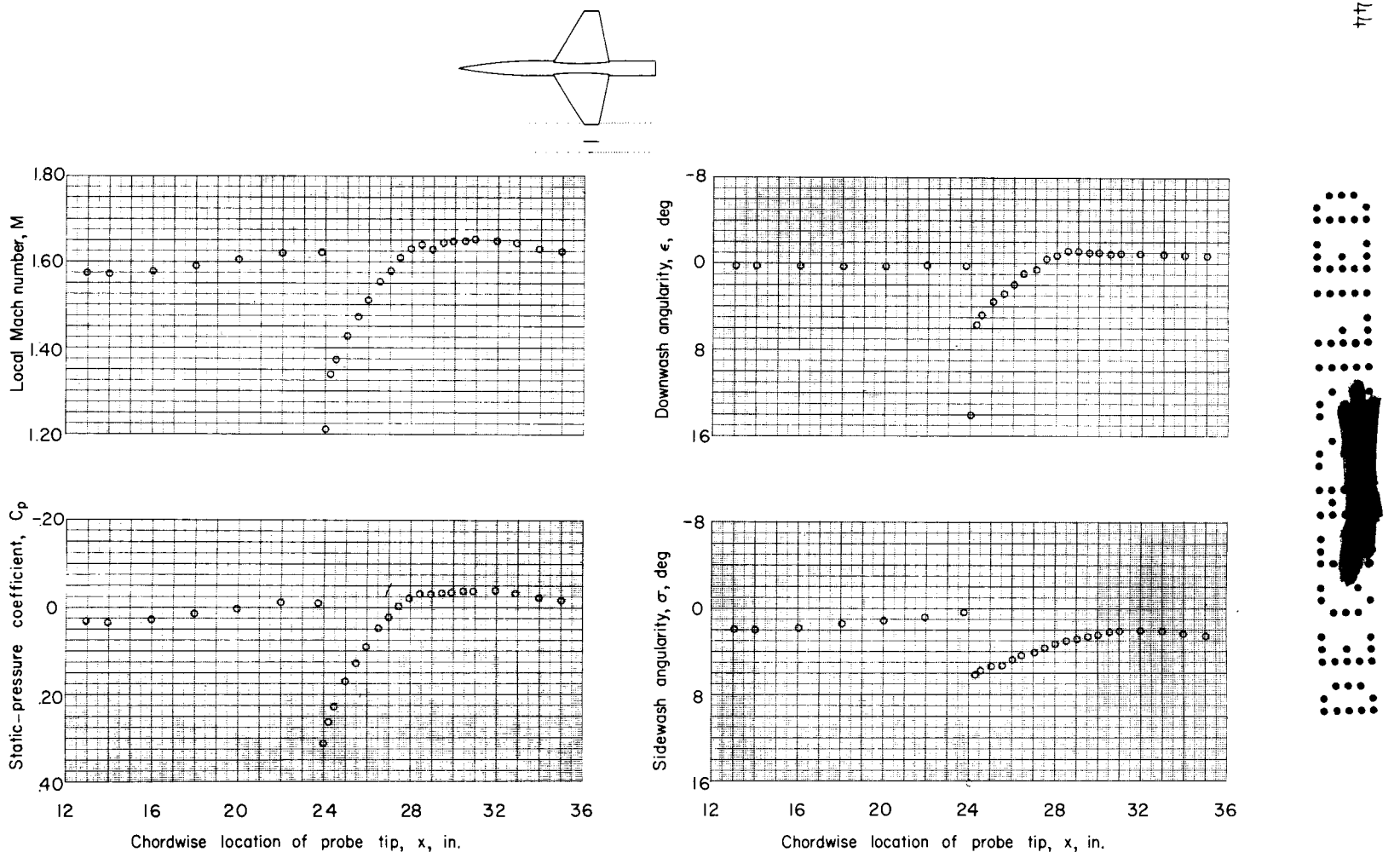

(c) y = 10.2 in.; z = 2.1 in.

Figure 9.- Concluded.

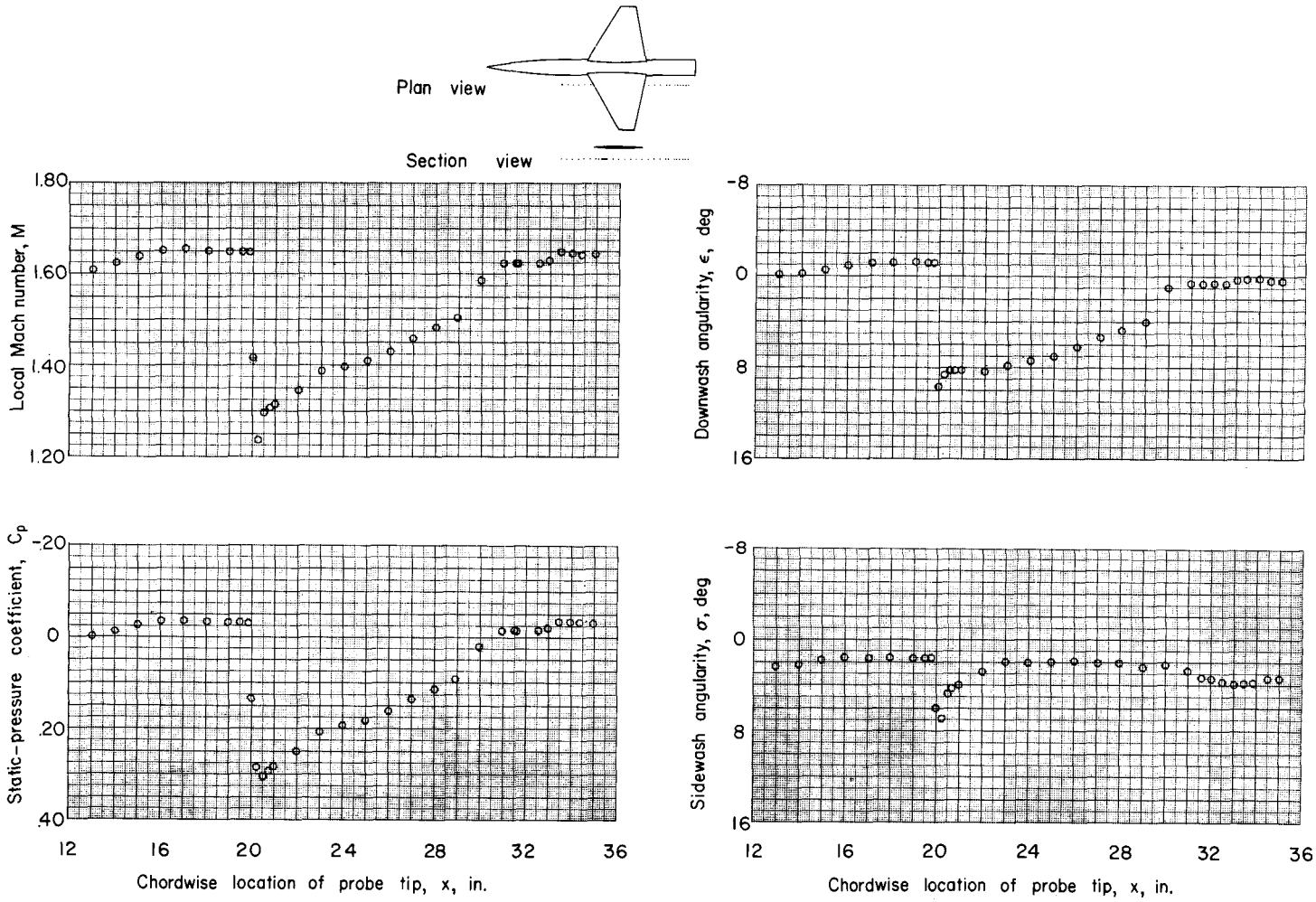

(a) y = 3.0 in.; z = 2.1 in.

Figure 10.- Flow properties measured in the vicinity of a trapezoidal-wing—fuselage configuration. $\alpha = 8^{\circ}$; $M_{\infty} = 1.61$.

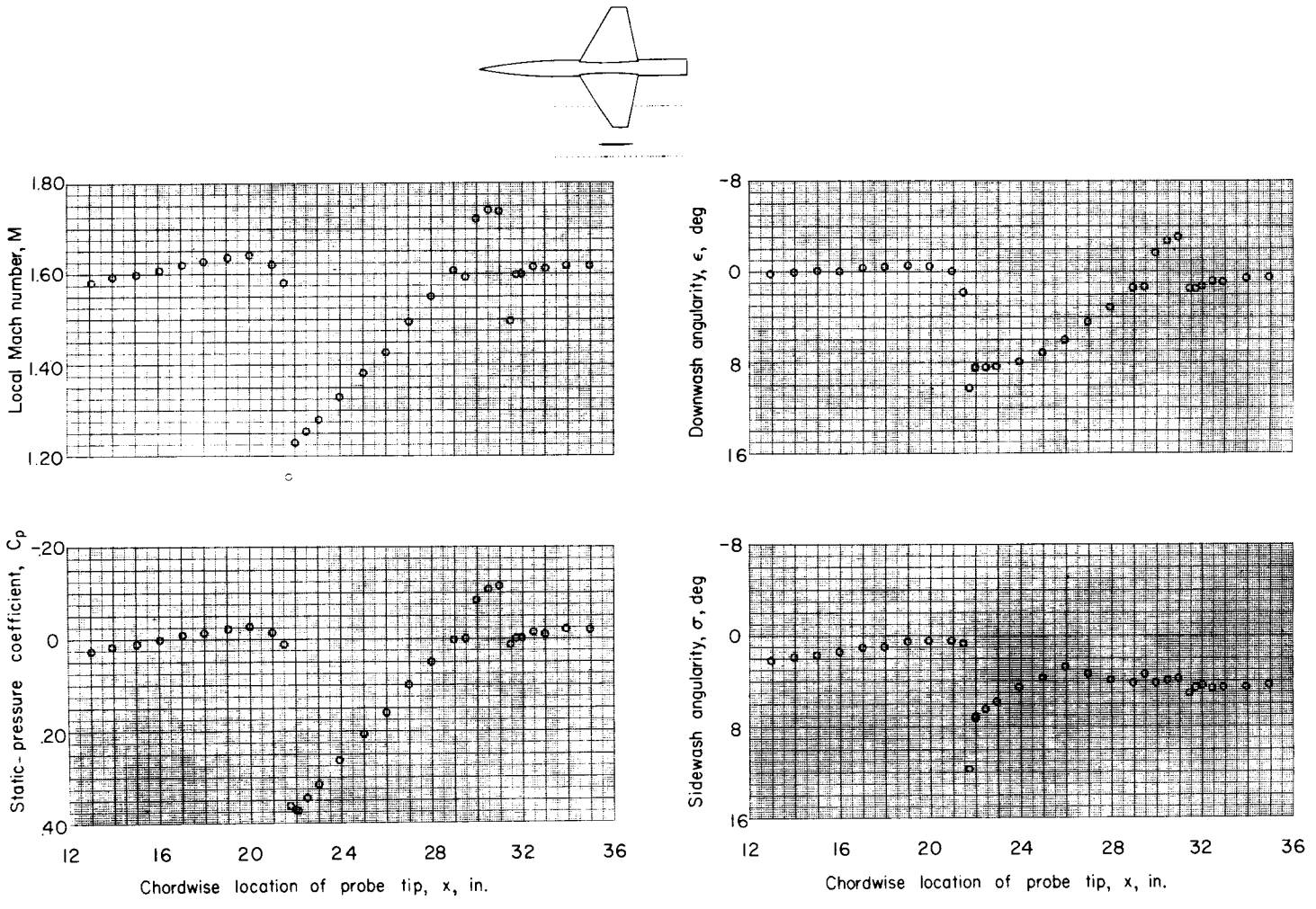

(b) y = 6.6 in.; z = 2.1 in.

Figure 10.- Continued.

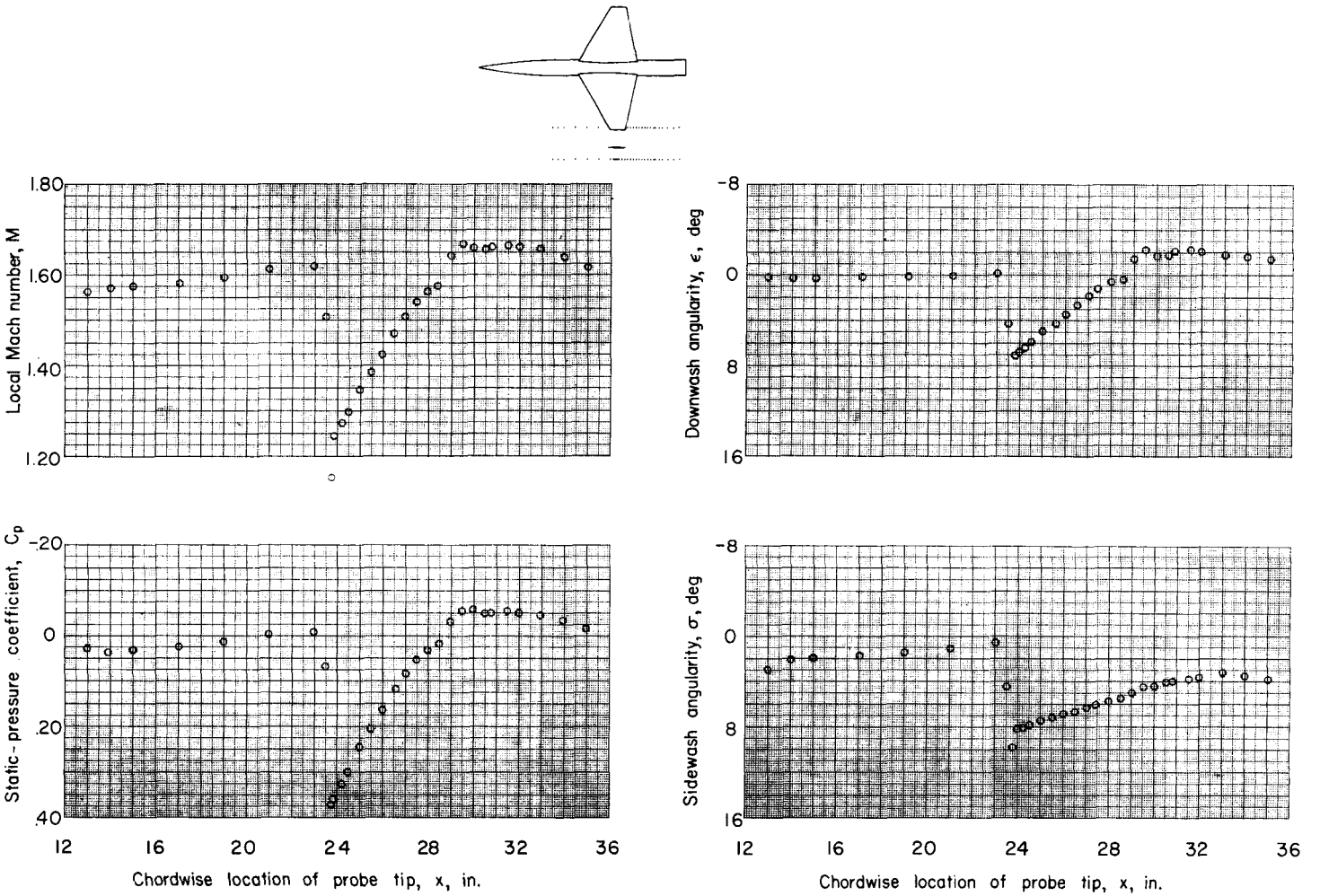

(c) y = 10.2 in.; z = 2.1 in.

Figure 10.- Concluded.

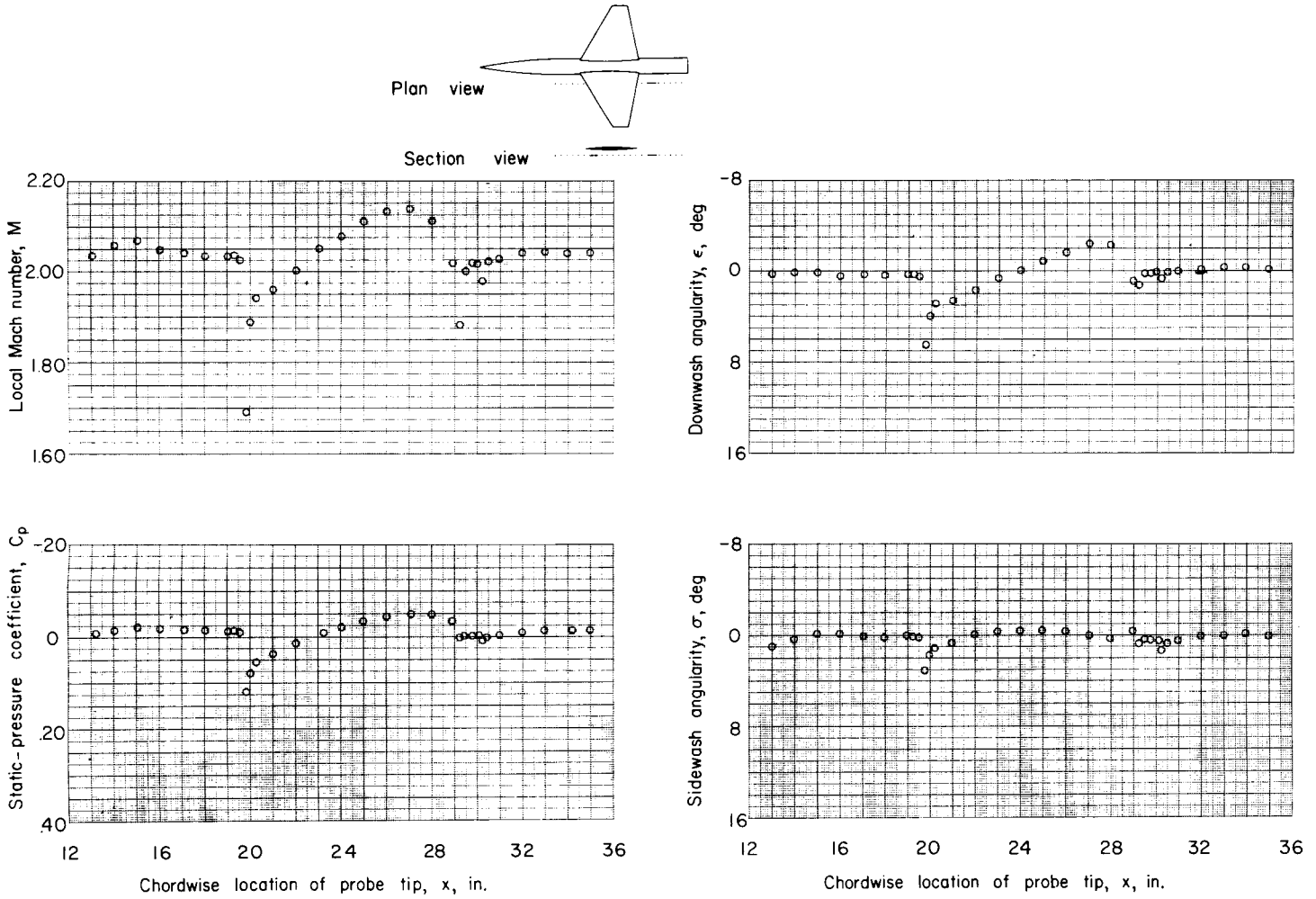

(a) y = 3.0 in.; z = 1.15 in.

Figure 11.- Flow properties measured in the vicinity of a trapezoidal-wing—fuselage configuration. $\alpha = 0^{\circ}$; $M_{\infty} = 2.01$.

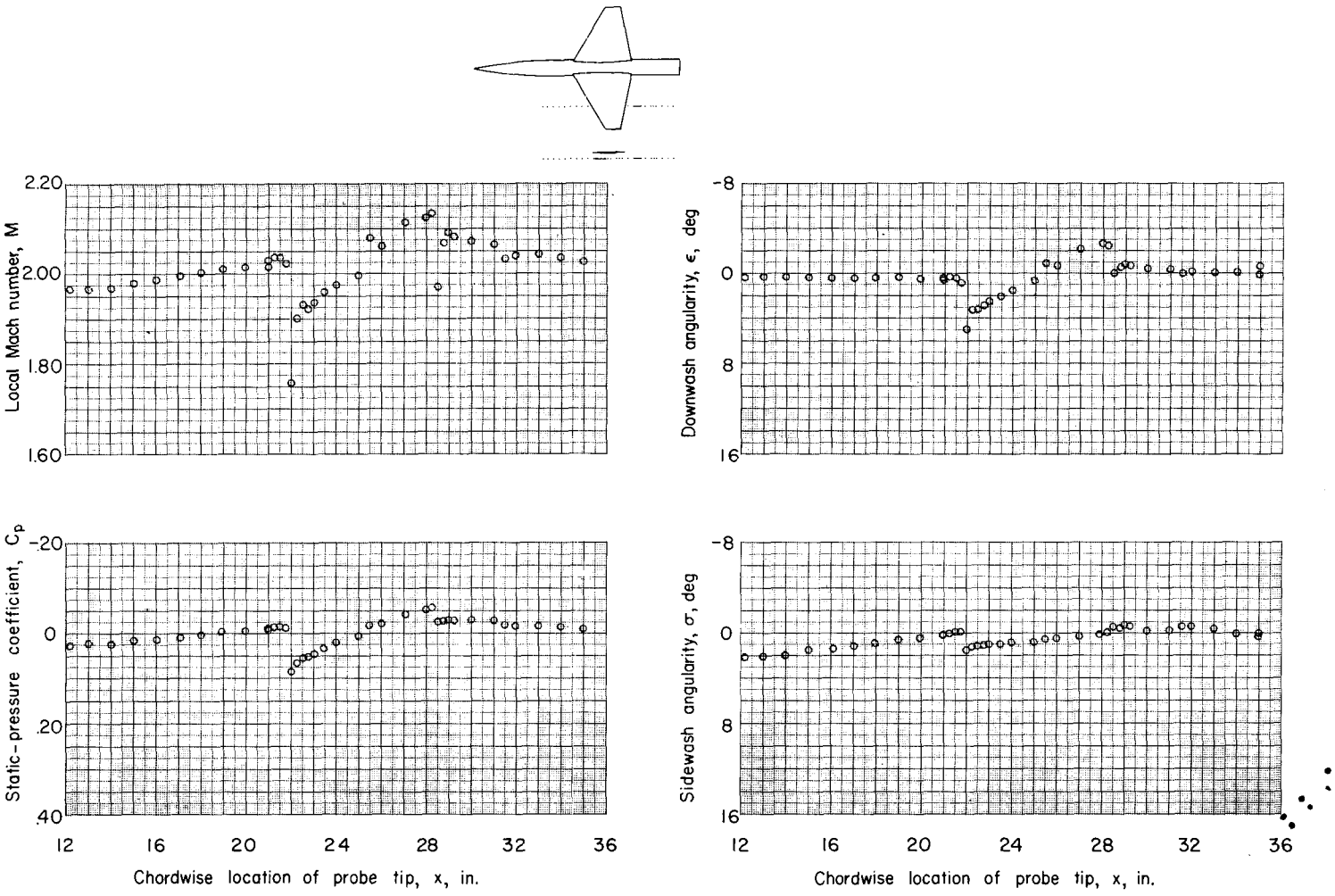

(b) y = 6.6 in.; z = 1.15 in.

Figure 11.- Continued.

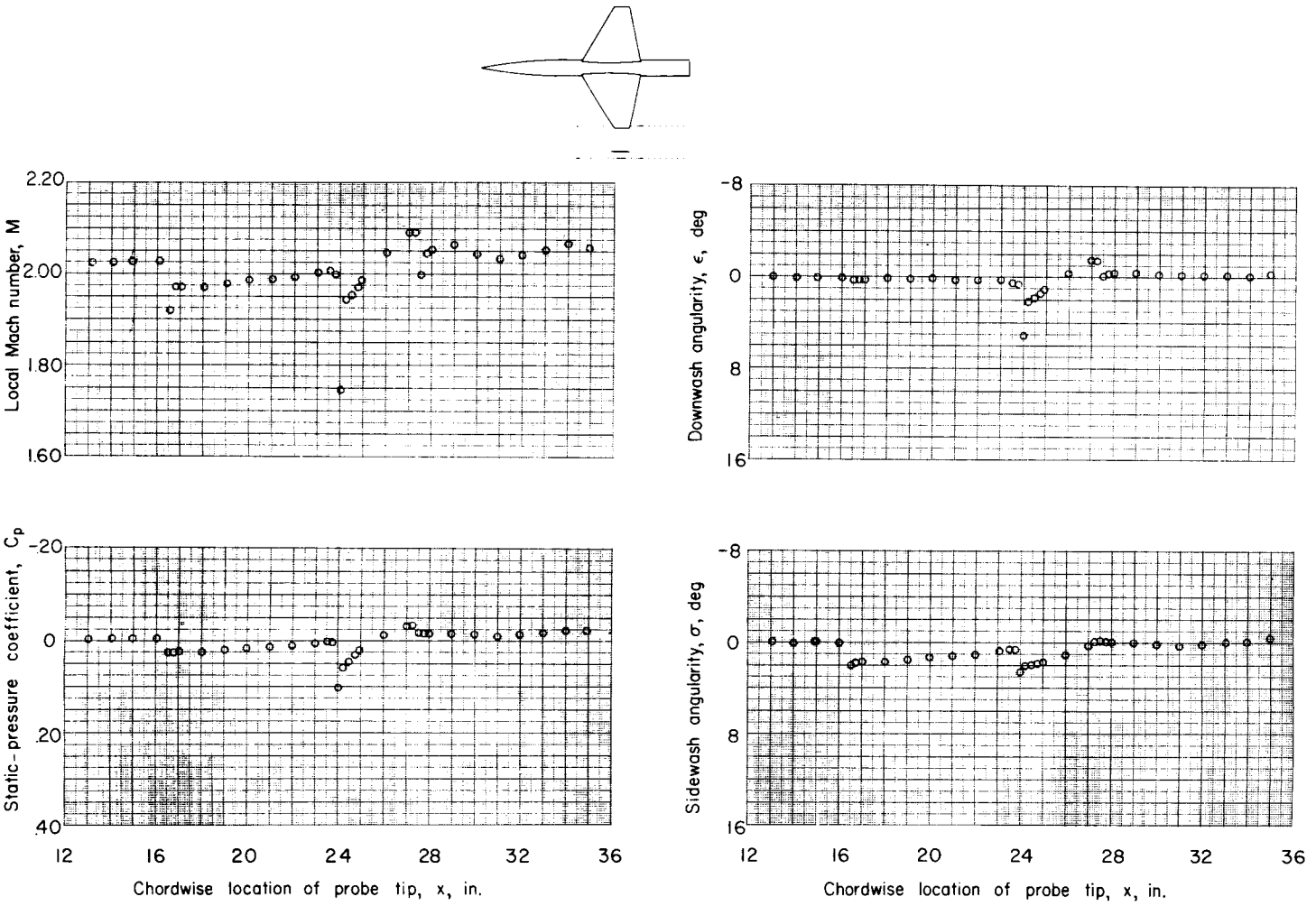

(c) y = 10.2 in.; z = 1.15 in.

Figure 11.- Continued.

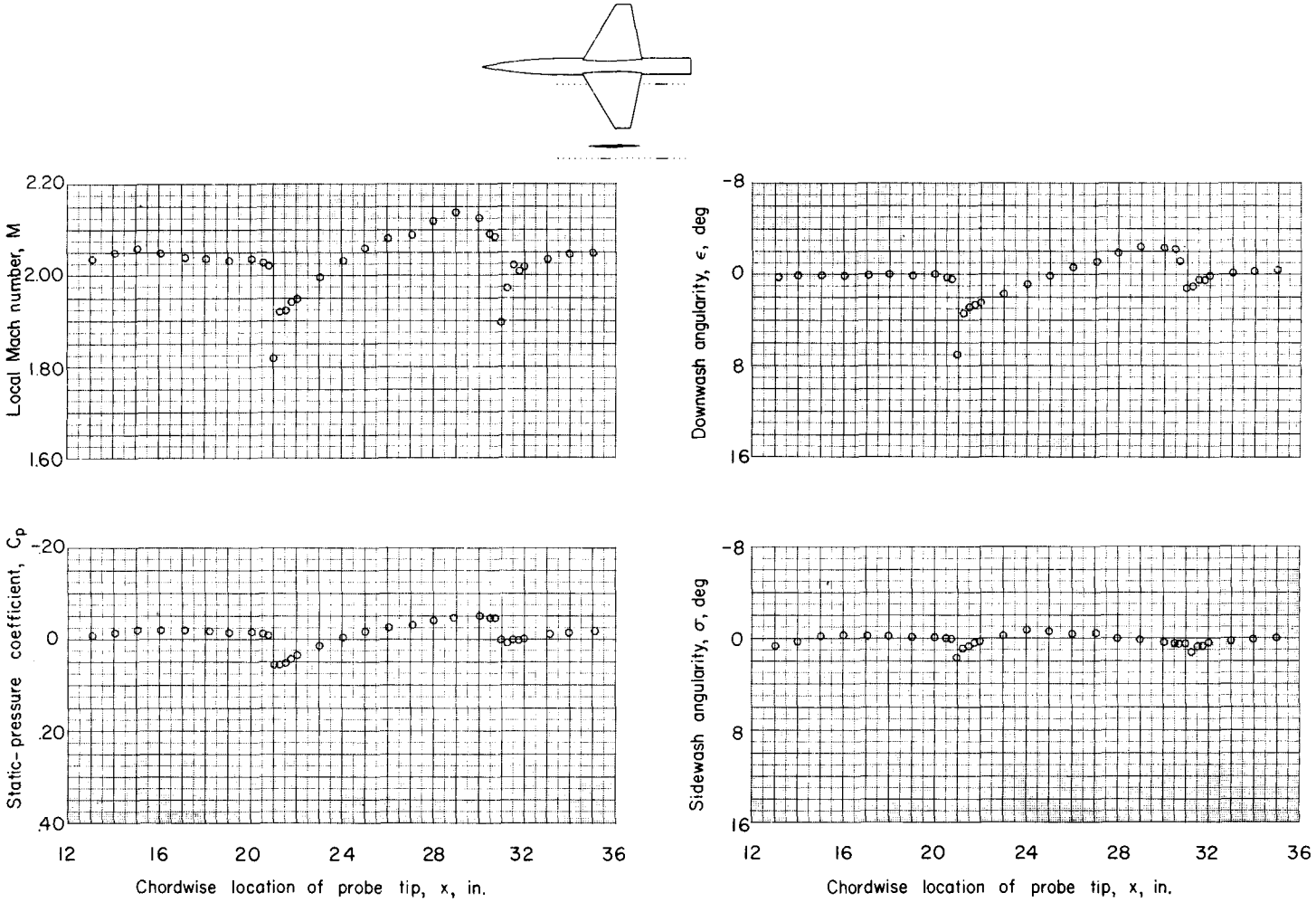

(d) y = 3.0 in.; z = 2.1 in.

Figure 11.- Continued.

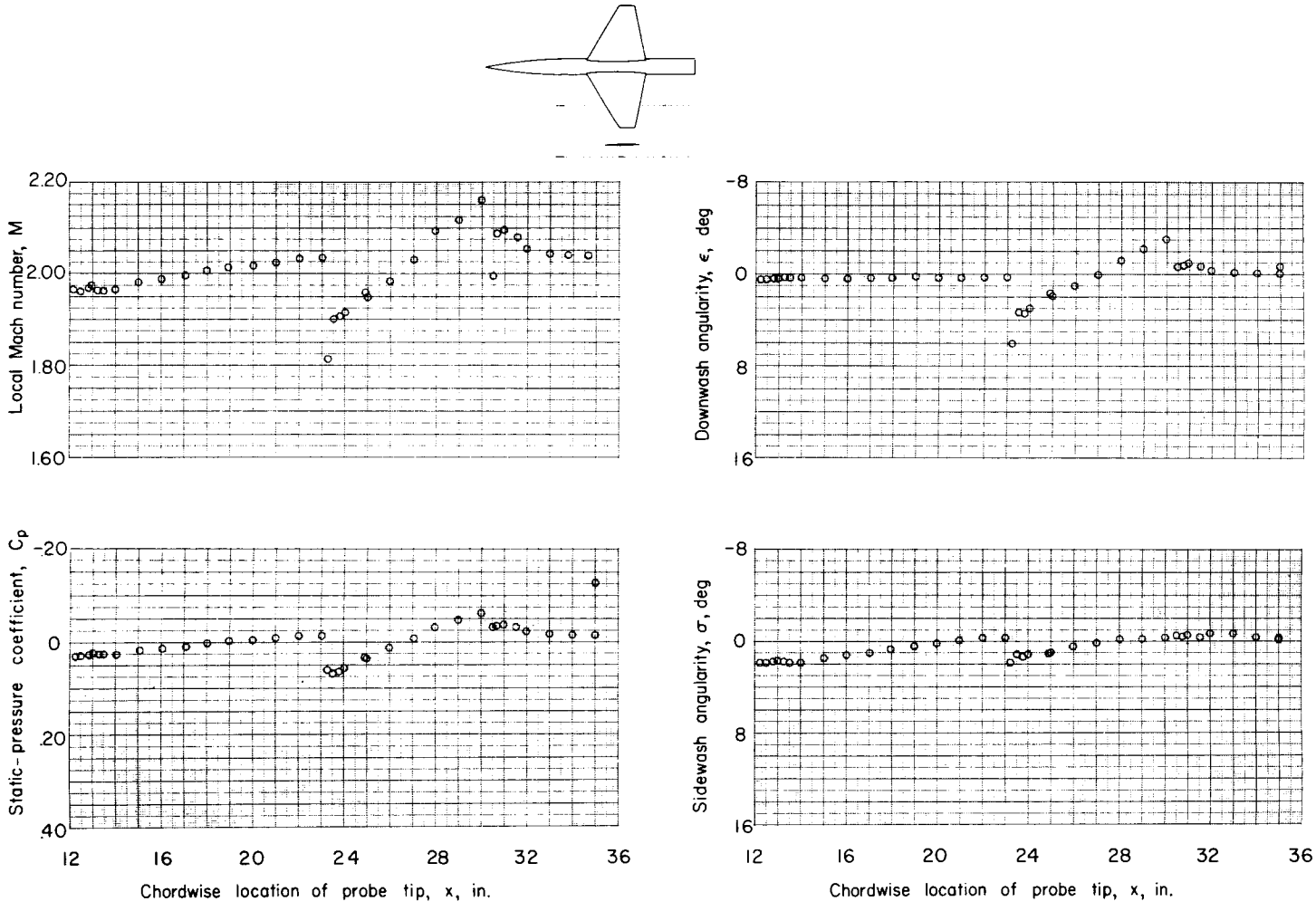

(e) y = 6.6 in.; z = 2.1 in.

Figure 11.- Continued.

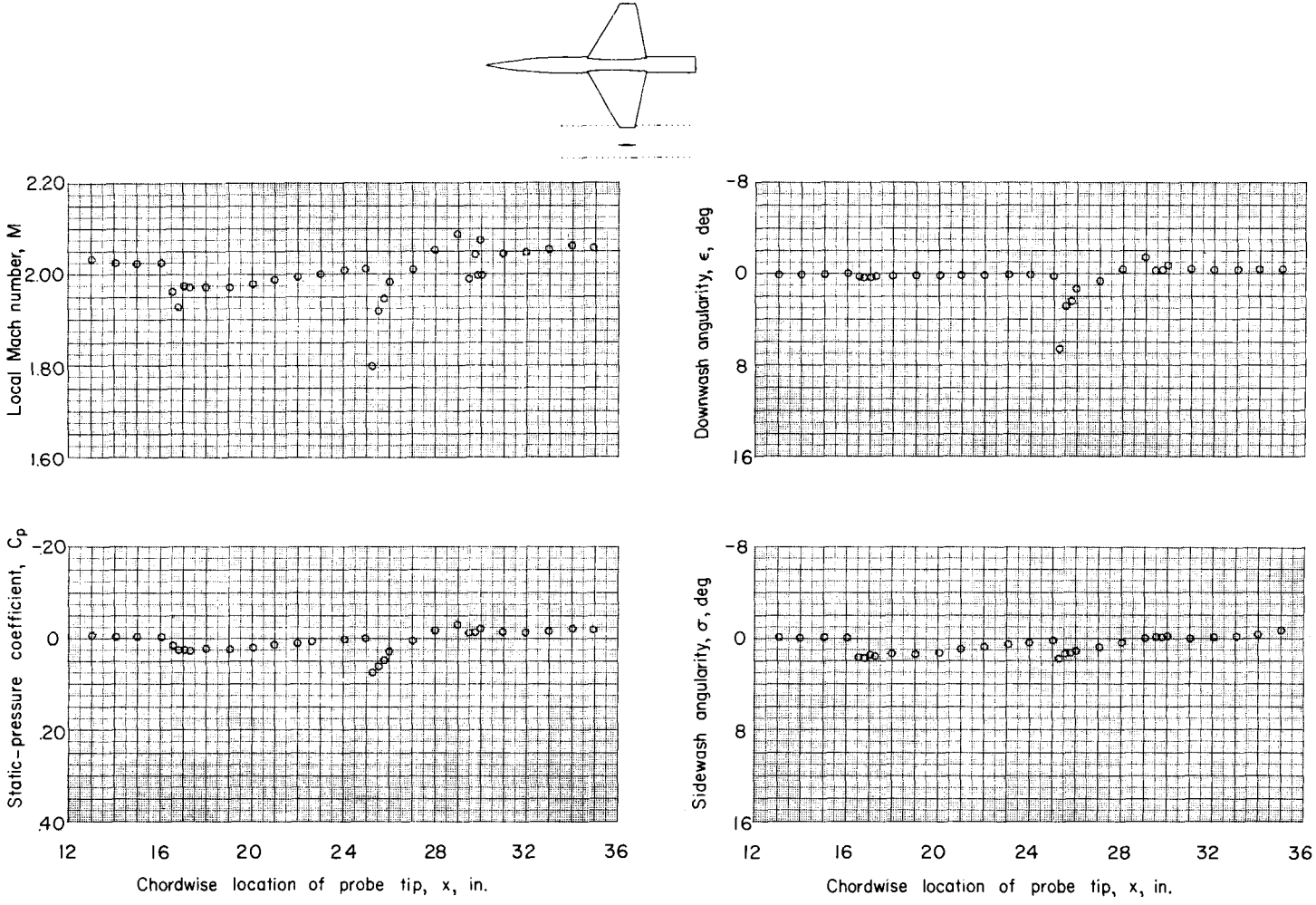

(f) y = 10.2 in.; z = 2.1 in.

Figure 11.- Concluded.

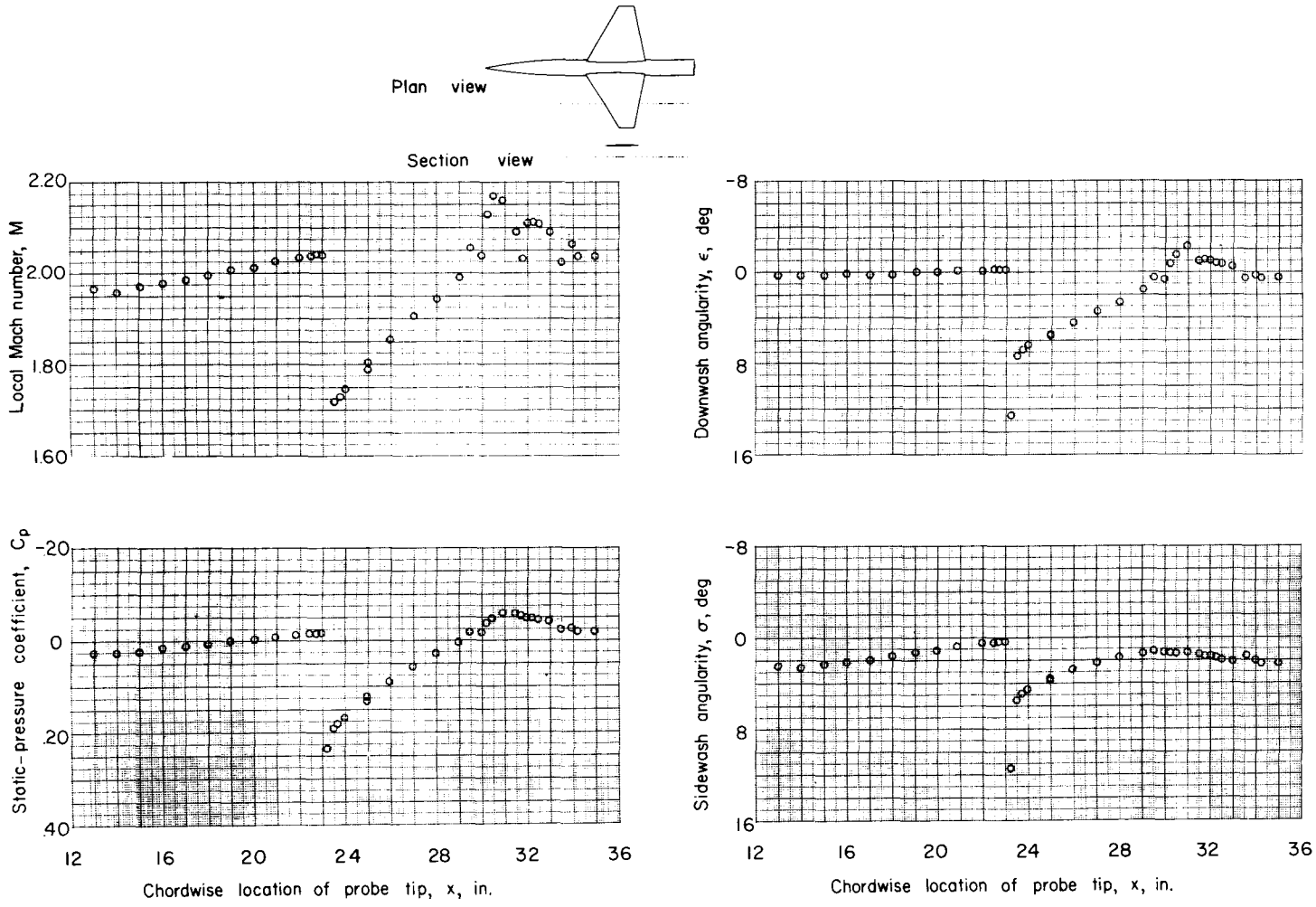

Figure 12.- Flow properties measured in the vicinity of a trapezoidal-wing—fuselage configuration. $\alpha = 4^{\circ}$; $M_{\infty} = 2.01$; $y = 6.6$ in.; $z = 2.1$ in.

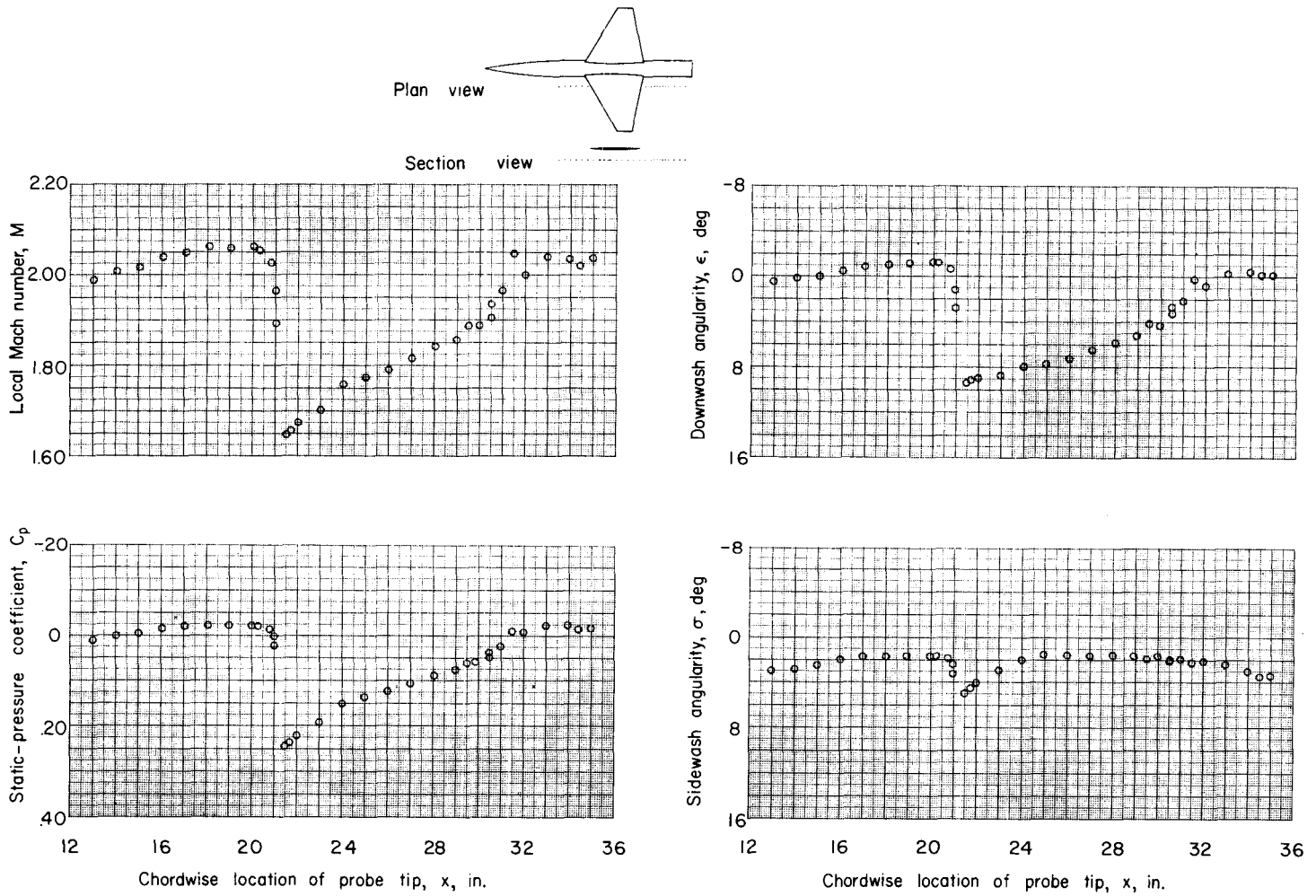

(a) y = 3.0 in.; z = 2.1 in.

Figure 13.- Flow properties measured in the vicinity of a trapezoidal-wing—fuselage configuration. $\alpha = 8^{\circ}$; $M_{\infty} = 2.01$.

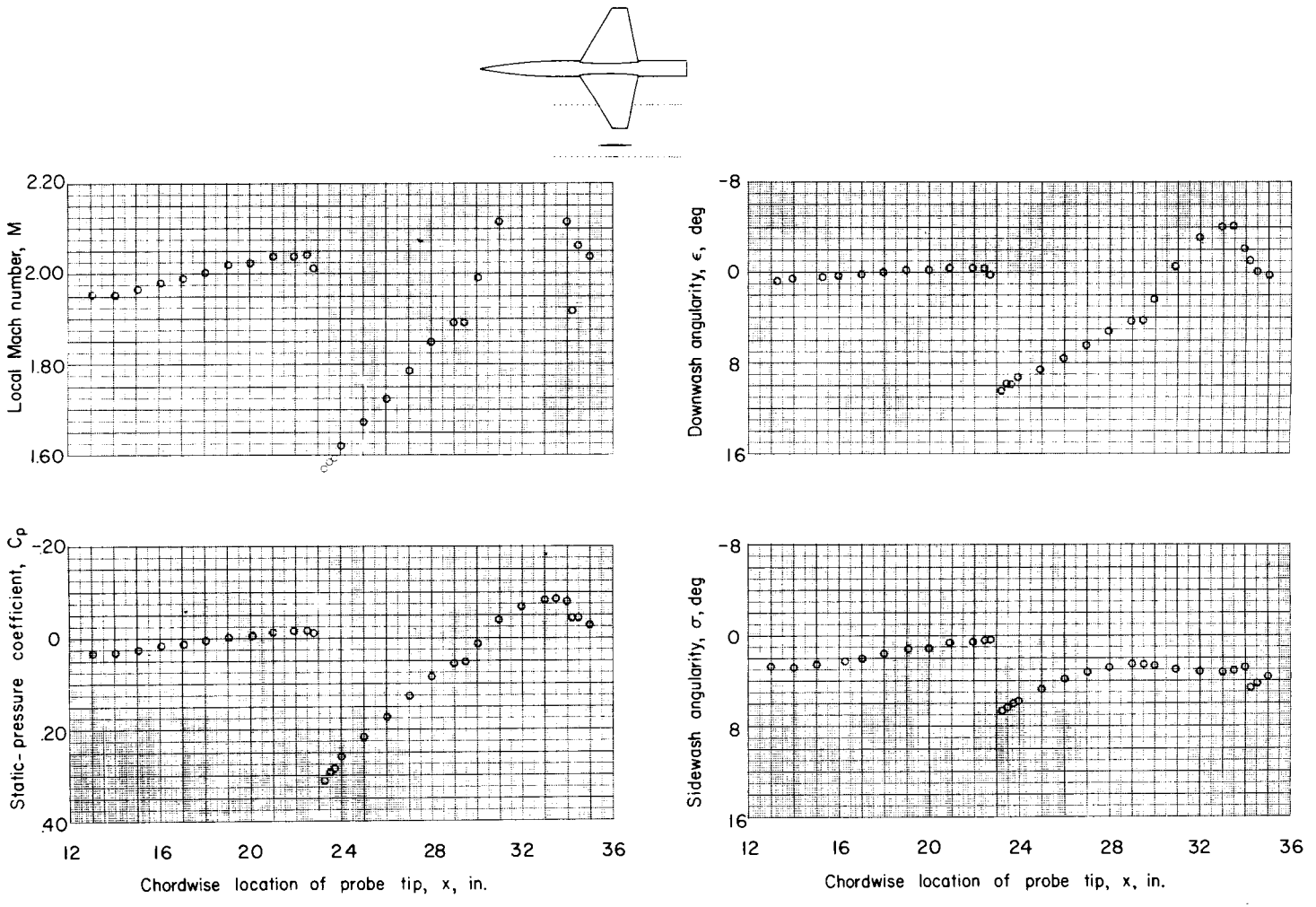

(b) y = 6.6 in.; z = 2.1 in.

Figure 13.- Continued.

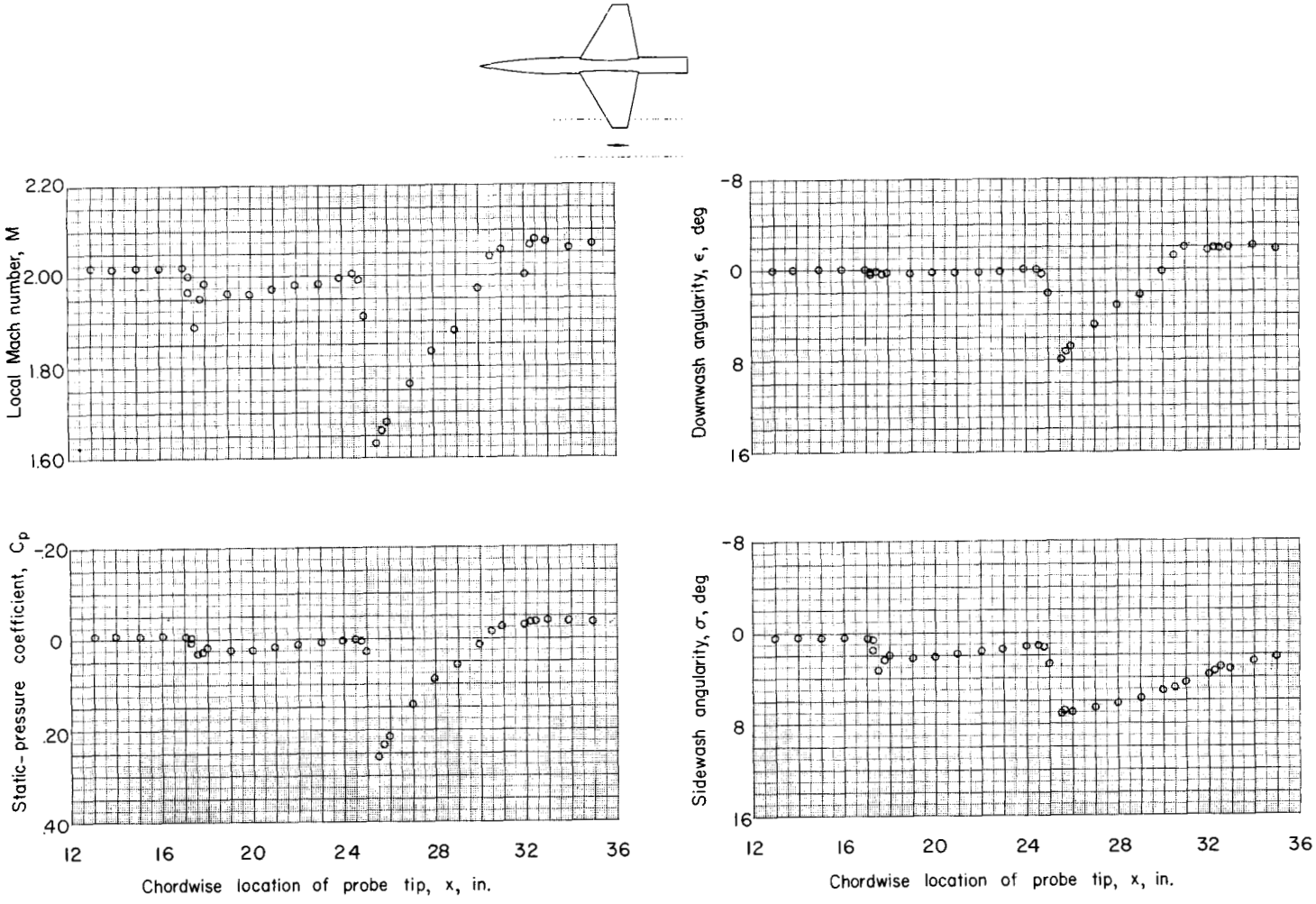

(c) y = 10.2 in.; z = 2.1 in.

Figure 13.- Concluded.

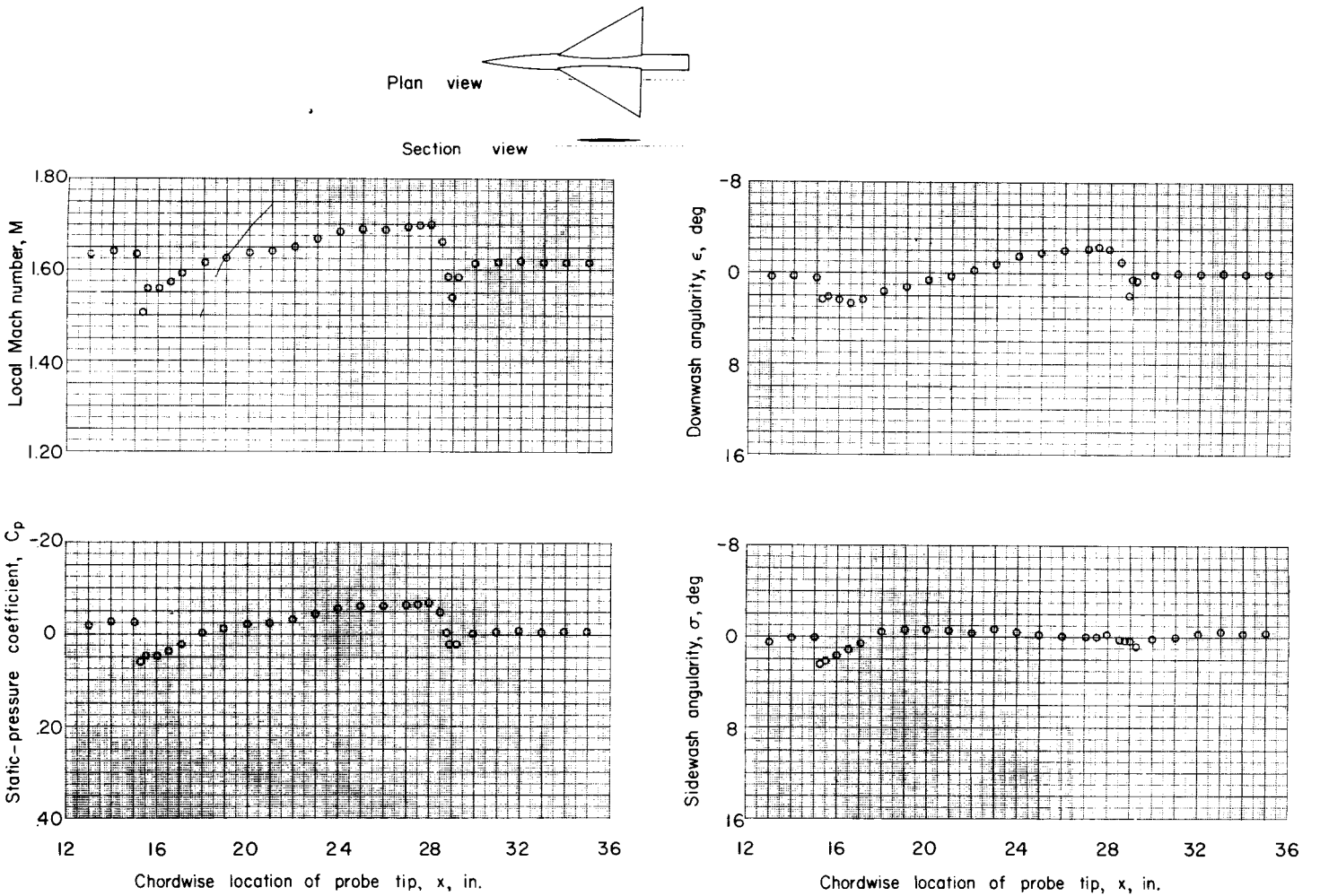

(a) y = 3.0 in.; z = 1.15 in.

Figure 14.- Flow properties measured in the vicinity of a delta-wing—fuselage configuration. $\alpha = 0^{\circ}$; $M_{\infty} = 1.61$.

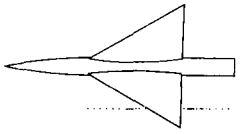

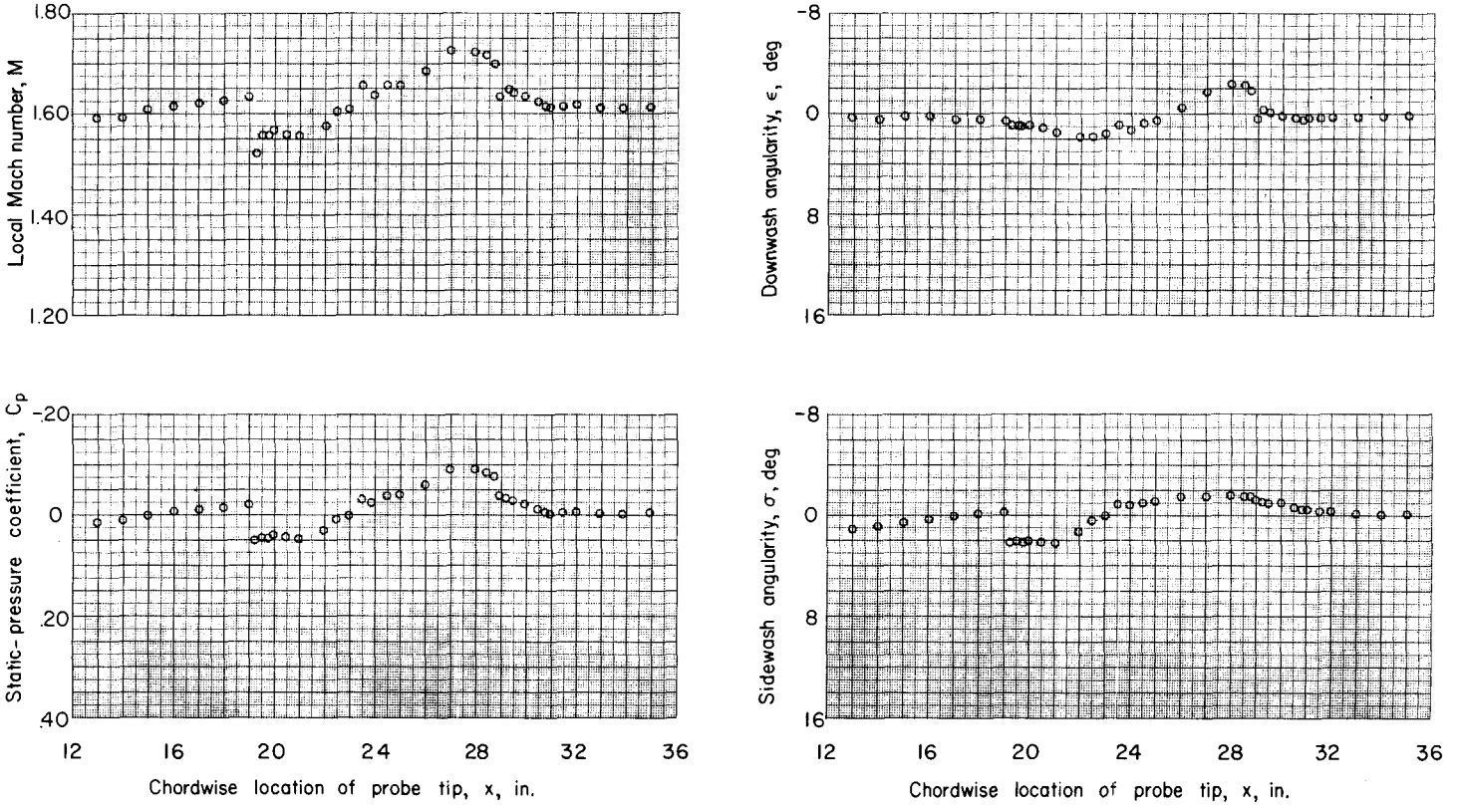

(b) y = 6.6 in.; z = 1.15 in.

Figure 14.- Continued.

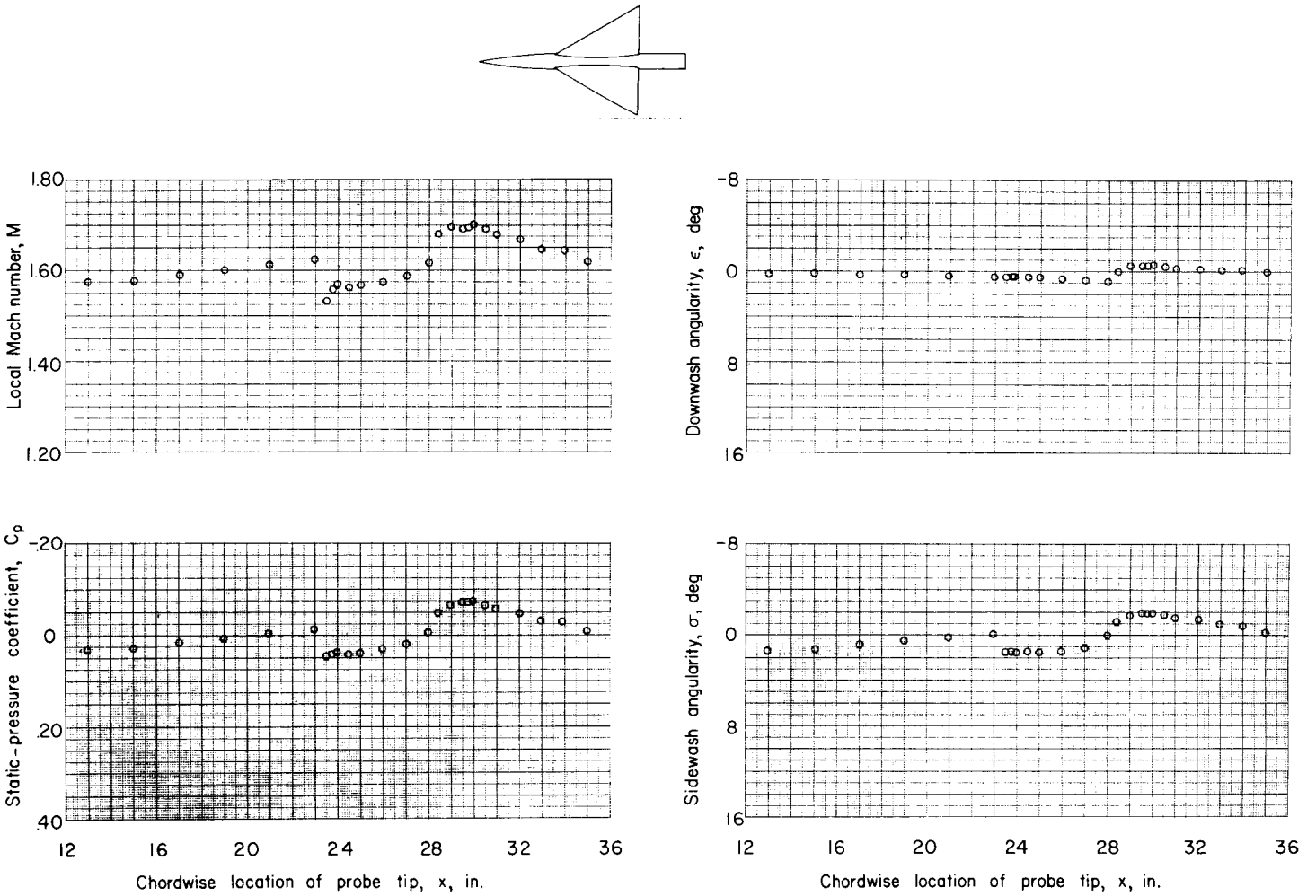

(c) y = 10.2 in.; z = 1.15 in.

Figure 14.- Concluded.

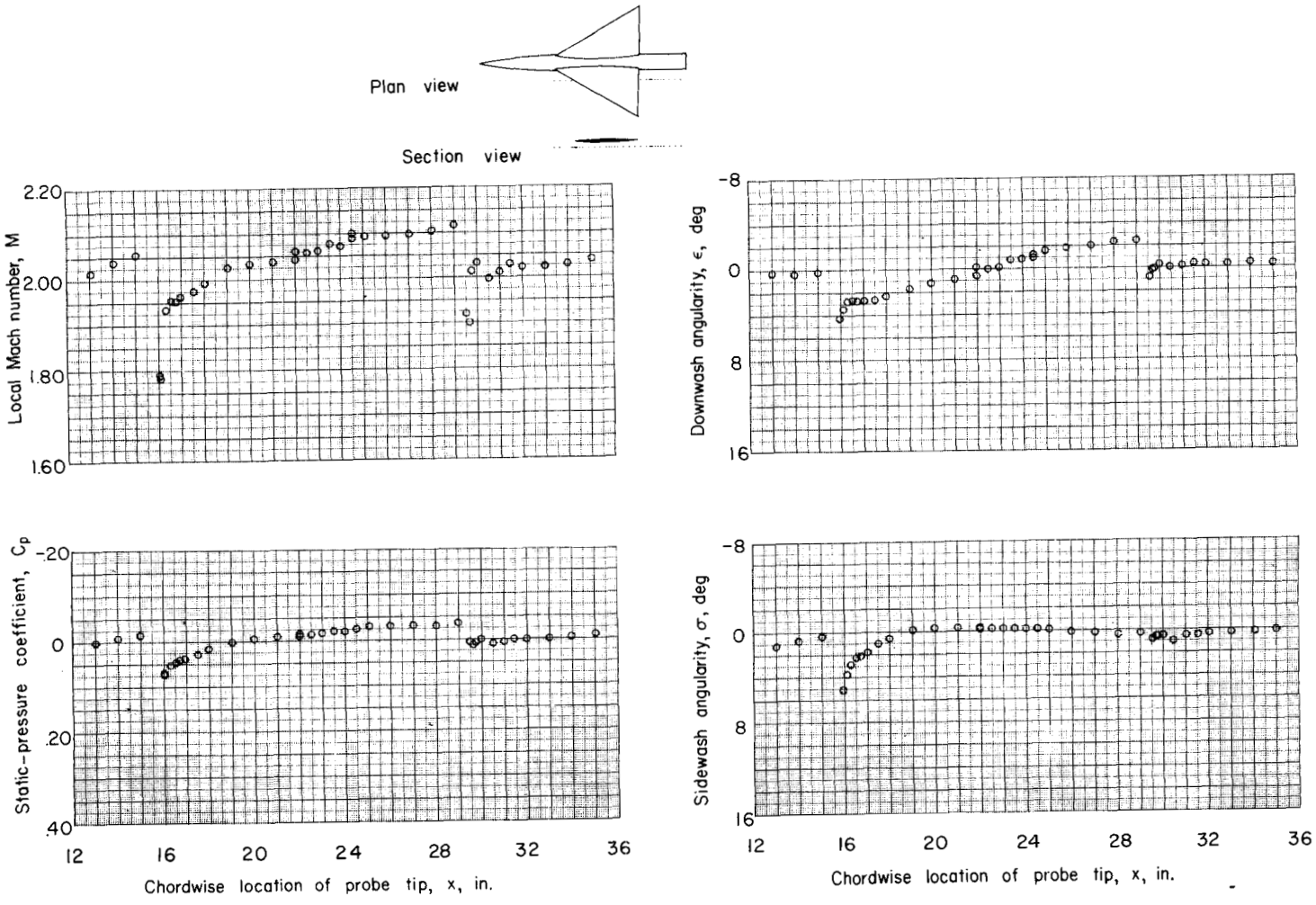

(a) y = 3.0 in.; z = 1.15 in.

Figure 15.- Flow properties measured in the vicinity of a delta-wing—fuselage configuration. $\alpha = 0^{\circ}$; $M_{\infty} = 2.01$.

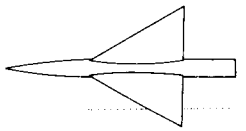

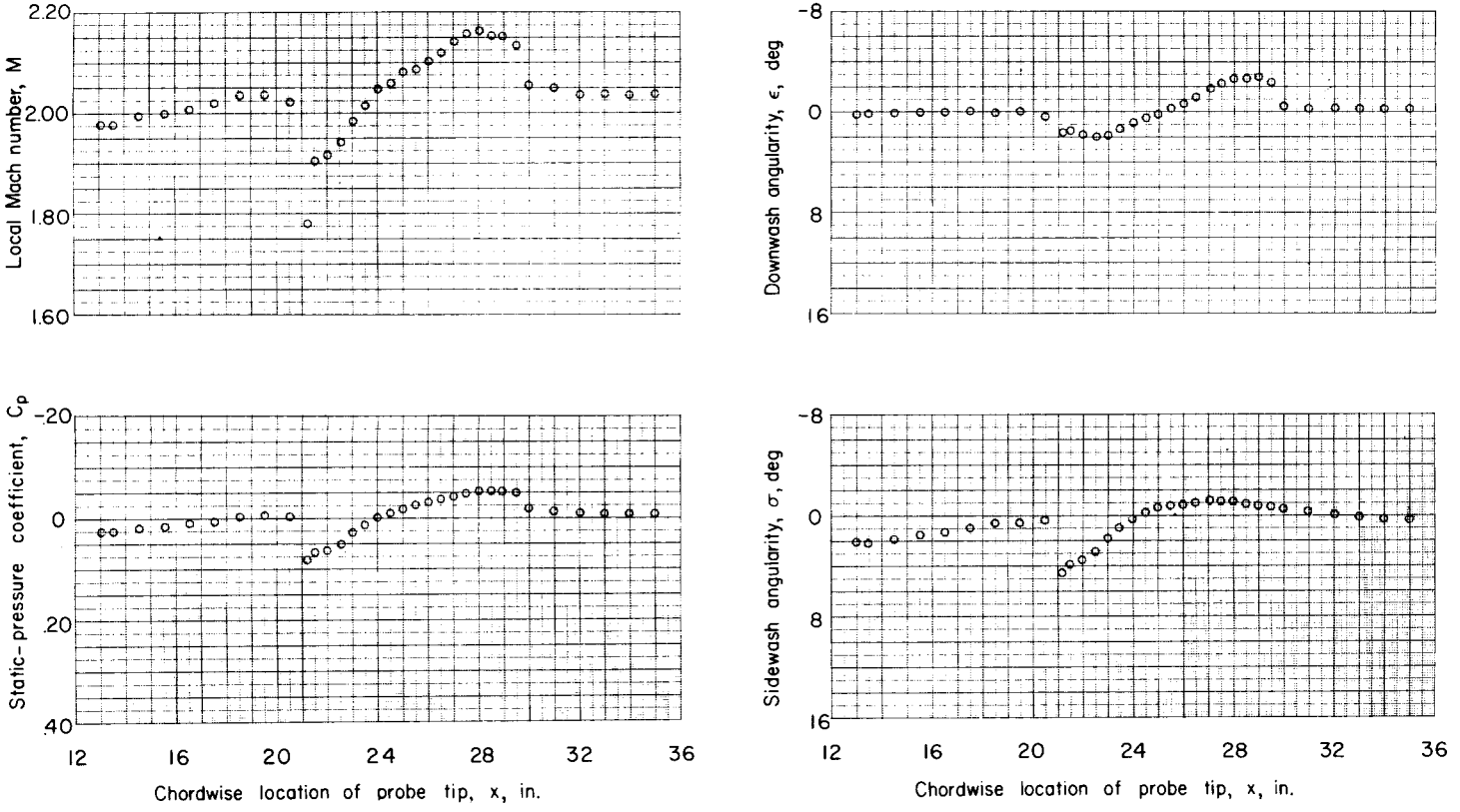

(b) y = 6.6 in.; z = 1.15 in.

Figure 15.- Continued.

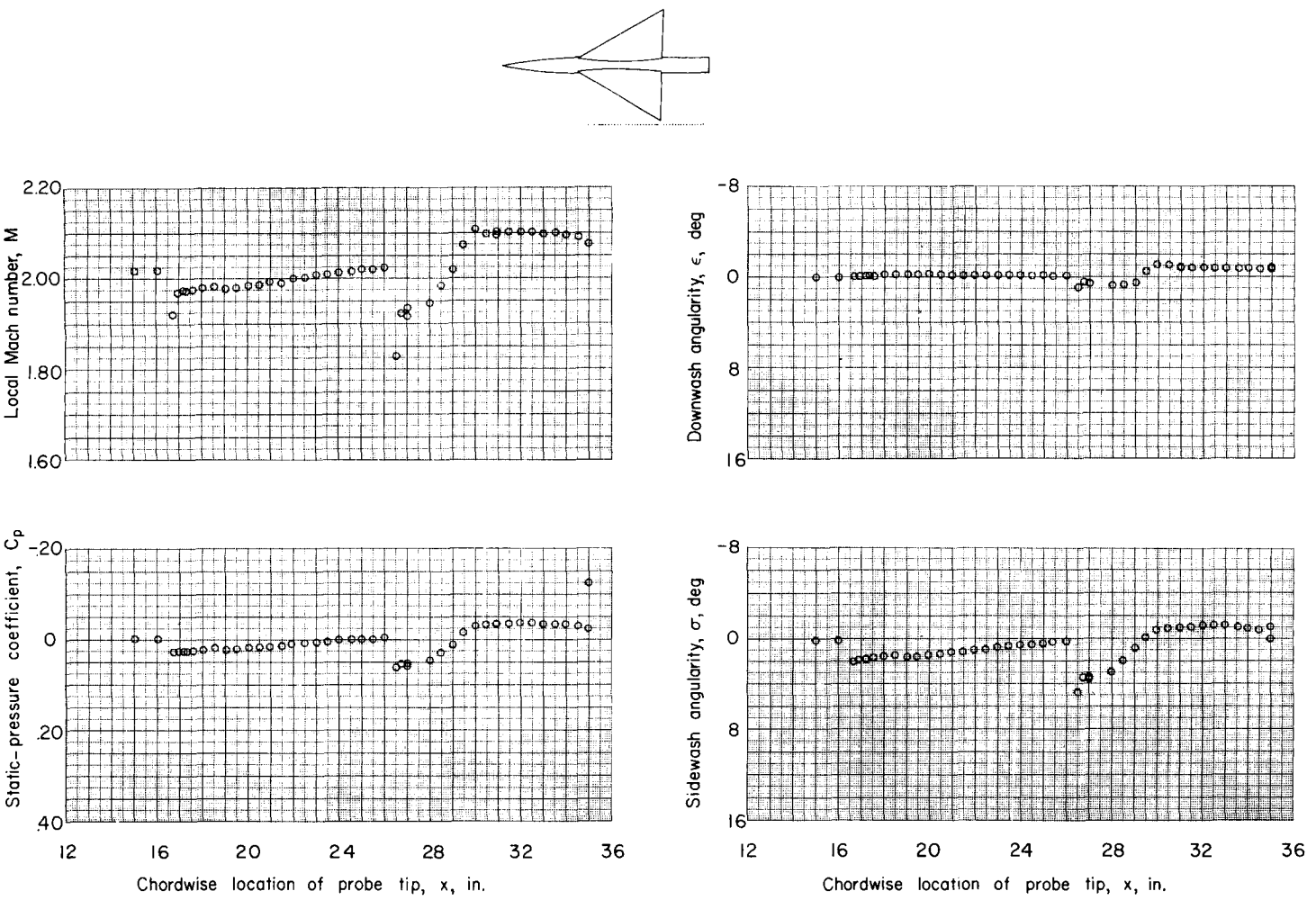

(c) y = 10.2 in.; z = 1.15 in.

Figure 15.- Concluded.

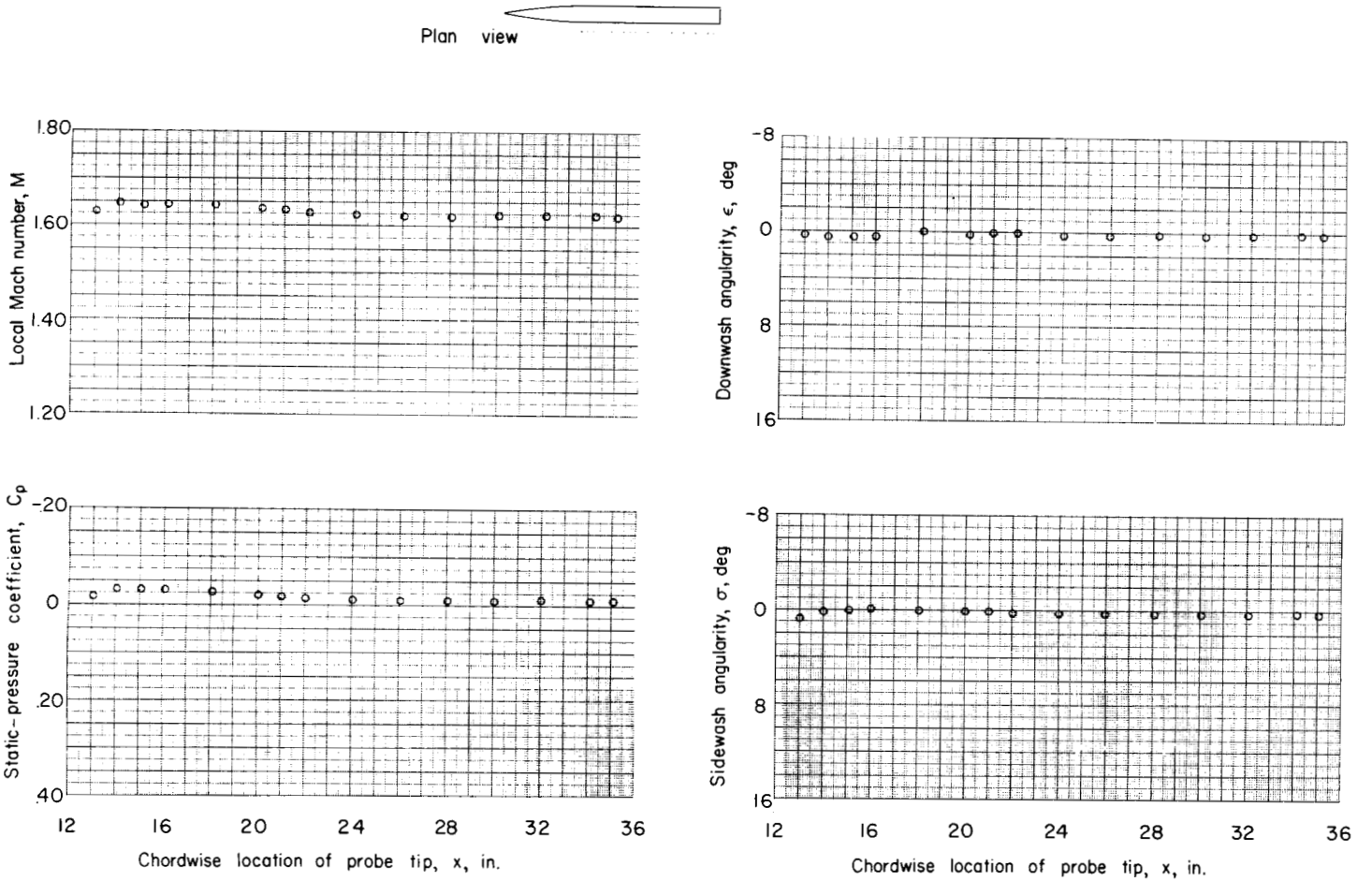

(a) y = 3.0 in.; z = 0 in.

Figure 16.- Flow properties measured in the vicinity of the fuselage. $\alpha = 0^{\circ}$; $M_{\infty} = 1.61$.

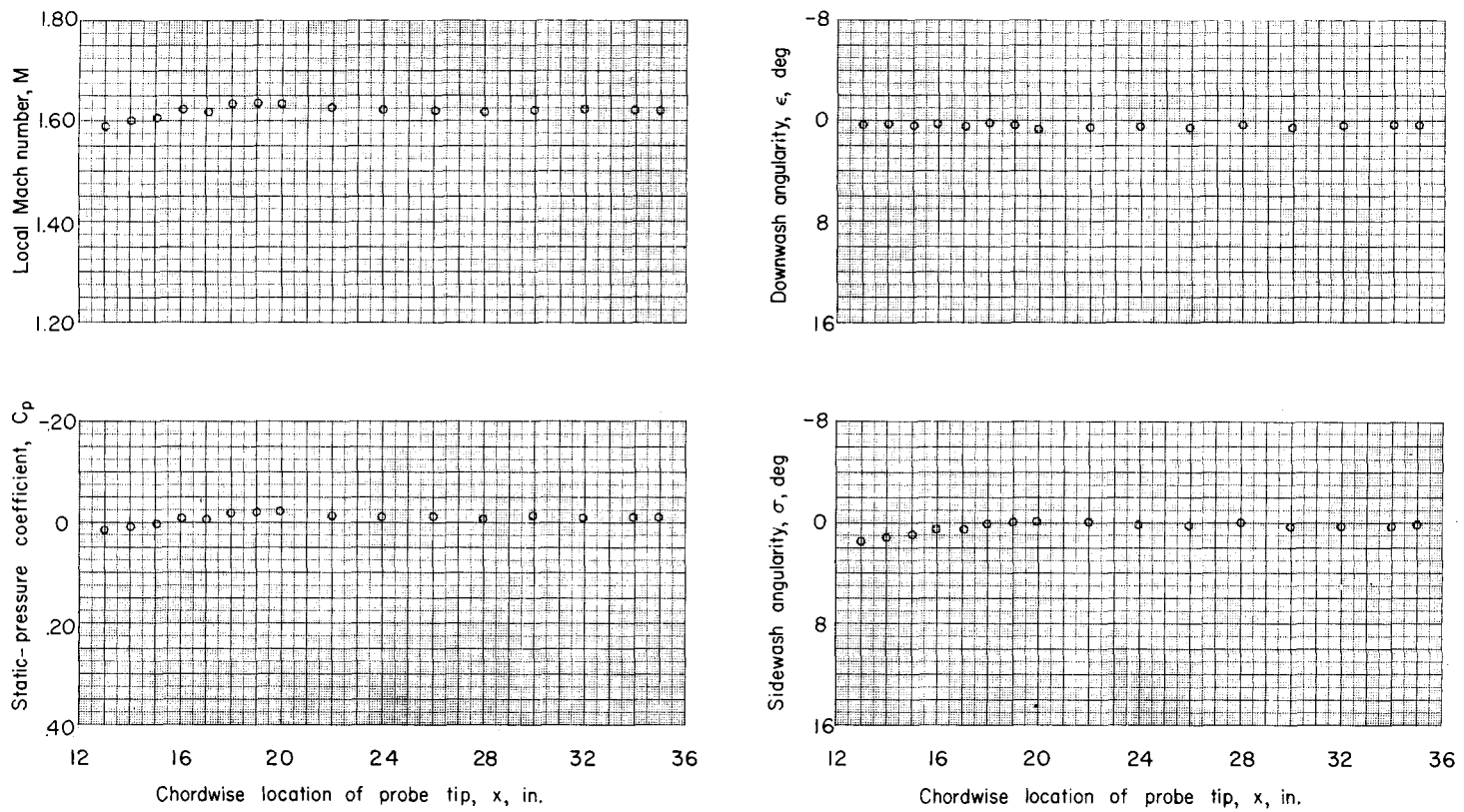

(b) y = 6.6 in.; z = 0 in.

Figure 16.- Continued.

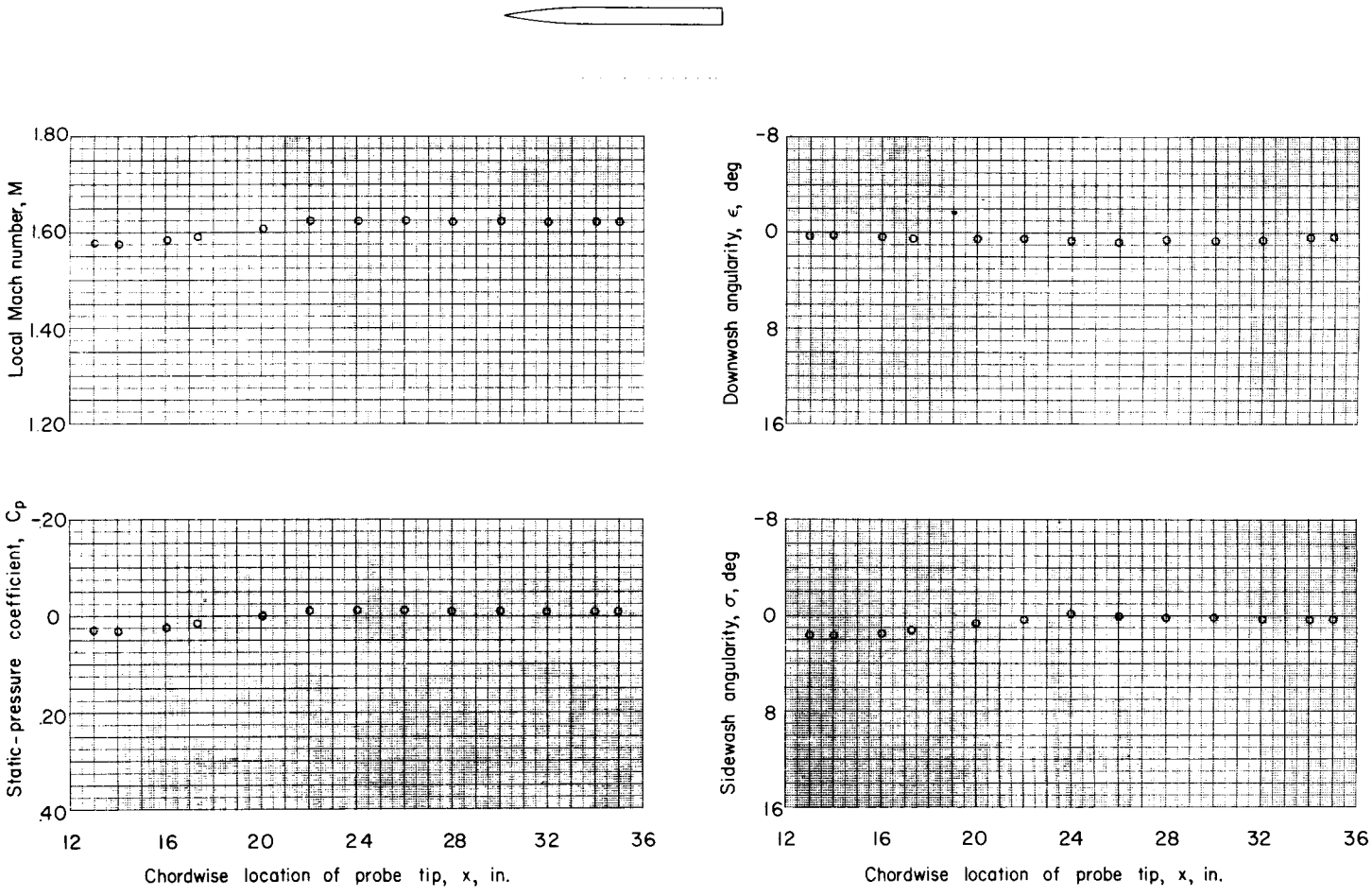

(c) y = 10.2 in.; z = 0 in.

Figure 16.- Concluded.

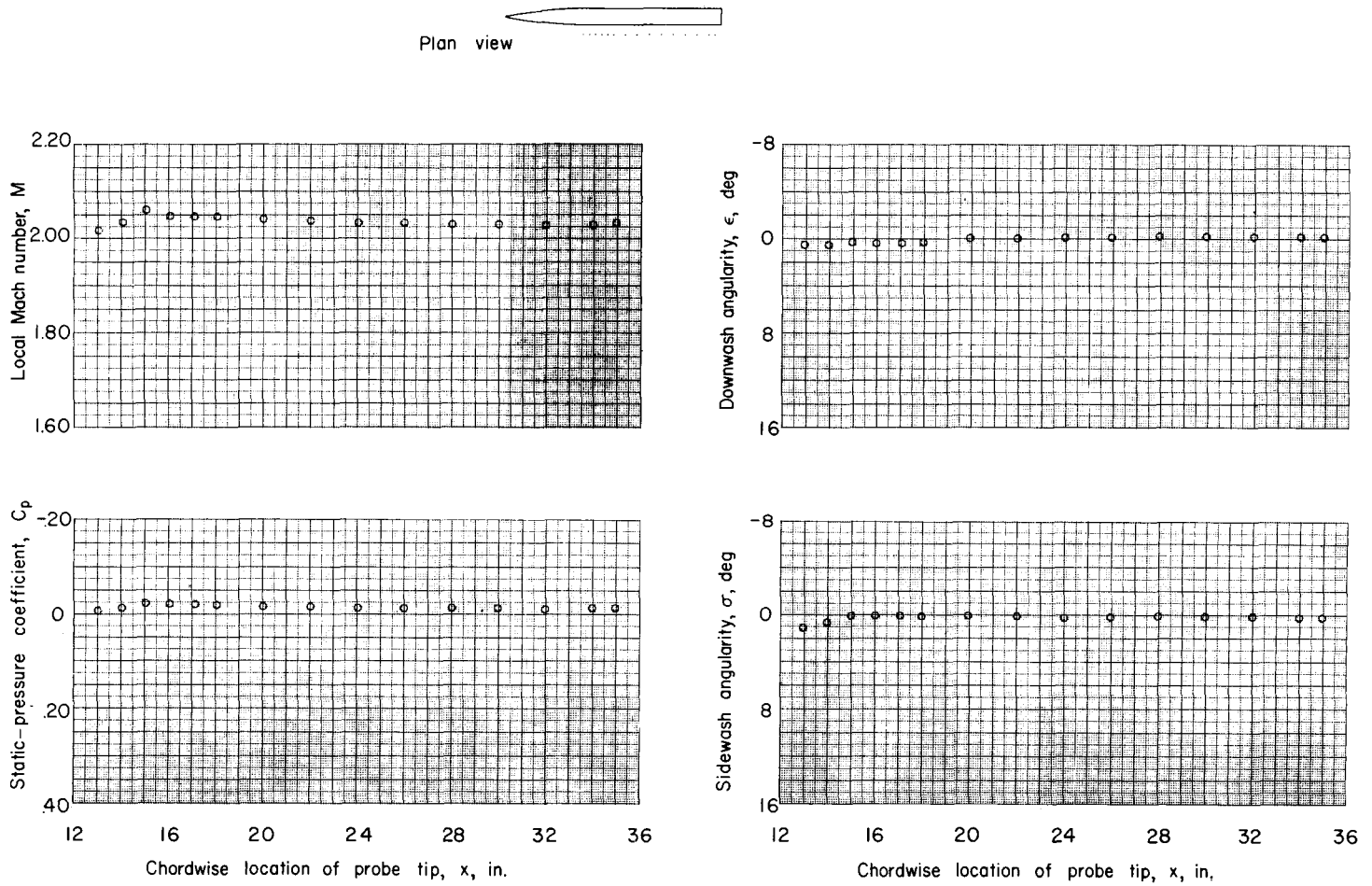

(a) y = 3.0 in.; z = 0 in.

Figure 17.- Flow properties measured in the vicinity of the fuselage. $\alpha = 0^{\circ}$; $M_{\infty} = 2.01$.

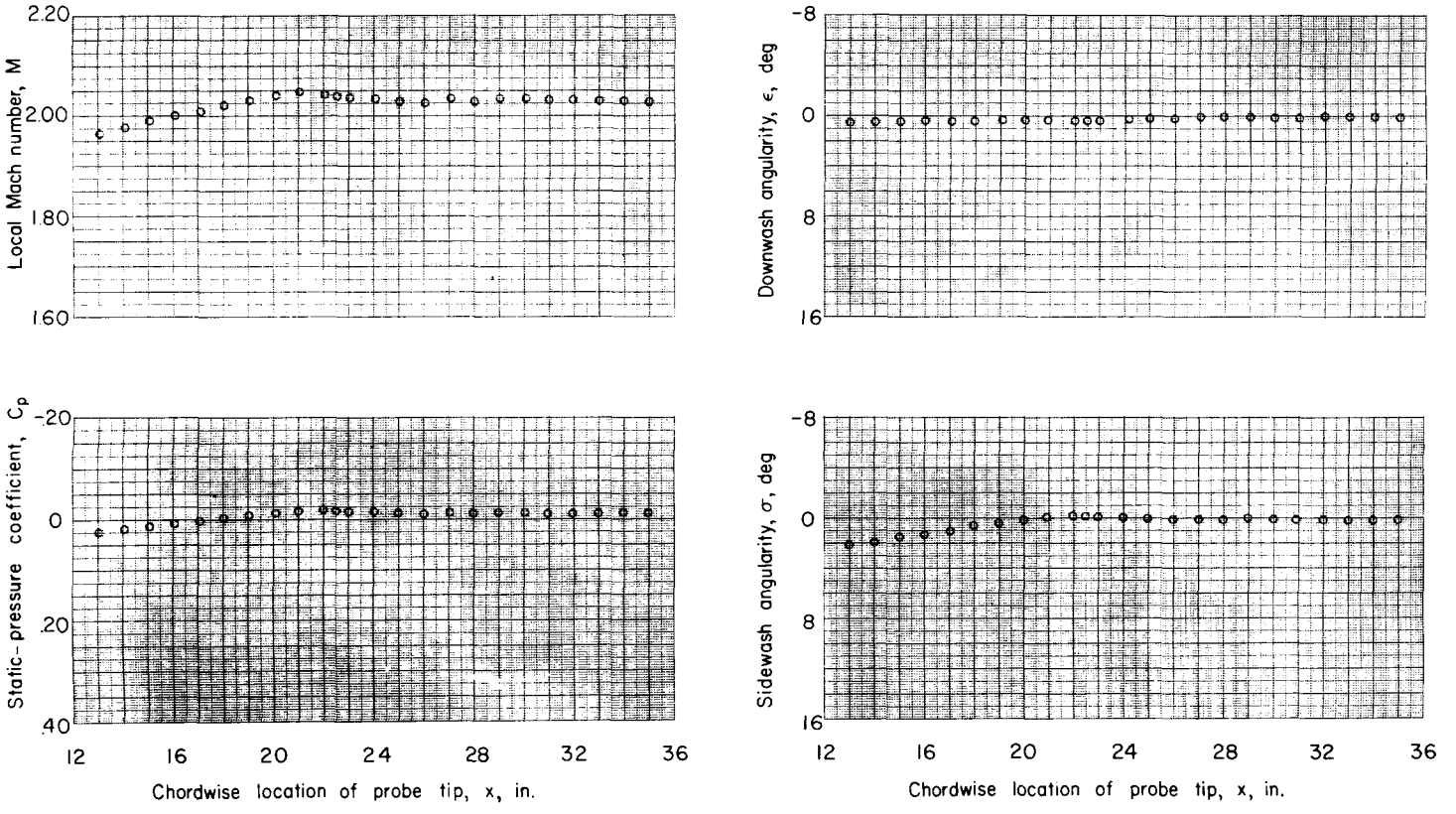

(b) y = 6.6 in.; z = 0 in.

Figure 17.- Continued.

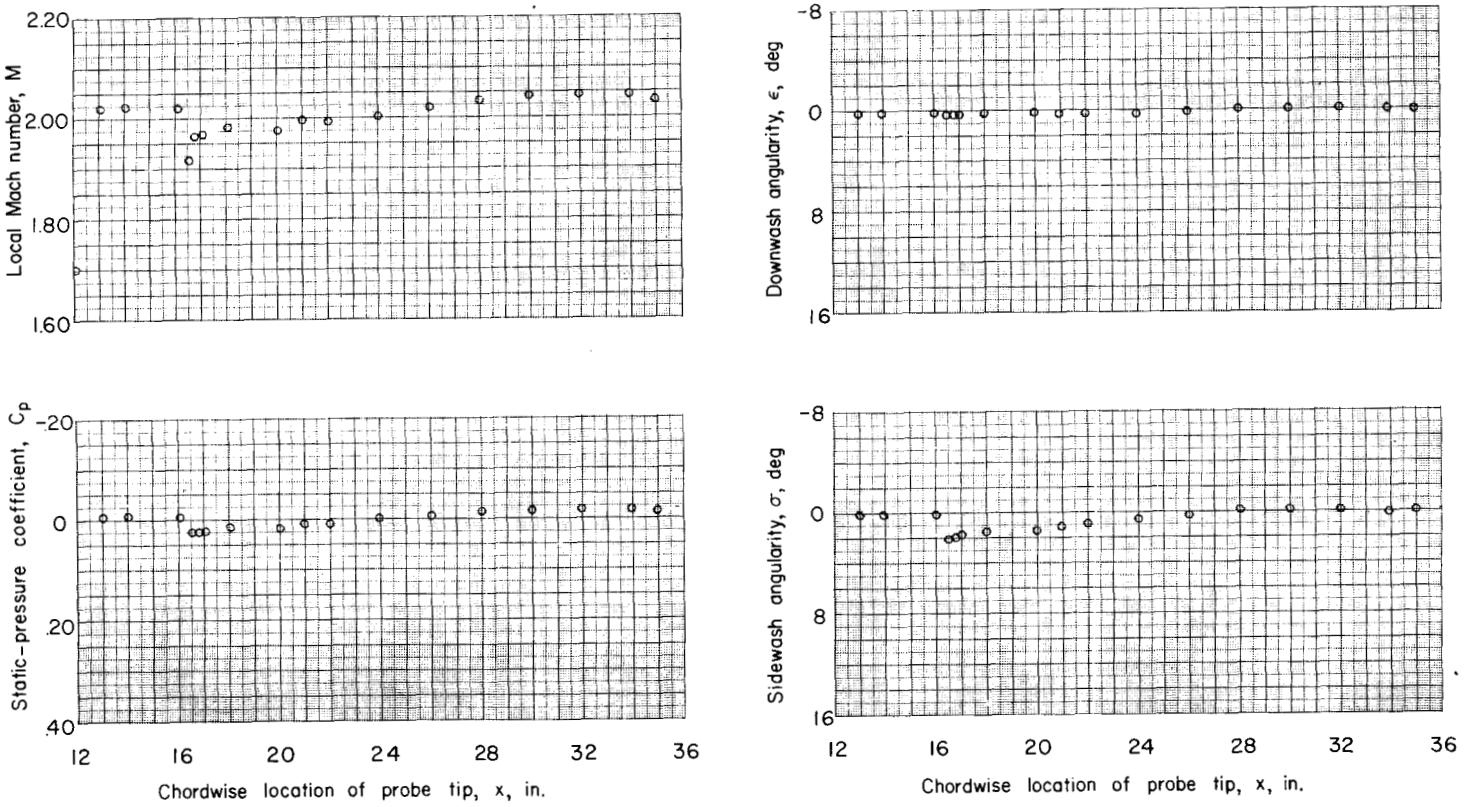

(c) y = 10.2 in.; z = 0 in.

Figure 17.- Concluded.

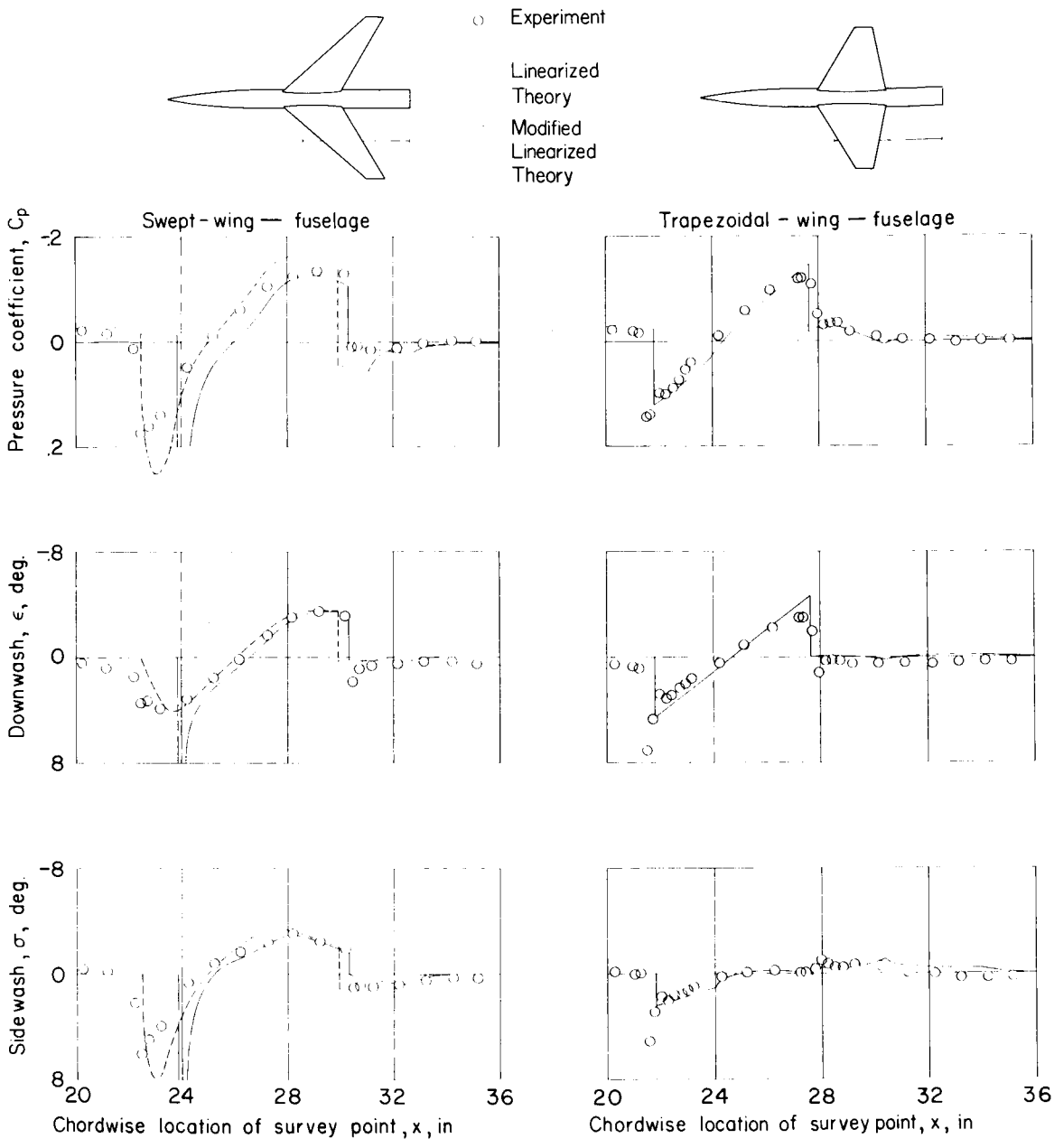

(a) $M_\infty = 1.61$.

Figure 18.- Comparison of theoretical and experimental flow properties of zero angle of attack for two wing-fuselage combinations. y = 6.6 in.; z = 1.15 in.

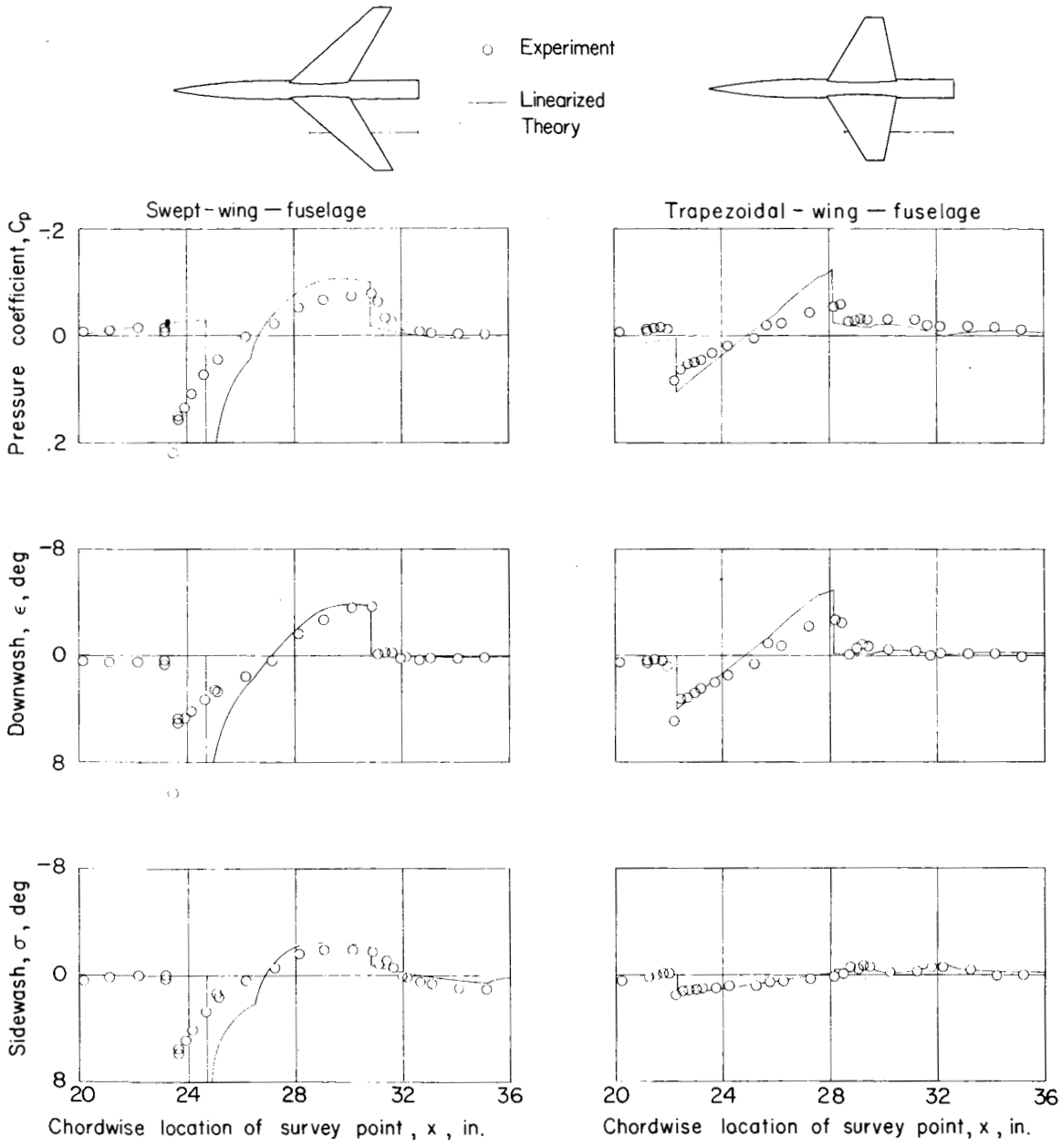

(b) $M_\infty = 2.01$.

Figure 18.- Concluded.

[redacted]

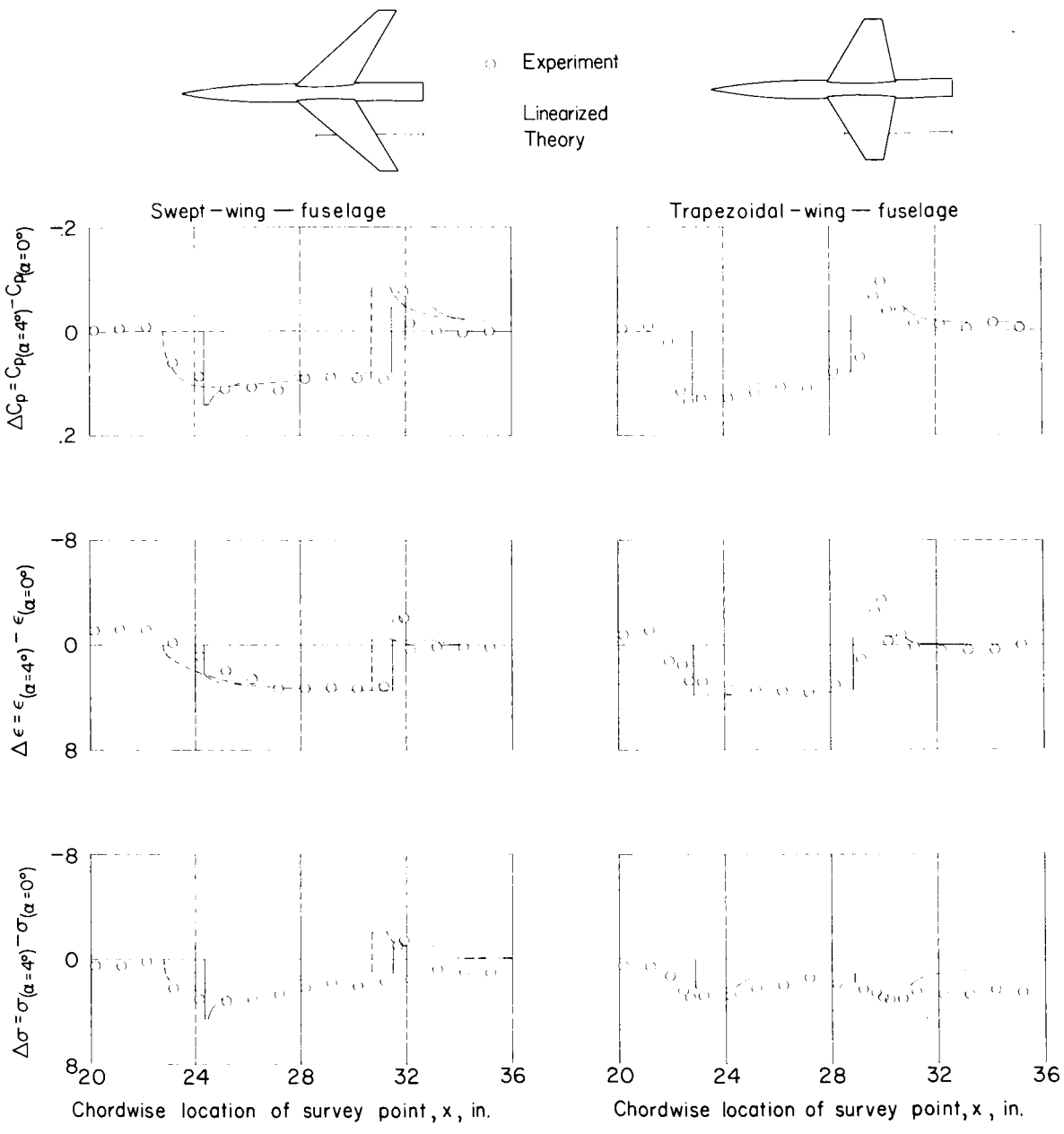

Figure 19.- Comparison of theoretical and experimental flow properties due to angle of attack for two wing-fuselage combinations. $y = 6.6$ in.; $z = 2.10$ in.; $M_\infty = 1.61$.

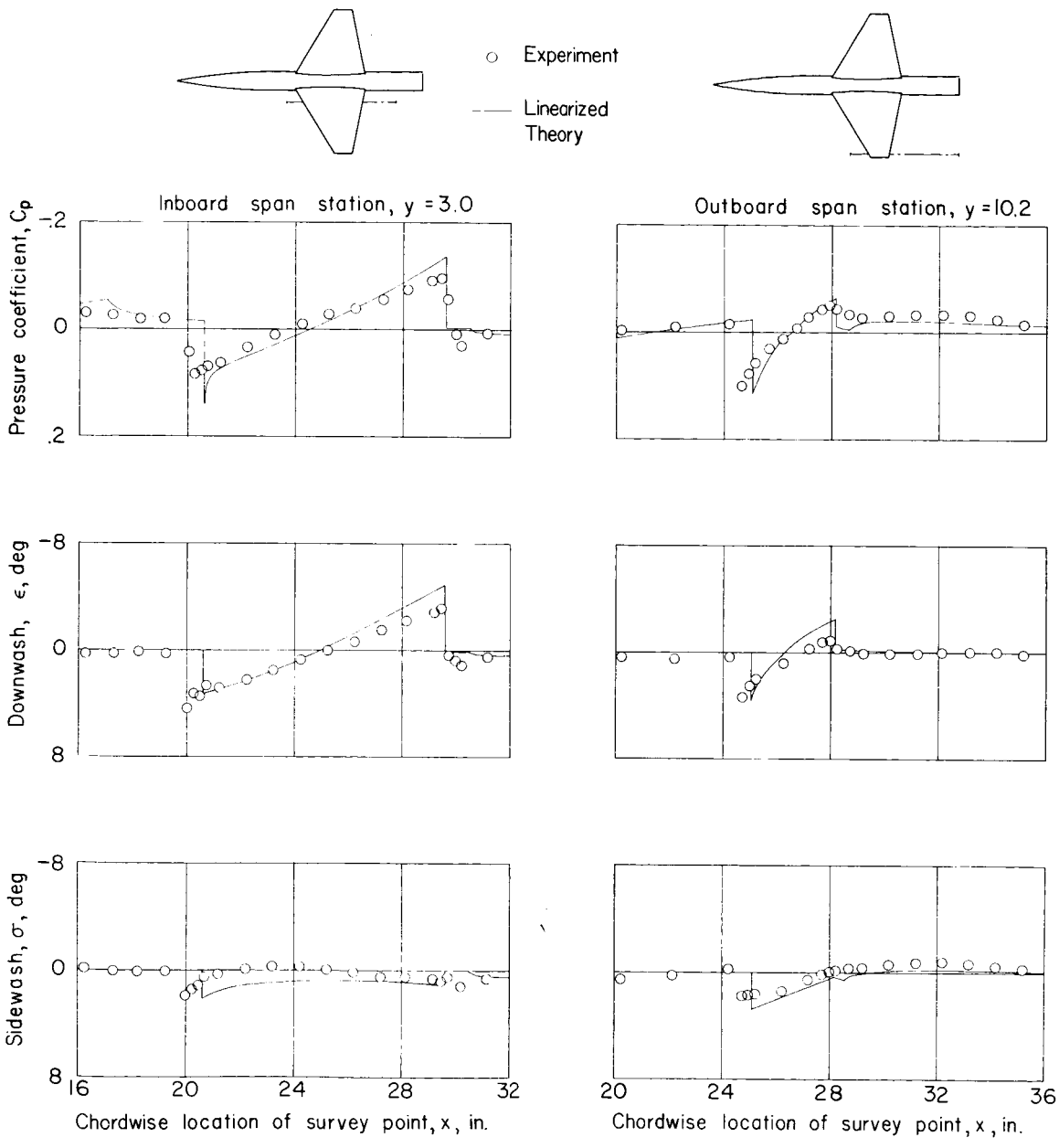

Figure 20.- Comparison of theoretical and experimental flow properties at zero angle of attack for an inboard and an outboard span station. Trapezoidal-wing—fuselage configuration; z = 2.1 in.; M_∞ = 1.61.

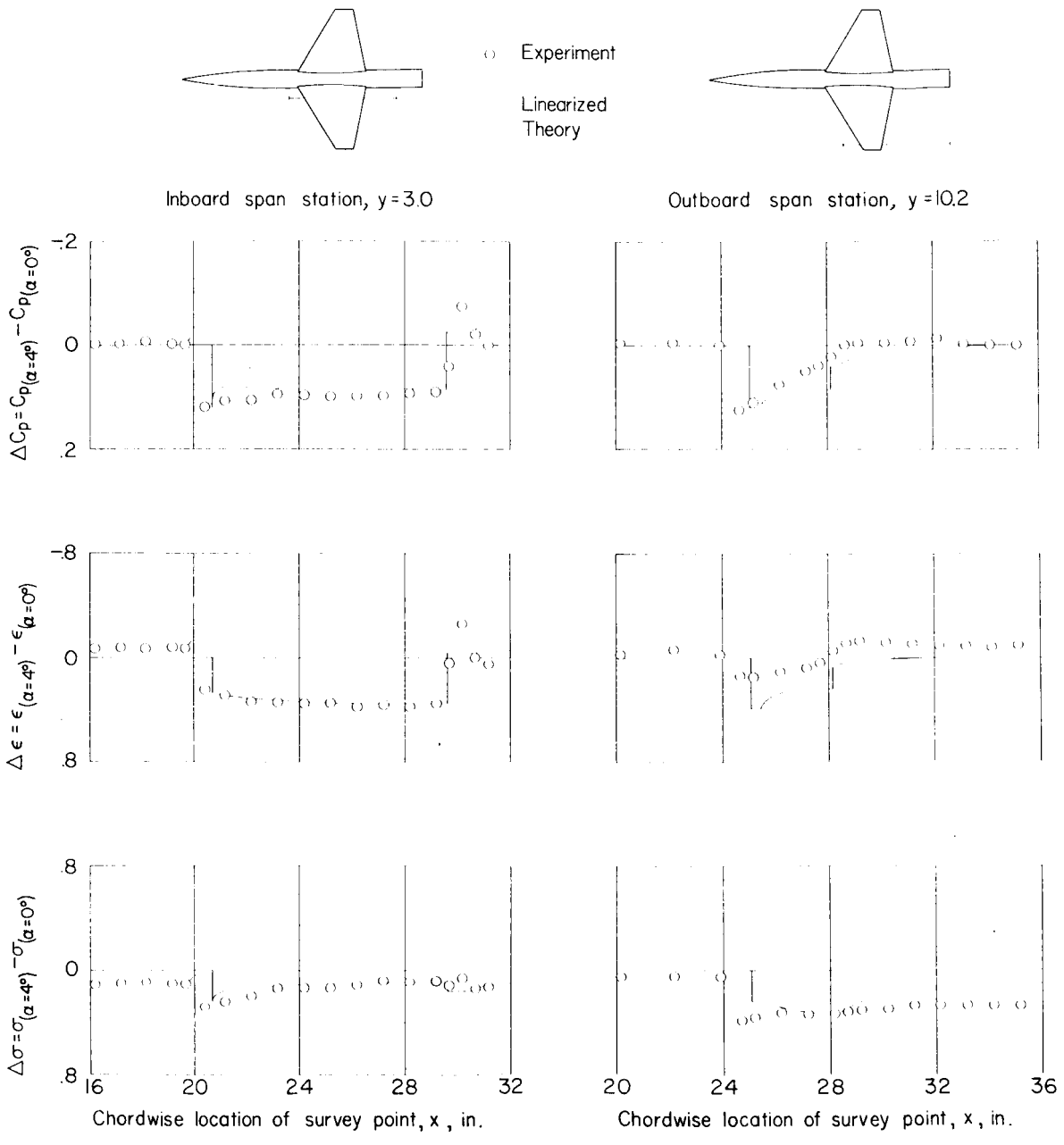

Figure 21.- Comparison of theoretical and experimental flow properties due to angle of attack for an inboard and an outboard span station. Trapezoidal-wing—fuselage configuration; z = 2.1 in.; M_∞ = 1.61.